

Design of Laterally Loaded Deep Piers to Resist River Scour

P. M. Kandarís¹, P.E. and B. Wahlin², Ph.D., P.E., D.WRE

¹Salt River Project, Mail Stop XCT317, P.O. Box 52025, Phoenix, AZ 85072-2025; PH (602) 236-8613; email: pmkandar@srpnet.com

²WEST Consultants, Inc., 8950 S. 52nd St. Ste. 210, Tempe, AZ 85284; PH (480) 345-2155; email: bwahlin@westconsultants.com

ABSTRACT

Expansion of the 91st Avenue Waste Water Treatment Plant in Phoenix, Arizona necessitated the relocation of a major Salt River Project (SRP) 500kV electric transmission power line. The project required installation of six reinforced concrete drilled shaft foundations at two structure sites within and along the Salt River banks to support the new single pole structures. WEST Consultants (WEST) performed hydraulic and sediment transport analyses to determine the local and long-term scour depths in the area near the supporting foundations. The hydraulic analysis consisted of determining average and maximum flow velocities as well as water surface elevations for various peak flow events. SRP utilized these values to determine the local scour that might be expected on the new foundations. WEST developed a sediment transport model for the study reach that was run through an observed 105-year flow hydrograph. Long-term scour near the new foundations was estimated from the sediment transport modeling results. WEST also conducted geomorphic analyses to evaluate the relative lateral stability of the channel in the vicinity of the proposed structures. SRP performed a geotechnical investigation to the full depth of proposed foundations to characterize subsurface soils and develop design parameters. Final design incorporating all study work resulted in the construction of 3-m diameter foundations ranging from 21.0-m to 23.9-m in length, with maximum reveals from scour and associated bank ground loss of up to 16.1-m.

This paper discusses a probabilistic approach for design of deep pier foundations with large reveals where structures and their structural elements must resist the transient environmental conditions of wind, temperature and stream flow.

INTRODUCTION

The 91st Avenue Wastewater Treatment Plant, located just north of the Salt River and east of 91st Avenue in Phoenix, Arizona, treats wastewater from the cities of Phoenix, Glendale, Mesa, Scottsdale, and Tempe. Plant reclaimed water is used for agriculture, running the Palo Verde Nuclear Power Plant, and helping provide a wildlife refuge in the adjacent Tres Rios Demonstration Wetlands Project. As part of ongoing capital improvements, the plant is undergoing a multi-year expansion to boost capacity from 678 MLD to 772 MLD by 2014.

A segment of the SRP Jojoba to Kyrene 500KV electric transmission power line extends through the planned waste water treatment plant expansion area and must be relocated to facilitate the work (see **Figure 1**). Work involves constructing five new structure sites using eleven single shaft poles that will wrap around the north, east, and south perimeters of the plant site and the demolition of two lattice tower

structures within plant property. Two new structure sites (CP-128 and CP-128A) along the south boundary are within the north bank of the normally dry Salt River and require drilled pier reinforced concrete foundations to be built at the edge of the river's floodplain. Both sites will use three cylindrical steel shaft poles, each founded on a drilled shaft pier, to support the power lines. The western site (CP-128) will be constructed 60-m southeast of an existing lattice tower structure within the same alignment as the present transmission line. The second site (CP-128A) is to be constructed approximately 365-m east-northeast of the same lattice tower structure.

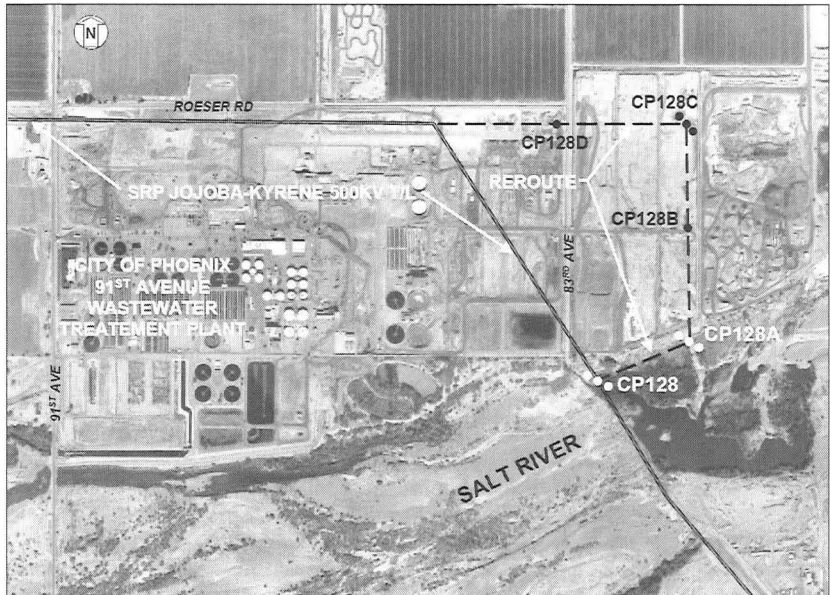


Figure 1. Site location.

Drilled shaft reinforced concrete foundations supporting poles must be designed to accommodate ephemeral river flow forces and corresponding ground loss from scour conditions along with maximum loads induced by electric power conductor lines from transient tension and wind loads. Structure design loads on foundations provided by the pole vendor are presented in **Table 1**. These loads are maximum design values (ultimate loads) at the top of the piers that include appropriate electric code overload factors.

Investigation Scope and Purpose

Nominal 21-m deep exploratory borings were performed at each structure site. Holes were advanced by use of percussion drilling with a Becker diesel hammer drill rig, Model AP1000; hammer rated at a maximum energy of 11 kN-m per blow. Percussion testing was performed by counting the number of hammer blows required

to drive the casing each 0.305-m into the subsurface. Standard penetration resistance tests (SPT) were also obtained within the exploratory borings beginning about 12-m below grade and about every 1.5-m thereafter for the full depth of each boring. Recovered samples were laboratory tested for soil strength properties and used along with blow counts to characterize the strata and estimate design properties.

Table 1. Foundation base plate loads (ultimate)

Structure		Structure w/ foundation number	Quantity	Reactions (maximum)		
Type	Height (m)			Shear (kN)	Moment (MN-m)	Compression (kN)
SPEC A	42.7	CP-128-1, 3	2	558	21.27	400
SPEC B	34.7	CP-128-2	1	503	19.00	354
SPEC C	42.7	CP-128A-1, 3	2	502	16.20	341
SPEC D	34.7	CP-128A-2	1	458	14.36	283

SRP employed WEST to perform hydraulic and sediment transport analyses for determining long-term degradation, parameters for use in local scour calculations at structure sites, and potential embankment loss. Hydraulic analyses were conducted for the 25-year, 100-year, and 500-year peak flow events. This analysis consisted of determining average and maximum flow velocities as well as water surface elevations for the various peak flow events. SRP then used these parameters to estimate the local scour that might be expected at the new foundations. WEST conducted a geomorphic and sediment transport analysis to evaluate the relative lateral stability of the channel in the vicinity of the proposed structures. Using existing HEC-6T sedimentation models developed for the Salt River, the general aggradation and/or degradation anticipated near the structure locations was also estimated.

Site and Geologic Setting

The site is on an elevated portion of the north bank of the Salt River and along the active flood channel bordering active and inactive sand and gravel mining operations. Two of the CP-128 foundations rest on a ridge at an elevation of 295-m (above mean sea level). The third foundation is located within an existing irrigation tail water ditch that drains into the river channel (invert at about at elevation 294-m). The foundations at CP-128A are also near the top ridge of the bank, but also lie within a graded earth-fill/cut ramp that extends down into the river channel (part of the mining operation). Ground elevations near these foundations range from about 300-m on the north end to 297-m on the south end. The steep bank of the river (primarily the result of mining operations) borders structure locations and the new transmission line alignment to the south, dropping down to a lower high-flow portion of the channel at an average elevation of 294-m. Invert elevations within numerous adjacent incised low-flow channels within the main river range from 290-m to 292-m.

Near-surface soil in the floodplain of the Salt River is primarily composed of recent alluvial deposits (Holocene to perhaps locally late Pleistocene) at least 18-m in thickness that overlay basin fill deposits (Demsey, 1989). Uppermost alluvium represents recent floodplain deposits, perhaps with minor aeolian and locally derived components and is mostly poorly graded silty sand, sand, gravelly sand, and gravel

with occasional interlayers of silt and silty clay (Fugro, 1979). Below this veneer is a very coarse and unconsolidated gravel unit mostly containing pebbles, cobbles, and boulders within a sandy matrix. The gravel (referenced as the Salt River Gravels) unit includes clasts of rocks not found in local mountains and represents deposits of the Salt River (Reynolds and Bartlett, 2002). These gravels have a siltier matrix in some areas, but lack any sandy or silty matrix found in some very coarse channel deposits.

ANALYSIS

Subsurface Characterization

Variable thickness layers of upper alluvium are encountered to a depth of 5.0-m at CP-128 and 5.5-m at CP-128A and are comprised of loose to medium dense (dense near the bottom of the deposit) non-plastic silty and gravelly sand and sandy gravel. Very dense, non-plastic sand/gravel/cobble deposits (locally referred to as SGC) underlay these upper strata to the full depth of borings. Interbedded within this SGC deposit are small fine-grained lenses of stiff, low plasticity clayey-silty sand to sandy silty clay and medium-dense to dense non-plastic sands ranging in thickness from 0.6-m to 1.5-m. These lenses are primarily found at the following intervals below grade: 8.8-m to 9.8-m, 12.2-m to 13.1-m, and 17.4-m to 18.9-m.

Groundwater was encountered during the investigation at 7.3-m below grade at CP-128 and at 9.8-m below grade at CP-128A. High groundwater levels within the active river channel and the surrounding floodplain have developed in response to recharge induced by long-term runoff and effluent from the adjacent wastewater plant in the normally dry river channel. A reduction in water level typically occurs soon after runoff ceases due to the highly permeable nature of river sediments. However, inundation and saturation of the entire soil column at structure locations can be expected periodically, thereby causing groundwater level fluctuations (Fugro, 1979).

Blow counts along with bore log subsurface soil descriptions are used to create an idealized subsurface soil profile for the site. The idealized soil layers are assigned low-bound normalized blow count values by statistical analyses that are then correlated with soil strength and deformation properties. A summary of the site geotechnical properties and design parameters assumed is presented in **Table 2**.

Previous Hydraulic and Sediment Transport Analyses

WEST performed two previous studies for the U.S. Army Corps of Engineers (USACE) in the area: the Rio Salado Oeste Feasibility Study (WEST, 2002) and the Preconstruction Engineering and Design (PED) of the Tres Rios North Levee (WEST, 2004). The Rio Salado project was a hydraulic and sediment transport analysis of the Salt River from 19th Avenue to 91st Avenue. The Tres Rios project provided a hydraulic PED for the proposed Tres Rios North Levee. The project reach included the Salt and Lower Gila Rivers in Phoenix, AZ, extending from the Agua Fria River confluence to 91st Avenue. For both of these studies, WEST created a hydraulic model using HEC-RAS and a sediment transport model using HEC-6T. The hydraulic model for the Rio Salado Oeste project was developed using 1.2-m contours. The various sand and gravel mining pits in the area were included as part of the topography when the cross-sections were generated. The hydraulic model for the Tres

Rios project was subdivided into three reaches: the Salt River, the Upper Gila River, and the Lower Gila River. The elevation data used to construct the Tres Rios hydraulic model consisted primarily of 0.3-m vertical resolution topography.

Table 2. Geotechnical properties and design parameters

Property/Value	Silty & gravelly sands	Very dense SGC	Sand	Dense SGC	Sand	Dense SGC	Very dense SGC	Silts & clays	Dense SGC
Depth, (m)	0 to 5	5 to 9	9 to 10	10 to 12	12 to 13	13 to 14.3	14.3 to 17.4	17.4 to 19	+19
SPT Blow Count, (blows/0.305m)	39	97	10	78	16	63	94	12	57
Total Unit Weight, (kg/m ³)	1922	2162	1682	2162	1682	2162	2162	1602	2162
Friction Angle, (deg)	34	50	30	45	31	42	47	30	41
Cohesion, (MPa)	0	0	0	0	0	0	0	0	0
Strength Reduction Factor	1.00	0.70	1.00	0.80	1.00	0.86	0.76	1.00	0.88
Elastic Modulus, (MPa)	27.6	55.2	6.2	48.3	12.4	41.4	855.2	5.5	37.9

Hydrology

The hydrology for the study is based on a report from the USACE (1996). Values for the 5-year through 500-year peak discharges are shown in **Table 3**.

Hydraulics

Because the study area is located right at the break between the two individual models, the Rio Salado Oeste model and the Tres Rios model were combined into a single HEC-RAS model to compute maximum water surface elevations, flow depths, flow velocities, and flow distributions for the 500-, 100-, and 25-year peak flow events. By combining the two models, the effects of the sand and gravel mining operations upstream of the study area and the backwater effects from the proposed levee near the study site were evaluated simultaneously. The cross-sections where the transmission structures are proposed in both the hydraulic model and sediment model are shown in **Table 4**. A summary of the hydraulic results appears in **Table 5**.

Geomorphic Analysis

The goal of the geomorphic analysis was to identify historical behavior of the Salt River by the collection and review of historical aerial photographs and the application of geomorphic relationships. A qualitative analysis of historical changes to river morphology was followed by a quantitative analysis for basic geomorphic factors of the Salt River. The Salt River was a perennial stream prior to construction of upstream water supply dams in the period 1908-1930. Historical accounts and photographs indicate that the Salt River was a wide braided channel that supported significant vegetation but was also prone to major flood events. Since completion of

the upstream dams on the Salt and Verde Rivers, the study reach has experienced significant periods of virtually no flow and is now an intermittent stream.

Table 3. Peak discharges used for hydraulic analysis (USACE, 1996)

Event	Flow rate (cms)
500-year	6,655
100-year	4,587
50-year	3,737
25-year	2,633 ¹
20-year	2,378
10-year	1,444
5-year	566

¹Interpolated from 20- & 50-yr events.

Table 4. Structure locations in the various hydraulic and sediment models

Structure location	Corresponding cross-section
CP-128	203.48
CP-128A	Between 203.67 & 203.77

Table 5. Hydraulic results at the various structure locations

Structure location	River Station	Water surface elev. (m)	Maximum channel depth (m)	Average velocity (m/s)	Maximum velocity (m/s)
25-year flows					
CP-128	203.48	296.95	5.00	2.32	2.81
CP-128A	203.67/203.77	297.36	3.98	1.59	1.91
100-year flows					
CP-128	203.48	297.78	5.83	2.90	3.37
CP-128A	203.67/203.77	298.27	4.90	1.99	2.37
500-year flows					
CP-128	203.48	298.47	6.52	3.34	3.79
CP-128A	203.67/203.77	299.01	5.66	2.42	2.85

The shifting, changing nature of braided channels and the fact that they are often generated by sediment deposition and bed aggradation leads many engineers and river scientists to associate them almost exclusively with disequilibrium in the fluvial system. However, as Leopold et al. (1964) pointed out, braided river systems are a distinct and viable category of dynamically stable planform, along with straight and meandering systems. The recent historical evidence examined here indicates that the project reach is in quasi-equilibrium, although adjustments to bank and thalweg lines within the historical meander belt are possible.

Sediment Transport Analysis

WEST estimated the general aggradation and/or degradation at the structure locations by combining the Rio Salado Oeste and the Tres Rios HEC-6T sediment transport model developed for the Salt River.

Hydrologic data for the simulation are taken from the more recent Tres Rios study and are comprised of a 105-year (1889-1993) series of hydrographs. Inflowing load from the Rio Salado Oeste model is used for each of the runs, because

introducing the lower Tres Rios inflowing load at the upstream end of the Rio Salado Oeste model is not consistent with the bed gradations in the Rio Salado Oeste model. The model is run using the Yang stream power sediment transportation function and the Toffaleti-Meyer-Peter-Muller combination sediment transport function. The worst case of all the runs was used to evaluate the potential degradation at the structure locations. In addition, a run was made in which the inflowing sediment load was cut in half to evaluate the sensitivity of the expected degradation.

The recommended scour depth and elevation due to long-term degradation are provided in **Table 6**. Total embedment depths for the structure foundation must also include a local scour component, which is not included in **Table 6** (local scour is calculated as part of the foundation design). The sum of scour components (long-term degradation and local scour) should be subtracted from the minimum channel elevation to compute the maximum scour elevation to account for possible thalweg migration within channel banks.

Table 6. Recommended long-term degradation depths

Structure location	Thalweg elev. (m)	Recommended long-term degradation depth (m) ¹	Recommended long-term degradation elev. (m) ¹
CP-128	291.9	-2.1	289.8
CP-128A	293.2	-0.9	292.3

¹The local scour component (pier scour) is not included in estimated values.

FOUNDATION DESIGN

Foundations must resist lateral forces introduced by wind on the conductors and pole, tension from conductors at angles that vary based on ambient temperature, and moving water on the foundation itself during periodic stream flow. The transient environmental factors of wind, temperature and water flow can be evaluated in terms of their maximum probable event frequency, with the understanding that peak wind and minimum temperature do not necessarily occur simultaneously with peak river flow. The goal is to match appropriate maximum probable events based upon time of year to provide a more reliable estimate of loads (a reliability-based approach). Maximum probable wind events, minimum expected temperatures and tension loads are governed by the National Electric Safety Code (NESC). Since the electric industry has no standard for hydraulic loads on foundations, SRP assumes a similar frequency for river flow events with foundation design. Project foundations are designed based on the largest dimensions provided by the following load cases.

- Case 1: Full bank washout + full long-term degradation + 100-yr event pier scour with NESC light wind loading on conductors and pole structures (≈ 25 yr return interval, ambient temperature at -1.1°C).
- Case 2: Full bank washout + full long-term degradation + 25-yr event pier scour with NESC extreme wind event on conductors and pole structures (100-yr return interval, ambient temperature at 15.6°C).

Water surface elevations, maximum flow velocities, and upstream channel depth values are obtained from **Table 5**. Embankment loss plus channel degradation values are obtained from the last column in **Table 6**. Top of piers are set above the

500-year event water surface elevations and at least 0.6-m above existing high adjacent grade (whichever is higher) or at elevation 298.9-m for CP-128 and elevation 300.1-m for CP-128A.

A 3-m diameter pier is used to accommodate the pole anchor bolt cage diameter and pier reinforcement clearance needs. The Colorado State University (CSU) equation is used in the analysis for determining local pier scour (FHWA equation 6.1, 2001). Other components of scour such as bend scour and contraction scour are not appropriate for this case.

Local design practice sets CSU equation constants as follows: $k_1 = 1.0$ (round piers), $k_3 = 1.1$ and $k_4 = 1.0$. The spacing effect in relation to the approach angle of flow is considered since there are three foundations within close proximity. To account for group effects, the term $K_S K_\Theta$, a combined shape and alignment factor for foundation groups, is substituted for k_2 (Melville and Coleman, 2000). Foundations are to be spaced (S) 17-m apart on a 45 degree angle to the direction of flow. Assuming a maximum pier diameter (D) of 3-m ($S/D = 5.5$), $K_S K_\Theta$ is equal to 1.17.

Lateral forces control the design of single shaft electric transmission line structures. These forces introduce high moments with moderate shear forces upon the tops of support foundations. Exposed portions of piers (including lengths in the scour zone) are also subject to additional longitudinal load due to stream pressure. To simplify the analysis, stream pressure forces from each load case are converted to an equivalent single shear force at the top of the foundation in the downstream direction. Detailed calculation methods are found in the literature (Kandaris et al., 2002). Since the channel can migrate to foundation locations, it is assumed that all scour originates at the thalweg elevations noted in **Table 6**. Lateral load analysis of the foundation includes the long-term degradation shown in **Table 6** and local scour calculated for each case. **Figure 2** shows an example configuration. **Table 7** summarizes the local scour and stream pressure forces for each case.

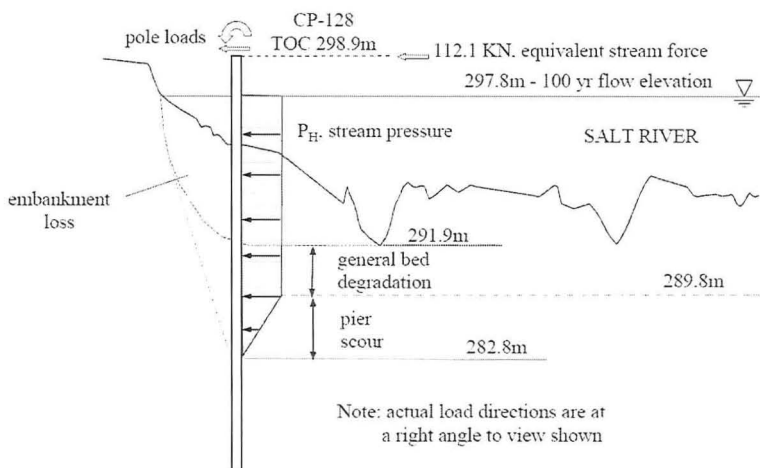


Figure 2. Scour and stream force model.

Table 7. Local scour and stream pressure design values

Structure number	Scour Event	Local pier scour depth (m)	Length of pier above scour (m)	Equivalent water shear force at top of foundation (kN)
CP-128	100-yr	7.0	16.1	112.1
	25-yr	6.3	15.4	66.0
CP-128A	100-yr	5.9	13.7	40.0
	25-yr	5.2	13.0	20.4

Foundation design results are summarized in **Table 8**. These dimensions are determined by applying the ultimate base reaction values with factored stream pressure forces. The combined loads are then multiplied by a dead-end geotechnical load condition factor of safety of 1.25 to account for soil variability, load repetition, long-term loading and to ensure equal to or greater foundation reliability than the pole structure. Rotational movement at the top of the pier is limited to one degree. Electric Power Research Institute Foundation Analysis and Design (FAD) methodology and computer software is utilized to perform detailed calculations.

Table 8. Foundation dimension summary

Structure w/ foundation number	Scour Event	Elevation to soil resistance (m)	Foundation embedment depth below scour (m)	Total pier length (m)
CP-128-1, 3	100-yr	282.8	7.8	23.9
	25-yr	283.5	7.9	23.3
CP-128-2	100-yr	282.8	7.4	23.5
	25-yr	283.5	7.4	22.8
CP-128A-1, 3	100-yr	286.4	7.6	21.3
	25-yr	287.1	8.0	21.0
CP-128A-2	100-yr	286.4	7.3	21.0
	25-yr	287.1	7.0	20.0

Controlling cases shown in **bold text**.

CONCLUSIONS

A methodology is presented to determine total pier embedment for electrical transmission line foundations placed within an ephemeral river channel. The methodology takes into account loading due to flowing water, scour due to bank loss, forces due to wind, and the subsurface characteristics of the river bed. Hydraulic and sediment transport analyses are used to calculate long-term degradation, bank loss from stream migration and local scour around the piers. In this case, other scour components such as bend scour are not applicable; however, these components should be added if appropriate at a given site. Field geotechnical and geologic investigation work characterize subsurface conditions, allowing development of soil strength and deformation parameters for use in lateral load analyses.

The case history shown applies reliability-based principles that take into account two different transient load scenarios: the maximum probable peak stream

flow event in conjunction with the seasonal high wind event and minimum low temperature condition; and a seasonal medium stream flow event with the maximum probable high wind event and seasonal low temperature condition. The lengths of the various 3-m diameter drilled shaft piers supporting structures CP-128 and CP-128A determined by the combined load and scour analyses range from 21.0-m to 23.9-m. Portions of piers extending above total scour elevations range from 13.0-m to 16.1-m.

Anderson Construction began drilling at CP-128A-1 on November 30, 2009 and completed their last concrete placement at CP-128-1 on February 3, 2010. Each pier foundation required an average of 5 working days to excavate and pour concrete to the planned cold joint within 3-m of ground surface. Use of both permanent metal liners and temporary steel casing above scour depths in conjunction with polymer slurry stabilization below scour depths held average foundation diameters within 3 percent of neat line values.

REFERENCES

- Demsey, K.A. (1989). *Geologic map of quaternary and upper tertiary alluvium in the Phoenix South 30' x 60' Quadrangle, Arizona*. Arizona Geologic Survey (AZGS) OFR 89-7, Tucson, AZ.
- Federal Highway Administration (FHWA) (2001). *Evaluating scour at bridges*. 4th Ed., HEC 18, Pub. No. FHWA-NHI 01-001. Washington, D.C.
- Fugro, Inc. (1979). *Palo Verde to Kyrene transmission line*. Salt River Project File Report CE-15, Phoenix, AZ.
- Kandaris, P.M., Kondziolka, R.E., and Adams, J. P. (2002). "Design and construction of scour foundations for electric power transmission line structures." Proc. ICFS-1, Vol. 2, College Station/TX: 954-967.
- Leopold, L.B., Wolman, M.G., and Miller, J.P. (1964). *Fluvial processes in geomorphology*. W.H. Freeman and Co., San Francisco, CA.
- Melville, B.W., and Coleman, S.E. (2000). *Bridge scour*. Water Resources Publications, LLC, Highlands Ranch, CO.
- Reynolds, S.J. and Bartlett, R.D. (2002). *Subsurface geology of the easternmost Phoenix Basin, Arizona: implications for groundwater flow*. AZGS CR-02-A, Tucson, AZ.
- USACE (1996). "Section 7 Study for Modified Roosevelt Dam, Arizona (Theodore Roosevelt Dam)." *Hydrologic Evaluation of Water Control Plans Salt River Project to Gila River at Gillespie Dam*, USACE Los Angeles District.
- WEST Consultants, Inc. (2004). *PED Hydraulic Design of Tres Rios North Levee, Maricopa County, Pre-Final Project Analysis Final Report*. Prepared for the U.S. Army Corps of Engineers, Los Angeles District, Contract Number DACW09-00-D-0021.
- WEST Consultants, Inc. (2002). *Rio Salado Oeste Study without Project Final Hydraulic Analysis Report*. Prepared for the U.S. Army Corps of Engineers, Los Angeles District, Contract Number DACW09-00-D-0021.

A LASER-BASED OPTICAL APPROACH FOR MEASURING SCOUR DEPTH AROUND HYDRAULIC STRUCTURES

Qing Tian¹, K. Todd Lowe¹, and Roger L. Simpson¹, Member, ASCE, P.E.

¹Applied University Research, Inc., 605 Preston Ave., Blacksburg, VA 24060; email: aur@aurinc.com

ABSTRACT

This paper describes a method using laser-based optical instrumentation to measure scour depth around hydraulic structures after flume tests. This laser-based optical approach utilizes a laser light sheet and digital camera. This method is nonintrusive, easy to setup and has high spatial resolution. A validation case of measuring a 3-D concave shape with known dimensions was conducted to evaluate the uncertainty of the proposed methodology. The intrinsic uncertainty limit represented by the laser sheet thickness is reached, and this simple procedure is suitable for obtaining meaningful results with an acceptable level of accuracy. The performance of applying a hooked collar as a scour countermeasure around a circular pier, rectangular pier and 2-D streamlined pier was studied and tested inside a flume. The scour depth data were measured and recorded with the described laser-based optical technique. The hooked collar reduced the maximum local scour depth by 60% at the optimal collar location; but it was importantly observed that this location strongly depends upon the local flow conditions such as the incoming flow speed, flow depth and pier width.

INTRODUCTION

Removal of riverbed substrate around bridge pier footings is known as scour. Excessive scour around bridge piers due to the large-scale unsteadiness and shedding of coherent vortices is the cause of failure of many bridges around the world (Batcho, 2001). Over the past decades, the local scouring mechanism around the circular pier has been studied intensively, well understood and documented. The horseshoe vortex and wake shedding vortices were identified as the major causes for the local scour around circular piers as described by Breusers et al. (1977), Melville (1975) and Dargahi (1990). The three-dimensional boundary layer separation due to large pressure gradients around a bridge pier is accompanied by large-scale vortices, characterized with intense turbulence, unsteadiness, shear stress and vorticity (Simpson, 2001).

Along with the understanding of local scour, various different methods for controlling local scour have been proposed. Bridge pier scour countermeasure techniques can be classified into three classes (Lagasse, et al. 2001), which are hydraulic countermeasures to enhance the resistance ability of the bed material to scour, structural countermeasures to reduce the power of the scour agents by modifying the local flow condition around the hydraulic structures, and scour monitoring. The structural countermeasures such as pier shape modifications and collars are primarily used to minimize local scour. The pier shape modifications

mentioned here refer to the bridge piers with streamlined cross sections. The performance of the streamlined piers on reducing local scour was studied by Laursen and Toch (1956) and Chabert and Engeldinger (1956). The conclusions were made that the streamlined piers greatly reduced the maximum scour depth. However, they also pointed out that the effectiveness of the streamlined piers on controlling local scour became questionable when the pier was not aligned with the flow, especially for the piers at a large angle of attack. This observation is intensified for piers with large length-to-width ratio. The results reported in the literature by Chabert and Engeldinger (1956), Thomas (1967), Tanaka and Yano (1967), Neill (1973), Ettema (1980) and Chiew (1992) showed that placing a collar or caisson around a bridge pier reduced the depth of scour. Thomas (1967), Tanaka and Yano (1967) and Dargahi (1990) also demonstrated that in order to be effective on controlling local scour, the collar has to be inside the separated flow region close to the riverbed and the collar diameter to pier diameter ratio has to be more than 3.

A typical real-world bridge pier with a diameter of some few meters yields flat collar diameters for effective scour control which are too large to be practical. Therefore, Chen et al. (2007) came up with the "hooked" collar idea. In their design, Chen et al. used a small diameter horizontal collar with a vertically oriented fence that forms an annulus around the periphery of the horizontal collar. The vertical "hook" section acts to prevent the downward jet flow of the horseshoe vortex that enhances local scour. The horizontal collar section has much smaller diameter than the flat collar necessary to mitigate local scour. Their results did show the improvement of local scour with the hooked collar at the optimal location along the vertical axis of the pier. The present work expands upon the work reported by Chen et al. The objectives are to investigate, by means of flow visualization and laser-based scour depth measurements, the effectiveness of the hooked collar design for different pier shapes and the coupling of the incoming flow and bed conditions, such as incoming flow speed, flow depth and sediment size, with the local scour observed.

Along with the research related to the scour countermeasures, the need of developing high spatial resolution and nonintrusive measurement instrumentation for studying sediment bed erosion becomes imperative. Traditional methods such as point gauges are intrusive and time consuming to use since they can only perform point-by-point measurements. Baglio and Foti (2003) developed a 3-D stereoscopic-type image processing method to measure three-dimensional coordinates of a scoured sediment bed surface. To do so, two video cameras at different viewing angles were applied during the process. Calibration was required for this process in order to get the coordinate transformation matrix. Younkin and Hill (2009) applied a planar laser sheet to illuminate the granular bed to capture the evolution of the sediment bed scour due to horizontal wall jet. In this paper, a simplified nonintrusive laser-based optical technique is proposed for rapidly measuring a scour hole. A 2-D laser sheet profile intersecting a scour hole is recorded with a digital camera and transformed from the image coordinates to the objective coordinates through a simple transformation formula. This simple technique affords detailed bed contour measurements in a fraction of the time required to probe the contoured surface mechanically.

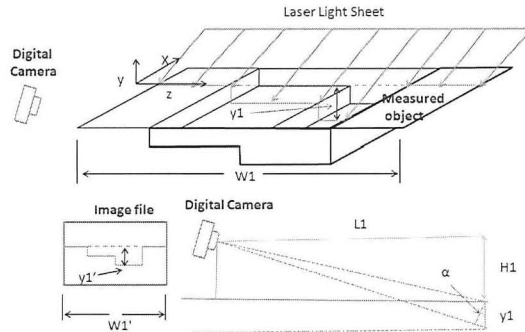


Figure 1. Laser optical approach for 2-D scour depth measurement.

MEASUREMENT METHODOLOGY

Laser-based Optical Approach for Measuring Scour Depth

A laser-based optical technique is applied for rapidly obtaining detailed bed elevation contours for scour testing. In the technique (figure 1), a laser light sheet is progressively positioned to illuminate slices of a scour hole from a flume test. The intersection of the laser sheet with the bed surface appears as a curved line to a viewer positioned out of the plane of the sheet. The image of this curved line is recorded with a digital camera, and post-processed using spatial calibration factors to convert the pixel coordinates of the line to surface elevations. Perspective distortion is eliminated through proper alignment of the camera relative to the sheet and by applying a geometric transformation from image coordinates to actual scour depth during post-processing. The following equations (1-3) are used as the transformation formulas from the image coordinates to the objective coordinates under the condition that $L1$ and $H1$ are much greater than $y1$. The equation (1) may be solved iteratively to obtain the scour depth given the instrument system parameters. The curved line profile from the laser sheet intersection with the scour hole is on the y - z plane in the objective coordinate as shown in figure 1 and the flat intersection line with the initial bed level is aligned with the z -axis. The third dimension coordinates of the curved line profile along the x -axis, which are constant, can be measured, and recorded manually. Therefore, the 3-D spatial coordinates of a scoured bed surface can be measured and reconstructed with only one still or video camera.

$$y1 \approx \frac{y1' \times M}{\cos(\alpha)} \quad \text{and} \quad \tan(\alpha) \approx \frac{y1' + H1}{L1}, \quad \text{if } L1, H1 \gg y1 \quad (1)$$

$$z1 = z1' \times M \quad (2)$$

$$M = \frac{W1}{w1'} \quad (3)$$

Where M is the calibration factor from pixel to the objective dimension before the perspective correction; $y1$ and $z1$ are the coordinates of the curved line profile in the objective coordinate; $y1'$ and $z1'$ are the coordinates of the curved line profile in the

image coordinate; $W1$ is the known width of the spanwise reference line in the objective coordinate; $W1'$ is the width of the spanwise reference line in the image coordinate; $L1$ is the horizontal distance between the laser sheet plane and the camera; and $H1$ is the vertical distance between the camera and the initial sediment bed level.

Discussion of the Uncertainty of the Developed Measurement System

A validation case of measuring the outline of a PVC coupler with known geometry is performed to evaluate the uncertainty of the developed measurement system. Figure 2 demonstrates the quality of the agreement between the measured and true value of the outline. The standard deviation of the difference between the measured and true value is about 0.5 mm. Given 21 to 1 odds, the uncertainty calculated as $\pm 2\sigma$ is about 1.0 mm. The actual thickness of the laser sheet is about 1.5 mm. Therefore, the measured uncertainty is very close to the thickness of the laser sheet.

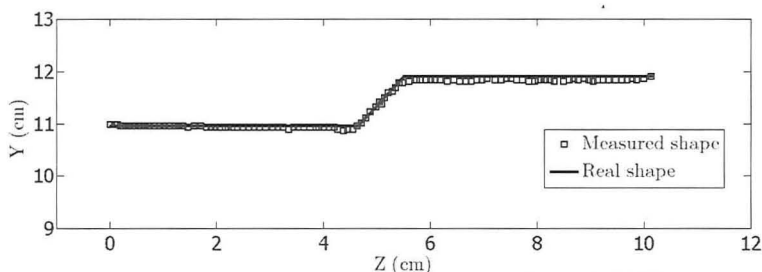


Figure 2. Comparison of the measured and real outlines of a PVC coupler.

EXPERIMENTAL SETUP AND PROCEDURES

Flume

The water flume facility was designed and constructed at the Applied University Research, Inc (AUR) laboratory in Radford, Virginia. The straight test section has a clear acrylic sidewall, and is about 2.44 m long and 1.22 m wide. The sidewall height is about 0.19 m and the water depth used for the current tests is 0.165 m. A layer of pea gravel bed was placed in the gravel tank. The pea gravel used for local scour tests has a specific gravity of three and is between 3.2 mm and 6.4 mm in size. The flume experiments were run at a nominal speed of 0.64 ± 0.03 m/s. The selected test speed produced an incipient scour condition for the pea gravel without any pier present. The influence of the sediment size on scour depth was studied by Ettema (1980); and it was found that for gravel size greater than 0.7 mm, there was a critical value of 18 for the pier width to gravel size ratio. If that ratio is above the critical value, the ratio of maximum scour depth to pier width reaches to a constant value. The corresponding pier width to gravel size ratio in following flume tests ranges between 12 and 24, with a mean value of 18. Therefore, there is little or no influence of gravel size on the maximum scour depths measured. The inflow boundary layer profile was measured with a Pitot-static probe and a U-manometer.

The results are presented in figure 3. The free surface boundary profile essentially follows the expected law of the wall (Elder 1959).

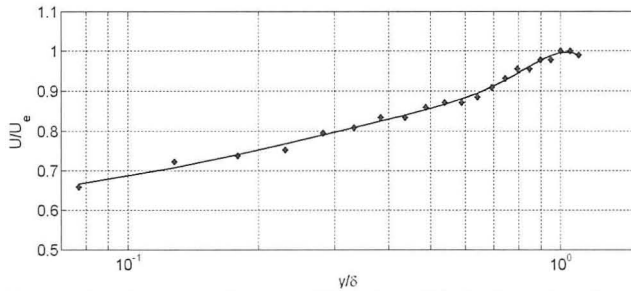


Figure 3. Free surface boundary layer profile, where δ is the boundary layer thickness at 99.5% of maximum velocity.

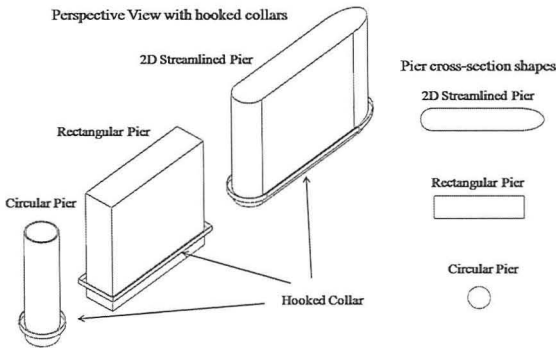


Figure 4. Sketch of the bridge pier models.

Experimental Test Models, Flow Cases, and Procedures

The bridge pier models with hooked collars are sketched in figure 4. Three different pier shapes have been tested: a circular pier, a rectangular pier and a 2-D streamlined pier. The length-to-width ratio of the rectangular pier is 4:1. The 2-D streamlined pier has a circular front nose and elliptical rear nose; and the middle section is a rectangle with 4:1 length-to-width ratio. The width of the pier models is 0.076 m. Each sheet-metal hooked collar has a flat horizontal bottom and a vertical surface. Hooked collars were used in some of the current tests. The design is based upon the work reported by Chen et al. (2007), as described in the introduction. The width and depth of the hooked collar are both 0.0127 m. For each pier model, the case without the hooked collar was tested and used as the reference for studying the effectiveness of the hooked collar. The hooked collar was placed at three different locations: $h_c/D=0$, 0.165 and 0.33 on each pier model. All tests—with or without hooked collars—were run with a water depth of $h_w/D=2.17$.

EXPERIMENTAL RESULTS AND DISCUSSION

Circular Pier Results

The bed elevation contour around a circular pier without the hooked collar was measured with the laser-based optical technique. The non-equidistantly-sampled scour depth data were interpolated onto a 6.5 mm by 6.5 mm square cell grid with a linear triangle-based interpolation. Scour depth contour results are presented in figure 5.a. The color in the contour represents the variation of the bed level. The scour pattern results are consistent with previous studies such as the work of Tanaka and Yano (1967) and of Lin (1993). Local scour was observed immediately upon initiation of the test. Before reaching equilibrium, the gravel in the separated flow region became loose, was carried away from the bed and was deposited downstream. As expected from much previous work, flow visualizations (in this case, performed using a single tuft) indicated the presence of a strong horseshoe vortex around the windward portion of the pier and wake shedding vortices behind the circular pier. The chaotic "bimodal" flow switching behavior of the horseshoe vortex described by Devenport and Simpson (1990) was also qualitatively observed in the tuft visualizations.

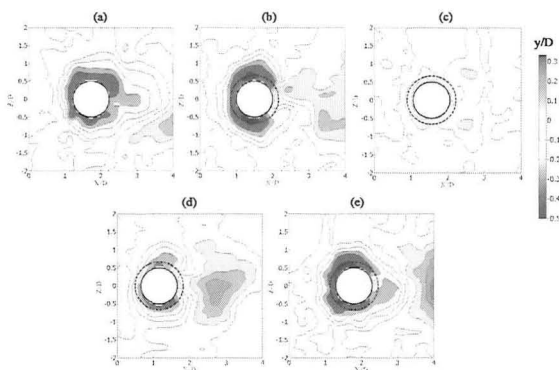


Figure 5. Measured final bed elevation contours around a circular cylinder pier with $h_w/D=2.17$ (a: no hooked collar; b: $h_c/D=0$; c: $h_c/D=0.165$; d: $h_c/D=0.33$; and e: $h_c/D=0.72$).

The results with the hooked collar located at $h_c/D=0, 0.165, 0.33$ and 0.72 are presented in figures 5.b-e. Results were obtained after the local scour rate appeared to reach zero. The hooked collar is plotted with a dashed line. For the cases $h_c/D=0, 0.165$ and 0.33 , local scour started very slowly around and under the hooked collar. The flow visualization showed that the downwash motion around the pier and under the hook was very chaotic. Unlike the case without the collar when scour was immediately observable, it took more than $15118D/U_c$ normalized time units before the local scour hole became observable, and then the local scour rate increased

dramatically. The scour rate later decreased and approached zero by $45354D/U_c$ time units after test initiation of the test case. The location $h_c/D=0.165$, was optimal, as it yielded the greatest reduction of local scour. Maximum scour depth was reduced by 65%, and there was almost no scour appearing in the wake region. The flow visualization results showed that the separated flow under the bottom edge of the hook flowed counter to the dominant mean vortical motion of the horseshoe vortex upstream of the circular pier, and the downwash motion along the pier was very weak. In contrast to the $h_c/D=0.165$ case, the $h_c/D=0.72$ collar location had almost no effect on local scour. The scour pattern for $h_c/D=0.72$ is very similar to the one without the collar and the maximum scour depth is about $0.45D$.

Chen et al. (2007) conducted a series of flume tests with hooked collars. The circular pier diameter and hooked collar dimension are very similar to current case. Their results did show reduction in the local scour with the hooked collar when placed at the optimal location. However, the specific optimal collar locations for these two cases are quite different. Chen's study showed that the best collar location was at $h_c/D=0.88$, while the current study yielded a value of 0.165 for optimal performance. This is mainly due to the difference in the incoming flow speed. The flow speed under the incipient scour condition in Chen's tests is about 0.24 m/s due to the relatively fine gravel, while the current test speed is 0.63 m/s. Such results indicate the most important challenge in practically implementing the hooked collar approach for reducing local scour.

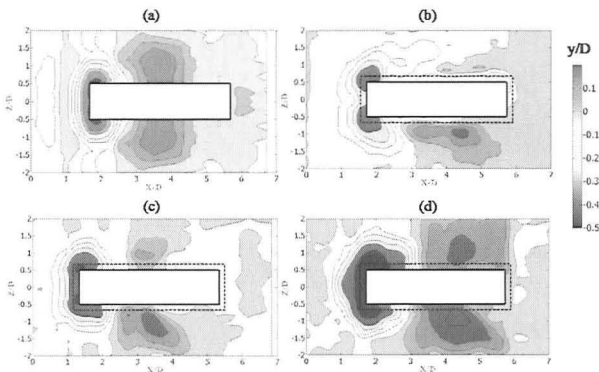


Figure 5. Measured final bed elevation contours around a rectangular pier with $h_w/D=2.17$ (a: no hooked collar; b: $h_c/D=0$; c: $h_c/D=0.165$; and d: $h_c/D=0.33$).

Rectangular Pier Results

The rectangular pier with length-to-width ratio equal to four, which is representative of a common class of bridge piers, was tested in the current study. The rectangular pier was installed at the middle of the test section. Under the influence of the horseshoe vortex, a deep scour hole appeared at the front nose of the rectangular pier at zero angle of attack, as shown in figure 6.a. The color in the contour represents the variation of the bed level. The maximum scour depth is about $0.4D$ around the nose and scour behind the pier is negligible. The above scour pattern and observations

are consistent with the experimental test results by Briaud et al. (2004). In that work, series of flume tests of rectangular piers were conducted to study pier shape effects (different length-to-width ratios) and angle of attack effect on local scour. It was found that for rectangular piers with aspect ratios greater than 4, the scour hole only appeared on the windward side, and no scour was observed in the wake region.

The test results for the rectangular pier with hooked collar at $h_c/D=0$, 0.165 and 0.33 are presented in figures 6.b-d. Similar to the case without the collar, gravels on the windward side were scoured out and one big scour hole was formed. As the collar was moved further away from the gravel bed, the local scour area and maximum scour depth were increased. There was no optimal location for hooked collar. Unlike the circular pier, the hooked collar around the rectangular pier actually increased local scour area and maximum scour depth. The hooked collar did not work as a scour countermeasure for the rectangular pier. There was no significant change in scour rate and local scour was observed right after the flume experiments were begun for each case. Results indicate that the corner separation around the rectangular hook is the main cause for the difference in performance as a scour countermeasure.

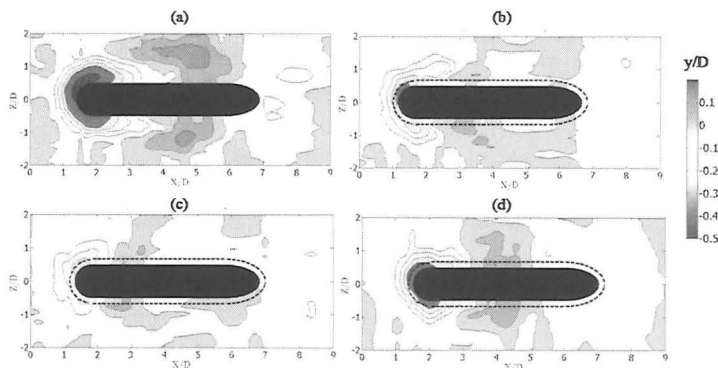


Figure 7. Measured final bed elevation contour around a 2-D streamlined pier with $h_w/D=2.17$ (a: no hooked collar; b: $h_c/D=0$; c: $h_c/D=0.165$; and d: $h_c/D=0.33$).

2-D Streamlined Pier Results

The 2-D streamlined pier has a half-circular front nose and a half-elliptical rear nose, and the middle section is a rectangle with 4:1 length-to-width ratio. The hooked collar is in the same shape as the streamlined pier and plotted with dash line as shown in figure 7. The hook dimensions normalized by the pier width are the same as hooked collars used for the circular and rectangular piers already discussed. In figure 7.a, a large scour hole developed under the influence of the horseshoe vortex around the circular front nose without the collar. The maximum scour depth is about $0.5D$. The scour hole is in the similar shape as for the circular pier without the collar and has a maximum width of $2D$.

The test result for the streamlined pier with the hooked collar installed so that the bottom rests on the initial gravel bed is included in figure 7.b. It does show some improvement on local scour by reducing maximum scour depth and its area. The

maximum scour depth is reduced from $0.5D$ without the hooked collar to $0.35D$ and concentrates in a smaller region. The hooked collar also caused a slightly more scour in the spanwise direction around the junction of the circular and straight sections. Figure 7.c shows that the best hook location for this pier model is located at $h_c/D=0.165$, which is also consistent with the location for the circular pier. The maximum scour depth is reduced to $0.2D$. Moving the collar further away from the bed, the local scour condition became worse as shown in Figure 7.d. Very slow scour rate was observed during the above collar tests. At the optimal location, the hooked collar reduced the maximum scour depth by 60%.

CONCLUSIONS

A nonintrusive method utilizing a laser light sheet and digital camera to measure scoured sediment bed surface around hydraulic structures after flume tests is presented in this paper. The major advantages of this method are that it is nonintrusive, spatially resolved, easy to setup and efficient for making whole-surface elevation measurements. The uncertainty analysis shows that the intrinsic uncertainty limit represented by the laser sheet thickness is reached. This simple procedure is suitable for obtaining meaningful results with an acceptable level of accuracy.

The flume test results of hooked collars around a circular pier, rectangular pier and 2-D streamlined pier demonstrate that the hooked collars at the optimal locations reduced the maximum scour depth by 60-65% for the circular pier and 2-D streamline shaped pier. In most of the cases studied, the hooked collars reduced the local sediment transport rate. However, the results also show that the optimal collar location greatly depends on and varies with the incoming flow conditions and other local conditions, such as the flow speed and pier width. For these reasons, the hooked collar becomes difficult to adopt in a real situation. The hooked collar did not work at all for the rectangular pier and even caused more severe local scour, because of the corner separation around the rectangular hooked collar.

References

- Baglio, S., & Foti, E. (2003). Non-Invasive Measurements to Analyze Sandy Bed Evolution Under Sea Waves Action. *IEEE TRANSACTIONS ON INSTRUMENTATION AND MEASUREMENT*, 52 (3), 762-770.
- Batcho, Paul F. Method and apparatus for mitigating junction flows. US: Patent 6186445, 2001.
- Breusers, H., Nicollet, G., & Shen, H. (1977). Local Scour Around Cylindrical Piers. *Journal of Hydraulic Research*, 15 (3), 211-252.
- Briaud, J.-L., Chen, H. C., Nurtjahyo, P., & Wang, J. (2004). *Pier and Contraction Scour in Cohesive Soils*. Washington, D. C.: NCHRP Report 516.
- Chabert, J., & Engeldinger, P. (1956). *Etude des affouillements autour des piles des ponts*. Chatou, France: Laboratoire National d'Hydraulique.
- Chen, S.-C., Wang, D.-Y., Chou, H.-T., & Yen, S.-C. (2007). The efficacy of hooked-collar on reducing bridge pier scour. *Journal of Taiwan Water Conservancy*, 55, 26-37.
- Chiew, Y.-M. (1992). Scour Protection at Bridge Piers. *Journal of Hydraulic Engineering*, 118 (9), 1260-1269.
- Dargahi, B. (1990). Controlling Mechanism of Local Scouring. *Journal of Hydraulic Engineering*, 116 (10), 1197-1214.

- Devenport, W. J., & Simpson, R. L. (1990). Time-dependent and time-averaged turbulence structure near the nose of a wing-body junction. *Journal of Fluid Mechanics*, 210, 23-55.
- Elder, J. (1959). The dispersion of marked fluid in turbulent shear flow. *Journal of Fluid Mechanics*, 544-560.
- Ettema, R. (1980). *Scour at Bridge Piers*. University of Auckland, New Zealand, School of Engineering. Report NO. 216.
- Lagasse, P., Zevenbergen, L., Schall, J., & Clopper, P. (2001). *Bridge Scour and Stream Instability Countermeasures*. FHWA Technical Report Documentation Hydraulic Engineering Circular No. 23.
- Laursen, E. M., & Toch, A. (1956). *Scour Around Bridge Piers and Abutments*. Iowa Institute of Hydraulic Research.
- Lin, G. H. (1993). *Study on the Local Scour around Cylindrical Bridge Piers*. Feng-Chia University, Taichung, Taiwan: M.S. Thesis.
- Melville, B. W. (1975). *Local scour at bridge sites*. Report NO. 117 The University of Auckland, School of Engineering, New Zealand.
- Neill, C. R. (1973). *Guide to bridge hydraulics*. Roads and Transportation Association of Canada, University of Toronto Press, Toronto, Canada.
- Simpson, R. L. (2001). Junction Flows. *Annual Review of Fluid Mechanics*, Vol. 33: 415-443.
- Tanaka, S., & Yano, M. (1967). Local scour around a circular cylinder. *Proc. 12th Congress I.A.H.R.*, (pp. 193-201).
- Thomas, Z. (1967). An interesting hydraulic effect occurring at local scour. *Proc. 12th Congress I.A.H.R.*, (pp. 125-134).
- Younkin, B., & Hill, D. (2009). Rapid Profiling of an Evolving Bed Form Using Planar Laser Sheet Illumination. *Journal of Hydraulic Engineering*, 135 (10), 852-856.

NOTATION

The following symbols are used in the paper

α = angle between the camera optical axis and the initial sediment bed level;

δ = boundary layer thickness

D = diameter or width of pier models;

h_c = vertical location for the hooked collars;

h_w = water depth inside the flume test section;

H1 = vertical distance from the digital camera to the initial sediment bed level;

L1 = horizontal distance between the laser sheet plane to the digital camera;

M = calibration factor from pixel to the objective dimension;

U_e = Free surface speed;

W1 = width of the spanwise reference line in the objective coordinate;

W1' = width in pixels of the spanwise reference line in the image coordinate;

$x1', y1'$ and $z1'$: coordinates in the image coordinate; and

$x1, y1$ and $z1$: coordinates in the objective coordinate

Effect of Post-Earthquake Bed Degradation on Bridge Stability

Jau-Yau Lu¹, Jian-Hao Hong², Yee-Meng Chiew³

¹Professor, Dept. of Civil Eng., Nat. Chung Hsing Univ., 250 Kuo-Kuang Rd. Taichung, Taiwan. Tel and Fax:+886-4-22853695. Email: jyly@mail.nchu.edu.tw

²Postdoctoral research fellow, Dept. of Civil Eng., Nat. Chung Hsing Univ., 250 Kuo-Kuang Rd. Taichung, Taiwan. Tel and Fax:+886-4-22809789. Email: jean6394@ms49.hinet.net

³Professor, School of Civil and Structure Engineering, Nanyang Technological Univ., Singapore. Tel: +65-67905256. Email: cymchiew@ntu.edu.sg

ABSTRACT

Earthquake and Typhoon are two major nature hazards in Taiwan. The Chi-Chi Earthquake with a magnitude of 7.3 on Richter scale occurred in central Taiwan on September 21, 1999. On September 14, 2008, nine years after the Chi-Chi Earthquake, Houfeng Bridge, located 4.5 km downstream of the Chelungpu Fault on Da-Chia River, collapsed due to the flood event induced by Typhoon Sinlaku. Three vehicles fell into Da-Chia River and six people died because of the collapse of the bridge. The main objective of this paper is to investigate the relative importance of different scour components in this event. The proposed methodology provides reasonable estimates for various scour components, and indicates that the bed degradation caused by the earthquake and all preceding Typhoon-induced floods contributed 27% to the total scour depth. It implies that the long-term general scour cannot be neglected in the bridge stability analysis.

INTRODUCTION

Taiwan is one of the archipelagos of islands in East Asia that frequently are exposed to two different major natural hazards: typhoon and earthquake. Bridges in Taiwan often are subjected to threats imposed by the rivers with steep slope gradient and rapid flows during floods associated with typhoons, which are common from June – October. This often leads to bridge failures. Typhoon Sinlaku pelted Taiwan in September 2008, the Houfeng Bridge, which crosses the Da-Chia River in central Taiwan, collapsed at 6:50 pm on September 14, 2008. Figure 1 shows the bridge one day after the actual collapse; it reveals that the direct cause of failure is the damage to a pier (P2) close to the right bank of the river. Figure 2(a) shows the flow condition upstream of the Houfeng Bridge after recession of the flood on September 24, 2008. The photograph clearly reveals the presence of an encased pipeline located at about 20 m upstream of the bridge, which causes the formation of an impinging jet flow towards the bridge. Figure 2(b), which is a photograph taken when the flood discharge was still high, clearly shows how the jet impinges directly onto the piers. Figure 2(a) also shows how the overall bed degradation associated with long-term general scour of the river bed had exposed the caisson, which forms the foundation of the bridge.



Figure 1. Damage of Houfeng Bridge on Sept. 14, 2008, looking downstream, with flow from right to left

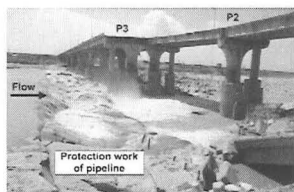


Figure 2(a). Flow field around Houfeng Bridge showing the presence of an upstream encased pipeline (Sept. 24, 2008)



Figure 2(b). Impinging jet downstream of encased pipeline at Houfeng Bridge (Sept. 15, 2008)

The cause of the failure of the Houfeng Bridge is complex. Although the direct cause of failure may be attributed to local pier-scour, it is naïve to suggest that it is the only factor. Based on visual evidences and all available data prior to and during the flood, we are attempting to put together an explanation on all contributing factors that lead to the eventual failure of the bridge. It is hoped that this thorough review and examination of events, either natural or man-made, will allow engineers to better tackle bridge safety worldwide in general, and in Taiwan in particular in the future. Moreover, an attempt is also made to evaluate the various scour depths, both general and local, associated with Pier 2 using published scour formulas. This will allow us to have a clearer understanding on how each of these components contributes to the eventual undermining of the caisson. If such formulas are found to be accurate in determining the extent of scour, they may be used for future design of pier foundation in Taiwan with a higher degree of confidence.

SITE DESCRIPTIONS AND FLOW INFORMATION

The Houfeng Bridge, which was opened to traffic in 1990, is a four-lane, two-way, provincial highway 13 bridge that spans the Da-Chia River in central Taiwan. It connects the Houli township in the north and the Fengyuan City in the south. The length of the bridge is 640 m with 16 spans. The superstructure consists of steel plate girders with a reinforced-concrete slab deck. Each pier consists of four 2-m-diameter reinforced-concrete cylinders tied with a reinforced-concrete capping

beam. These circular piers were founded on cylindrical concrete caissons with diameter of 4 m and length of 14 m (see Figure 2a). All the caissons were originally designed to be completely embedded within the river bed.

The Da-Chia River Basin upstream of the Houfeng Bridge has a drainage area of 1,204 km². As the third longest river in Taiwan, Da-Chia River, which has a total length of 124 km, flows westward for another 25 km from the Houfeng Bridge before reaching the Taiwan Strait. The tidal effect from the river mouth does not influence flows at the bridge. The Shihkang Dam, which was constructed in 1977 to supply water for domestic use in the central part of Taiwan, is located about 5 km upstream of the Houfeng Bridge. The aerial photograph in Figure 3 shows the braided character of Da-Chia River in the reach between the Houfeng Bridge and National Expressway No. 1 Bridge. According to surveys conducted by the Third River Management Office in Taiwan from 1999 to 2004, the thalweg of Da-Chia River in the reach near the Houfeng Bridge is generally located on the northern side of the river (right bank). The river approaches the bridge at an angle of 15° to the longitudinal axis of the bridge.

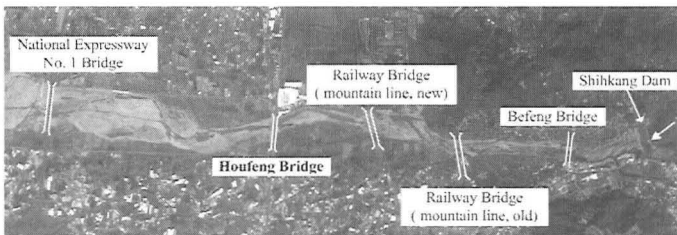


Figure 3. Aerial photograph around Houfeng Bridge in 2007. Flow is from right to left. (courtesy of the Shihkang Dam Water Resources Management)

Bed samples obtained in the vicinity of the Houfeng Bridge has a median size (D_{50}) of about 80 mm and a geometric standard deviation (σ_g) of about 6.32. This shows that the bed sediments are small cobbles and the sediment particles are poorly sorted.

AUXILIARY MAN-MADE ENGINEERING STRUCTURES

A search through the records in engineering works carried out around the Houfeng Bridge reveals that three important auxiliary man-made structures were constructed before the demise of the bridge in September 2008. They are (1) an encased pipeline; (2) a tetrahedron type grade-control structure; and (3) a steel-fence type grade-control structure. The first one was located upstream while the others were located downstream of the bridge (see Figure 4). It is envisaged that items (1) and (3) have important influence in contributing to the eventual collapse of the bridge. Table 1 summarizes all pertinent information on the bridge geometry, channel geometry, and the bed material relevant to the Houfeng Bridge.

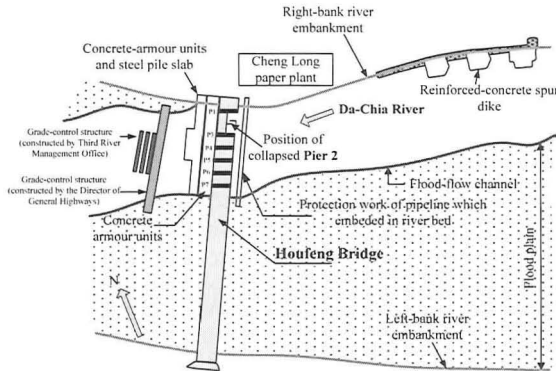


Figure 4. Schematic site plan of the Houfeng Bridge near-field at failure

Table 1. Site description of Houfeng Bridge

Bridge Geometry	Cylindrical pier, caisson
Bridge length (m)	640
Number of piers	14
Bridge span (m)	40
Cylindrical pier	2
Caisson width	4
Drainage area (km ²)	1,204
Channel geometry	Braided channel, curved reach
Centre-line bend radius (km)	2.78
Channel slope	1/90
Bed material	Gravel, cobble
D_{50} (mm)	80
D_{90} (mm)	230
Standard deviation of particles, σ_g	6.32

MAJOR EVENTS AND CAUSES OF THE COLLAPSE

An extremely important factor that has significantly contributed to the collapse of Houfeng Bridge is the considerable bed degradation due to general scouring of the Da-Chia River. It is interesting to note that the Chi-Chi Earthquake, which took place on September 21, 1999, had a direct influence on long-term riverbed degradation, which in turn may have significantly contributed to the collapse of the bridge. The destructive Chi-Chi Earthquake with a magnitude of 7.3 on the Richter scale occurred in the center of Taiwan. The death toll in this catastrophe reached more than 2,000. Figure 5 shows variations of the longitudinal riverbed profiles of the Da-Chia River from 1993 to 2008.

The bed level has reached a quasi-equilibrium condition over the period from 1993 to 1998. In 1999, nine years after the opening of the Houfeng Bridge, the Chi-Chi Earthquake occurred, resulting in the lifting of the surrounding ground levels along a fault line just upstream of the Shihkang Dam to create an average 10-m drop in the Da-Chia River. Over the subsequent years from 1999 to 2008, the Da-Chia River

responded to this abrupt lifting through significant bed degradation in the river reach downstream of the dam. Coupled with this scour potential, the flood flows associated with typhoons have contributed to extensive general scour of the river. The combined effect of both these occurrences leads to an average lowering rate of the river bed at the Houfeng Bridge of about 0.5 m/year or a total of 4.51 m over the past 9 years. In the next section, quantitative evaluation of scour depths relating to different scour processes will be given to confirm our hypotheses.

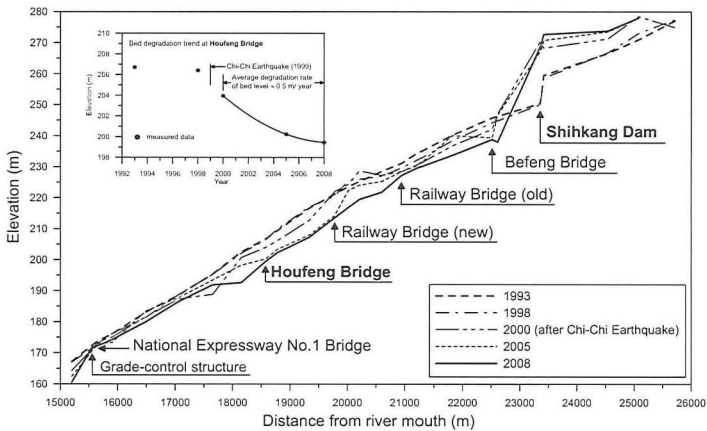


Figure 5. Variations of longitudinal riverbed profiles for Da-Chia River

ANALYSIS OF DIFFERENT SCOUR COMPONENTS

Field evidences and thorough analysis of available data associated with the Houfeng Bridge reveal that failure of the bridge likely is due to undermining of the caisson connected to Pier 2 (P2). Hence, it is reasonable to surmise that the total depth of scour at this location may have approached the embedment depth of the caisson, which is at 191.27 m MSL (the caisson top level = 205.27 m MSL; the depth of caisson = 14 m). Examinations of all the events before and during the flood associated with Typhoon Sinlaku show that the total scour depth is a combination of the following scour depths: (1) general scour, both long-term and short-term; (2) contraction scour depth; (3) bend scour depth; (4) pier scour depth; and (5) impinging jet scour depth. The overall effect of each of these inter-related scour processes is a very complex phenomenon. So far, interactions of the processes of general scour, contraction scour, bend scour, local scour and impinging jet scour are unknown. Federal Highway Administration guidelines (Richardson and Davis, 1995) and bridge scour texts such as Melville and Coleman (2000) recommended that all the components of scour depths can be assumed to be independent. Based on this assumption, the total depth of scour at the bridge is then simply the sum of all the scour components to provide a conservative estimate. In this section of the paper, an attempt is made to compute the total depth of scour at the pier by independently evaluating

each of these scour depths using published formulas.

General scour

General scour, which occurs irrespective of the presence of a hydraulic structure, such as a pier, is defined as the continuous lowering of the river bed with time. It may be in the form of long-term (bed degradation) or short-term general scour. The former occurs over a considerably length of time, normally in the order of several years or longer, while the latter occurs during floods (Melville and Coleman, 2000). Measured field data show that the Houfeng Bridge experienced both these types of scour.

Long-term general scour (bed degradation)

Table 2 shows the extent of bed degradation downstream of the Shihkang Dam before and after the Chi-Chi Earthquake. Figure 6 shows how this severe bed degradation has caused the caisson at Pier 2 to be protruded above the mean river bed level, which was at 199.45 m MSL in 2008. The field data in Table 2 also show how the bed degradation rate of Da-Chia River is significantly affected by the Chi-Chi Earthquake. For example, the respective rates of degradation are 0.93 versus 0.11 m/year at the new Railway Bridge and 0.50 versus 0.05 m/year at the Houfeng Bridge, i.e. the post-earthquake bed degradation rate being close to one order of magnitude larger than its pre-earthquake counterpart.

The extent of bed degradation regarded as long-term general scour depth of 4.51 m at the Houfeng Bridge from 1999 to 2008 is not directly related to Typhoon Sinlaku. It is a response of the river to the cumulative effect of the Chi-Chi Earthquake and all preceding Typhoon-induced floods. Notwithstanding the severity of this effect, it still is unable to undermine the caisson attached to Pier 2 of the Houfeng Bridge. Its final demise must therefore be related to the Typhoon Sinlaku-induced flood on September 14, 2008. In the next section, each of the scour components is computed using the available information and actual flood data.

Table 2. Bed degradation downstream of the Shihkang Dam in Da-Chia River after the Chi-Chi Earthquake from 1999 to 2008

Site	Distance to Shihkang Dam (km)	Degradation between 1993 to 1999 (m)	Degradation between 1999 to 2008 (m)	Average degradation Rate between 1993 to 1999 (m/yr)	Average degradation Rate between 1999 to 2008 (m/yr)
Befeng Bridge	0.84	1.55 (245.75-244.2)	3.31 (242.15-239.38)	0.26	0.37
Railway Bridge (old)	2.41	1.45 (231.1-229.65)	1.28 (228.52-228.47)	0.24	0.14
Railway Bridge (new)	3.58	0.64 (221.21-220.57)	8.35 (221.97-214.32)	0.11	0.93
Houfeng Bridge	4.78	0.31 (206.72-206.41)	4.51 (203.96-200.24)	0.05	0.50
National Expressway No.1 Bridge	7.70	0.86 (173.78-172.92)	1.31 (172.78-172.13)	0.14	0.15

Note: The above data were reported by the Water Resources Planning Institute (2005).

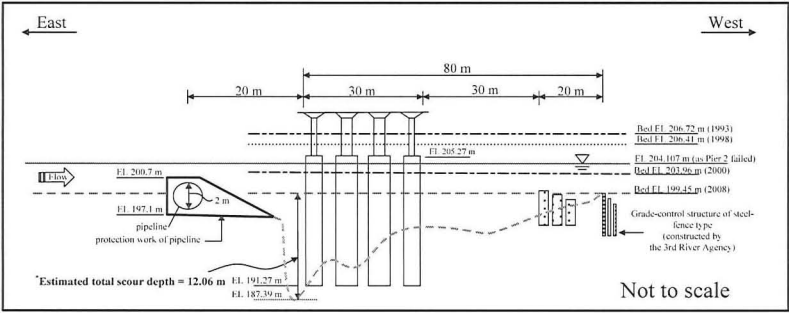


Figure 6. Schematic diagram for the quantitative analysis of scour depth

Evaluation of scour depth induced by typhoon sinlaku

Melville and Coleman (2000) proposed a methodology to calculate scour depths quantitatively. In this paper, their method is adopted and modified as shown in Figure 7 to evaluate the scour depth. Table 3 summarizes all relevant data needed for the scour calculation.

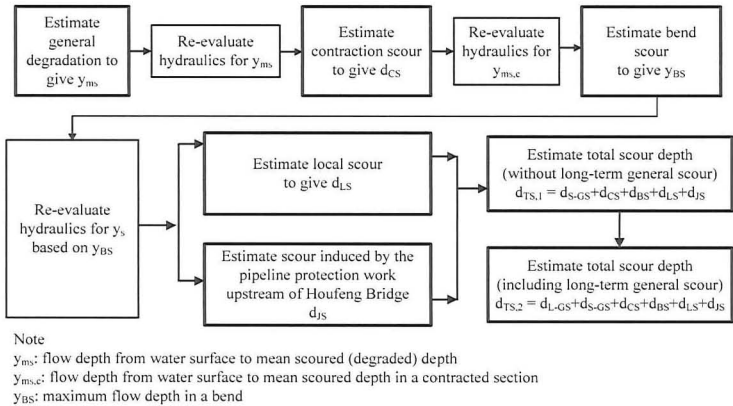


Figure 7. Methodology for quantitative prediction of scour depth (modification of method proposed by Melville and Coleman, 2000)

Short-term general scour

The short-term general scour depth is assumed to be directly related to the peak flood associated with Typhoon Sinlaku on Sept. 14, 2008. Based on the peak flow condition, the average scoured flow depth of 5.63 m is calculated using the relationships proposed by Lacey (1930), Blench (1969) and Maza Alvarez and Echavarria Alfaro (1973). The value based on Lacey's (1930) method was

disregarded because the y_{ms} -value is less than the upstream unscoured flow depth y_u , and the size of the sediment particles of the Da-Chia River is markedly higher than that recommended by this approach.

Table 3. Basic data for the scour analysis of Houfeng Bridge

Category	Basic data	Typhoon Sinlaku (Sept. 14, 2008)
Channel	Channel centre-line radius of curvature r_c (m)	2870
	Channel slope S_b	0.011
	Channel width W (m)	230
Flow	Flow discharge Q (m ³ /s)	4230
	Average upstream un-scoured flow depth y_u (m)	4.657
	flood peak duration t (days)	0.0625
Bed material	Median size d_{50} (mm)	80
	Geometric standard deviation σ_g	6.32
	Specific gravity G_s	2.65
Pier	Pier width b (m)	2
	Caisson width b^* (m)	4
	Caisson depth L_c (m)	14
	Angle of attack θ (degree)	15
Protection work of pipeline	Downstream slope of protection work S_m (V:H)	0.31
Grade-control structure	Length of grade-control structure L_g (m)	81
Elevation	Water stage as pier failed EL_{wrf} (m)	204.107
	Caisson top level (in main channel) EL_c (m)	205.27
	Caisson toe level EL_{ct} (m)	191.27
	Top level of pipeline protection work EL_p (m)	200.70
	Flood-level warning 1 EL_{fwt} (m)	204.27

Contraction scour

Recently, Dey and Raikar (2005) investigated the long contraction scour depth and the bed variation in the streamwise direction under the clear-water scour conditions. Based on Laursen's (1962) equation and Dey and Raikar's (2005) experimental results, the long contraction scour depth and the ratio of the contraction scour depth at Pier 2 to equilibrium contraction scour depth $d_{sc}/d_{sc,e}$ are estimated to be 2.08 m and 0.25, respectively. Based on this calculation, the contraction scour depth at Pier 2 is found to be 0.52 m.

Bend scour

Computation of bend scour was conducted using three different approaches: Chatley (1931); Thorne (1988); and a simple graphical solution proposed by Lacey (1930). The results from the calculation conducted using the methods of Thorne (1988), Lacey (1930), and Chatley (1931) are 7.56 m, 7.66 m and 5.35 m, respectively; they yield an average maximum bend scour depth of 6.86 m (y_{BS}) or 197.25 m MSL.

Local pier and jet scour

The scour relationship proposed by Melville and Coleman (2000) was used to calculate the local pier scour depth, while the jet scour formula proposed by Bormann and Julien (1991) was used to compute the jet scour depth induced by the upstream

encased pipeline. Table 4 summarizes all the computed scour depths in the study. First of all, the results show that the total depth of scour (without long-term general scour) is 12.06 m. With the addition of the long-term general scour depth of 4.51 m over the past 9 years since the Chi-Chi Earthquake, the total scour depth at Pier 2 of the Houfeng Bridge (P2) is a whopping 16.57 m! This value confirms the hypothesis that undermining of the caisson at Pier 2 is completely plausible since it is 3.88 m below the bottom of the caisson level. This undermining is, to a large extent, confirmed by field evidences at the bridge site after the flood.

Considering only the total scour depth without contribution from long-term general scouring, the results reveal that local pier-scour contributes 53% of the overall scouring at the pier-caisson, while the short-term general scour (8%), contraction scour (4%), bend scour (6%) and impinging jet scour (29%) combine to contribute the remaining 47%. The data also show that the impinging jet generated by the encased pipeline had contributed significantly to the overall scour at the pier. This issue must be addressed if the Houfeng Bridge were to be re-built at its present location.

Table 4. Comparison of scour components calculated by the proposed methodology

Scour components			Ratio of scour components to total scour			
			without bed degradation		including bed degradation	
Long-term general scour depth	$d_{L-GS}(m)$	4.51	—	—	$d_{L-GS} / d_{TS,2}$	0.27
Short-term general scour depth	$d_{S-GS}(m)$	0.98	$d_{S-GS} / d_{TS,1}$	0.08	$d_{S-GS} / d_{TS,2}$	0.06
Contraction scour depth	$d_{CS}(m)$	0.52	$d_{CS} / d_{TS,1}$	0.04	$d_{CS} / d_{TS,2}$	0.03
Bend scour depth	$d_{BS}(m)$	0.70	$d_{BS} / d_{TS,1}$	0.06	$d_{BS} / d_{TS,2}$	0.04
Local scour depth	$d_{LS}(m)$	6.34	$d_{LS} / d_{TS,1}$	0.53	$d_{LS} / d_{TS,2}$	0.38
Jet scour depth	$d_{JS}(m)$	3.52	$d_{JS} / d_{TS,1}$	0.29	$d_{JS} / d_{TS,2}$	0.21
Total scour depth without long-term general scour depth	$d_{TS,1}(m)$	12.06	$d_{TS,1} / d_{TS,1}$	1.00	$d_{TS,1} / d_{TS,2}$	1.0

Note: Bed degradation from 1999 to 2008 in the vicinity of Houfeng Bridge, d_{L-GS} = 4.51 m

$$d_{TS,1} = d_{S-GS} + d_{CS} + d_{BS} + d_{LS} + d_{JS} \quad (\text{without long-term general scour})$$

$$d_{TS,2} = d_{L-GS} + d_{S-GS} + d_{CS} + d_{BS} + d_{LS} + d_{JS} \quad (\text{including the long-term general scour})$$

Additionally, if long-term general scour (bed degradation = 4.51 m) from 1999 to 2008 are included in the consideration, the total scour depth ($d_{TS,2}$) at Pier 2 is 16.56 m. About 27% of the total scour depth is attributed to long-term general scour of the Da-Chia River around the Houfeng Bridge, while the short-term general scour (6%), contraction scour (3%), bend scour (4%), local pier-scour (38%), and the impinging jet scour (21%), combine to contribute the remaining 73%.

CONCLUSIONS AND SUGGESTIONS

Based on the case study of the Houfeng Bridge failure, the following conclusions and suggestions can be drawn:

- 1. The destructive Chi-Chi Earthquake (7.3 on the Richter scale) has a significant long-term effect on bed degradation downstream of the Shihkang Dam.

According to the analysis with the consideration of long-term general scour caused by the Chi-Chi Earthquake in the present study, the calculated results reveal that about 27% of the total scour depth is attributed to long-term general scour of the Da-Chia River around the Houfeng Bridge. Both long-term general scour and the impinging jet generated by the encased pipeline have contributed significantly to the overall scour at the pier.

2. Proper precautions need to be taken if damage to or failure of the downstream bridges is identified. The failure of the Houfeng Bridge also highlights the potential risk associated with human interventions, e.g., construction of the encased pipeline or grade-control structures to overall bridge stability.
3. With proper modifications, quantitative analysis of the Houfeng Bridge using Melville and Coleman's (2000) method provides reasonable estimates for various scour components in such a complex inter-related scour phenomenon. It implies that before the construction of a new bridge or the rebuilding of an old bridge, one can use appropriate methodology and formulas to evaluate the scour potential and improve bridge design.

REFERENCES

- Blench, T. (1969). *Mobile-bed fluviology*, University of Alberta, Edmonton, Canada.
- Bormann, N. E. and Julien, P. Y. (1991). "Scour downstream of grade-control structures." *J. Hydraul. Eng.*, ASCE, 117(5), 579-594.
- Chatley, H. (1931). "Curvature effects in open channels." *Engineering*, London, England, Vol. 131.
- Dey, S. and Raikar, R. V. (2005). "Scour in long contractions." *J. Hydraul. Eng.*, ASCE, 131(12), 1036-1049.
- Lacey, G. (1930). "Stable channels in alluvium," Paper 4736, Minutes of the Proc., Institution of Civil Engineers, Vol. 229, William Clowes and Sons Ltd., London, Great Britain, 259-292.
- Laursen, E.M. (1962). "Scour at bridge crossings." *Transactions, A.S.C.E.*, Vol. 127, Part 1, 116-179.
- Maza Alvarez, J. A. and Echavarria Alfaro, F. J. (1973). "Contribution to the study of general scour," Proc., International Symposium on River Mechanics, I.A.H.R., Bangkok, Thailand, 795-803.
- Melville, B. W., and Coleman, S. E. (2000), *Bridge Scour*, Water Resources Publication, Littleton, Colorado, USA.
- Richardson, E. V., and Davis, S. R. (1995). "Evaluating scour at bridges." *Federal highway Administration Rep. No. FHWA-IP-90-017, Hydr. Engrg. Circular No. 18*, 3rd Ed., Ofc. Of Technol. Applications, HTA-22, Washington, D. C.
- Thorne, C. R. (1988). "Bank processes on the Red River between Index, Arkansas, and Shreveport, Louisiana." *Final Rep. to the U.S. Army Eur. Res. Ofc., Contract No. DAJ445-88-C0018*, Dept. of Geography, Queen Mary College, London.

Submerged-Flow Bridge Scour under Maximum Clear-Water Conditions (I): Experiment

J. Guo¹, K. Kerenyi², J. E. Pagan-Ortiz², K. Flora³, and B. Afzal¹

¹Dept. of Civil Engineering, University of Nebraska-Lincoln, PKI 204D, 1110 67th ST, Omaha, NE 68182; PH (402)-554-3873; email: jguo2@unl.edu

²Office of Infrastructure R&D, Turner-Fairbank Highway Research Center, Federal Highway Administration, 6300 Georgetown Pike, McLean, VA 22101.

³Hydraulics Branch, Structure Maintenance and Investigation, California Dept. of Transportation, P.O. Box 942873, Sacramento, CA 94273-0001.

ABSTRACT

Submerged-flow bridge scour at clear water threshold condition has been studied experimentally. The experiments were conducted in a self contained recirculating tilting flume where two uniform sediment sizes and two model bridge decks with eight different inundation levels were tested for scour morphology. The experiments showed that the longitudinal scour profiles before the maximum scour depth can be approximated by a 2-D similarity profile, while the scour morphology after the maximum scour depth is 3-D. Finally, two empirical similarity equations for scour profiles were proposed for design purpose, and the collected data set could be used for analytical studies of bridge scour.

INTRODUCTION

Bridges are a vital component of the transportation network. Evaluating their stability and structural response to hydrodynamic loading is critical to highway safety in design phase and after flooding. The studies of bridge scour usually assume an unsubmerged bridge flow, but the flow regime can switch to submerged flow when the downstream edge of a bridge deck is partially or totally inundated during large flood events. For example, a submerged bridge flow occurred in the Cedar River in Iowa after heavy rains in June 2008 (Figure 1), which interrupted traffic on I-80. Submerged flow most likely creates a severe scouring capability because to pass a given discharge, the flow under a bridge can only scour the channel bed to dissipate its energy.

Investigations on submerged-flow bridge scour have been reported by Arneson and Abt (1998), Umbrell et al. (1998), and Lyn (2008). Arneson and Abt (1998) did a series of flume tests and proposed the following regression equation



Figure 1: Bridge-submerged flow in Iowa in 2008

$$\frac{y_s}{h_u} = -0.93 + 0.23 \left(\frac{h_u}{h_b} \right) + 0.82 \left(\frac{y_s + h_b}{h_u} \right) + 0.03 \left(\frac{V_b}{V_{uc}} \right) \quad (1)$$

where y_s = maximum equilibrium scour depth, h_u = depth of approach flow before scour, h_b = vertical bridge opening height before scour, V_b = velocity through a bridge before scour, and V_{uc} = upstream critical approach velocity defined by

$$V_{uc} = 1.52 \sqrt{g(s-1)d_{50}} \left(\frac{h_u}{d_{50}} \right)^{1/6} \quad (2)$$

where g = gravitational acceleration, s = specific gravity of sediment, and d_{50} = median diameter of bed materials. Although Eq. (1) has been adopted in the FHWA manual (Richardson and Davis 2001), it suffers from a spurious correlation where both sides of the equation include y_s/h_u . In the meanwhile, Umbrell et al. (1998) also conducted a series of flume tests in the FHWA J. Sterling Jones Hydraulics Laboratory. Using the mass conservation law and assuming that the velocity under a bridge at scour equilibrium is equal to the critical velocity of the upstream flow, they presented the following equation

$$\frac{y_s + h_b}{h_u} = \frac{V_u}{V_{uc}} \left(1 - \frac{w}{h_u} \right) \quad (3)$$

where V_u = approach flow velocity that is less than or equal to the critical velocity V_{uc} , and w = depth of weir flow when flow overtops a bridge deck and $w = 0$ for partially submerged flow. By comparing Eq. (3) with their flume data, Umbrell et al. modified Eq. (3) as follows

$$\frac{y_s + h_b}{h_u} = 1.102 \left[\frac{V_u}{V_{uc}} \left(1 - \frac{w}{h_u} \right) \right]^{0.603} \quad (4)$$

where the critical velocity is estimated by Eq. (2) except that the coefficient, 1.52, is replaced by 1.58. Eq. (3) or (4) was based on the mass conservation law, but the dynamic law of momentum or energy was overlooked, which weakens the foundation of predictions because scour is a dynamic process. Besides, Umbrell's tests were run only for 3.5 hours which is not enough time for equilibrium scour to develop although they extrapolated their results to equilibrium states. The latest study was reported by Lyn (2008), who reanalyzed Arneson's and Umbrell's data sets and proposed the following power law

$$\frac{y_s}{h_u} = \min \left[0.105 \left(\frac{V_b}{V_{uc}} \right)^{2.95}, 0.5 \right] \quad (5)$$

where V_b and V_{uc} are the same as in Eq. (1). Lyn's equation is empirical, but he identified the spurious regression of Eq. (1) and the low quality of Umbrell's data.

In brief, the two existing data sets are insufficient to develop a general description of submerged-flow scour, especially for a scour profile. Moreover, all the existing methods lack understanding of the physical mechanism of submerged flow scour. Therefore, the objectives of this study were to collect a detailed data set of submerged-flow scour at a model bridge in a flume, and to develop a theoretical

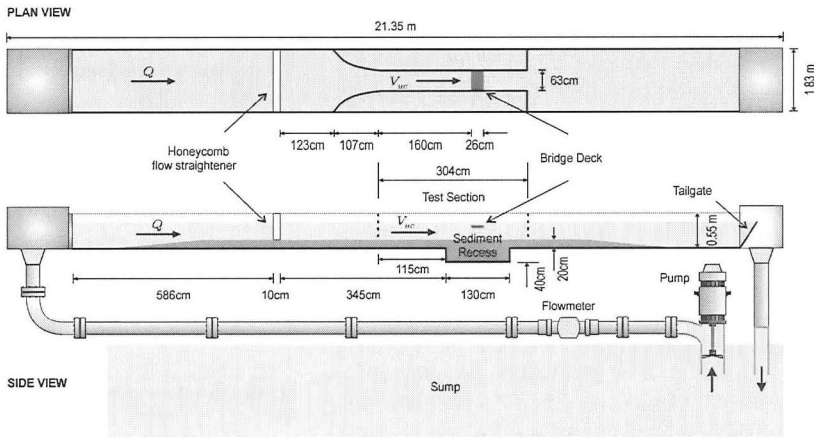


Figure 2: Experimental flume

model for the maximum scour depth under threshold clear water conditions. This paper emphasizes the experimental study that includes the experimental setup, results, discussion, and conclusions. A theoretical model for equilibrium scour depth is discussed in a separate paper.

EXPERIMENTAL SETUP

The experiments aimed to understand the flow and scour phenomena of submerged bridge flow by collecting scour data at a model bridge in a flume under controlled flow conditions. Specifically, the experiments tried to answer how sediment size, bridge girders and bridge inundation affect the longitudinal scour profile and maximum scour depth of submerged bridge flow.

The experiments were conducted in the FHWA J. Sterling Jones Hydraulics Laboratory, located at the Turner-Fairbank Highway Research Center in McLean, VA. The experimental flume (Figure 2) had a length of 21.35 m, width of 1.83 m, and depth of 0.55 m, with clear sides and a stainless steel bottom whose slope was about horizontal. In the middle of the flume was installed a test section that consists of a narrowed channel with length of 3.04 m and width of 0.63 m, a 40-cm sediment recess, and a model bridge above the recess. A honeycomb flow straightener and a trumpet-shaped inlet were carefully designed to smoothly guide the flow into the test channel. The water in the flume was supplied by a circulation system with a sump of 210 m³ and a pump with capacity of 0.3 m³/s; the depth of flow was controlled by a tailgate; and the experimental discharge was controlled by a LabView program and checked by an electromagnetic flowmeter.

To test the effect of sediment size on scour morphology, two uniform sands (the coefficient of gradation $C_g < 1.5$, and the coefficient of uniformity $C_u < 5$)

were used in the experiments: a median diameter $d_{50} = 1.14$ mm with $C_g = 1.45$ and $C_u = 1.77$, and a median diameter $d_{50} = 2.18$ mm with $C_g = 1.35$ and $C_u = 1.59$. The effect of bridge girders was examined by a three-girder deck and a six-girder deck (Figure 3). Both decks had rails at the edges (Figure 3c) that could pass over-flow on the deck surface whose elevation was adjustable, permitting the deck to have eight different inundation levels. A LabView program was used to control an automated flume carriage that was equipped with MicroADV for records of velocities and a laser distance sensor for depths of flow and scour. The MicroADV (SonTek 1997) measures 3-D flow in a cylindrical sampling volume of 4.5 mm in diameter and 5.6 mm in height with a small sampling volume located about 5 cm from the probe; the range of velocity measurements is from 1 mm/s to 2.5 m/s. In this study, velocity measurements were taken in a horizontal plane located at a cross-section 22 cm upstream of the bridge. The LabView program was set to read the MicroADV probe and the laser distance sensor for 60 seconds at a scan rate of 25 Hz. According to the user's manual, the MicroADV has an accuracy of $\pm 1\%$, and the laser distance sensor has an accuracy of ± 0.2 mm.

Two discharges were applied in the experiments. They were determined by a critical velocity and the flow cross-section in the test channel that had a width of 0.63 m and a constant flow depth of 0.25 m. The critical velocity was preliminarily calculated by Neill's (1973) equation and adjusted by a trial-and-error method. The critical velocity of sediment $d_{50} = 1.14$ mm was approximately 0.41 m/s and the corresponding experimental discharge Q was 0.0646 m³/s. The critical velocity of sediment $d_{50} = 2.18$ mm was approximately 0.53 m/s and the corresponding experimental discharge was 0.0835 m³/s. The experimental conditions are summarized in Table 1 where the Froude and Reynolds numbers mean the approach flows were subcritical turbulent flows.

The experiments proceeded as follows: 1) Filled the sediment recess with sand and evenly distributed sand on the bottom of the flume until the depth of sand was 60 cm in the sediment recess and 20 cm in the test channel. 2) Installed a bridge deck at a designated elevation and positioned it perpendicular to the direction of flow. 3) Pumped water gradually from the sump to the flume to the experimental discharge that was checked with the electromagnetic flowmeter. 4) Ran each test for 36-48 hours and monitored scour processes by grades in a clear side wall; an equilibrium state was attained when scour changes at a reference point were less than 1 mm for three continuous hours. 5) Gradually emptied water from the flume and scanned the 3-D scour morphology using the laser distance sensor with a grid size of 5 cm \times 5 cm.

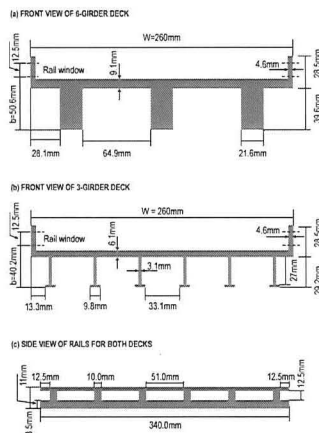


Figure 3: Decks of bridge models

Table 1: Test conditions of approach flow, bridge deck and sediment

Approach flow	3-girder deck	6-girder deck
$V_{uc} = 0.41$ m/s	$d_{50} = 1.14$ mm	$d_{50} = 1.14$ mm
$Q = 64.6$ l/s	$C_g = 1.45, C_u = 1.77$	$C_g = 1.45, C_u = 1.77$
$R_h = 13.9$ cm	$h_b = (21.0, 19.5,$	$h_b = (22.0, 20.5,$
$Re = 5.7 \times 10^4$	$18.0, 16.5, 15.0,$	$19.0, 17.5, 16.0,$
$Fr = 0.17$	$13.5, 12.0, 10.5)$ cm	$14.5, 13.0, 11.5)$ cm
$Q = 83.5$ l/s		$d_{50} = 2.18$ mm
$R_h = 13.9$ cm		$C_g = 1.35, C_u = 1.59$
$V_{uc} = 0.53$ m/s		$h_b = (22.0, 20.5, 19.0,$
$Re = 7.37 \times 10^4$		$17.5, 16.0, 14.5,$
$Fr = 0.22$		$13.0, 11.5)$ cm

Note: $h_u = 0.25$ m, $Fr = V_{uc}/\sqrt{gh_u}$, $Re = R_h V_{uc}/\nu$ where R_h = hydraulic radius, and, ν = kinematic viscosity of water.

RESULTS

The results include the records of 3-D scour morphology, the width-averaged 2-D longitudinal scour profiles, and the width-averaged maximum scour depths. A representative 3-D scour morphology is shown in Figure 4 that was measured for a test of six-girder deck under conditions $V_{uc} = 0.41$ m/s, $h_b =$

17.5 cm and $d_{50} = 1.14$ mm. The width-averaged longitudinal scour profiles of 26 tests are plotted in Figure 5 where $x = 0$ is at the maximum scour point that is 4 cm from the downstream deck edge, and $y = 0$ is at the channel bed before scour. The most important results, the width-averaged maximum scour depths, are shown in Figure 5 and will be detailed in Guo et al. (2010).

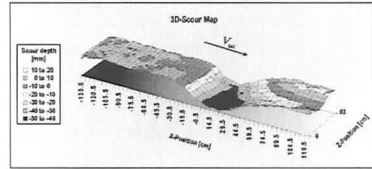


Figure 4: A representative of 3-D scour

DISCUSSION

Figure 4 shows that the scour morphology before the maximum point is approximately 2-D, after the maximum scour point it is 3-D. Furthermore, it is found that the 2-D scour morphology is subjected to pressurized flow while the 3-D scour morphology corresponds to free surface flow where the flow just exits the bridge, as shown in Figure 5, which plots 26 measured width-averaged longitudinal scour profiles. From Figure 5 one can see that: (1) The measured data are reproducible, as shown in subplot (a) where the data of two tests with $h_b = 15$ cm almost collapse into a single curve; similarly, a reproduction for two tests with $h_b = 20.5$ cm in subplot (b) can also be found before the maximum

scour point, the difference after the maximum scour point is due to the effect of free surface. (2) The longitudinal scour profiles are bell-shaped curves, but not symmetrical because the eroded materials deposit approximately two to three times the deck width downstream of the bridge. (3) The scour decreases with increasing sediment size, though the approach velocity in subplot (c) is larger than that in subplot (b). (4) The number of bridge girders has little effect on scour, as shown in subplots (a) and (b), but further test of this hypothesis is needed later since the values of h_b in the two plots are not the same. (5) The scour increases as bridge opening height, h_b , decreases, which means the scour increases with deck inundation level, $h_u - h_b$. (6) The maximum scour point occurs at 15% of bridge width (or 4 cm for the present experiments) to the downstream bridge edge.

Moreover, by looking at all the profiles in Figure 5, it is hypothesized that a similarity profile may exist for the 2-D profiles before the maximum scour point by scaling the horizontal length, x , with the deck width, W , and the local scour depth, y , with the maximum equilibrium scour value, y_s . This hypothesis is tested in Figure 6 (where the shallowest scour profile in Figure 5c is excluded because of large relative measurement errors), which confirms the similarity for $x \leq 0$. A least-squares curve-fitting process with MatLab gives a mean similarity equation

$$\frac{y}{y_s} = -\exp\left(-1.1 \left|\frac{x}{W}\right|^{2.41}\right) \quad (6)$$

where $x \leq 0$. The corresponding correlation coefficient is $R^2 = 0.995$ and the standard deviation is $\sigma_1 = 0.032$, which implies that 68% of the data can be described by Eq. (6) with an error of ± 0.032 , and 95% of the data with an error of ± 0.064 . Accordingly, the scour depth at the upstream edge of a bridge deck where $x/W = -0.846$ is approximately

$$\frac{y}{y_s} = -0.479 \pm 0.064 \quad (7)$$

with 95% confidence interval. Eq. (7) may be used for field scour evaluation. Considering that a significant scour starts at $y/y_s = -0.1$, from Eq. (6) and considering 95% confidence interval the x -coordinate of the initiation of scour is between $-1.58 \leq x/W \leq -1.23$.

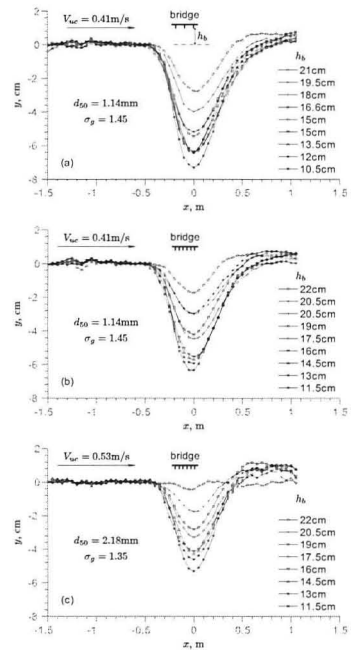


Figure 5: Measured width-averaged longitudinal scour profiles

For the 3-D profiles where $x > 0$ in Figure 6, a similarity profile does not exist, which results from the effect of free surface at the downstream of bridge. A mean profile equation for $x > 0$ does not have any meaning in practice. Thus, only a lower envelope equation is proposed for engineering design

$$\frac{y}{y_s} = -\exp\left[-\frac{1}{3}\left(\frac{x}{W}\right)^2\right] \quad (8)$$

which is plotted in Figure 6 and denoted by the dashed line. Note that although the width of deck in the experiments was constant, it was the only length in the flow direction so that it is natural to be the horizontal length scale. It is expected that Eqs. (6)-(8) are valid for similar bridge decks that are neither very thin like a sluice gate nor very wide like a water tunnel where a uniform scour profile may be developed after an entrance region.

Briefly, the horizontal scour range of a submerged flow depends on the width of bridge deck, but the design of a scour profile by Eqs. (6) and (8) needs the maximum scour depth y_s , which may be calculated by the methods reviewed in the introduction. Comparisons between the existing methods and the maximum scour depths in Figure 5 are plotted in Figure 7, which shows that: (1) the Arneson and Abt method has an adverse tendency with the test data, which means the functional structure of the equation is not correct; (2) the Umbrell et al. method, in general, agrees with the present data, in particular for sediment $d_{50} = 1.14\text{mm}$; and (3) the Lyn method underestimates most of the present data. For a better estimation of y_s , a theoretical model, based on the mass and energy conservations, will be proposed in Guo et al. (2010).

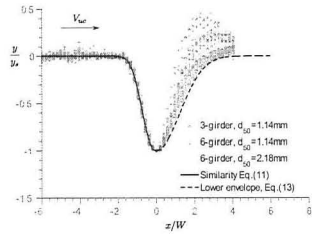


Figure 6: Test of similarity of hypothesis

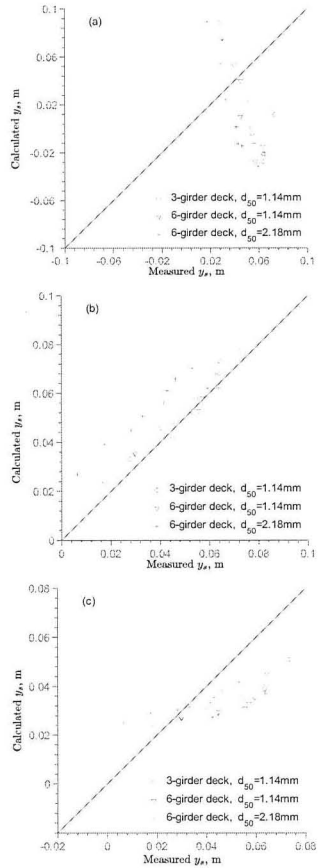


Figure 7: Comparison of existing methods with measured data

CONCLUSIONS

The experiments showed that under threshold clear water conditions: (1) a similarity longitudinal scour profile, Eq. (6), for submerged flows exists before the maximum scour point that is approximately 15% of deck width to the downstream bridge edge; (2) after the maximum scour point, scour morphology is 3-D and the lower envelope of scour can be empirically described by Eq. (8); (3) the maximum scour depth increases with deck inundation level, but decreases with increasing sediment size; and (4) the maximum scour depth is independent of the number of deck girders.

ACKNOWLEDGMENT

This study was financially supported by the FHWA Hydraulics R&D Program with Contract No. DTFH61-04-C-00037. The writers would like to thank Mr. Oscar Berrios for running the tests and preparing some of the figures. The writers are also thankful to Mr. Bart Bergendahl at FHWA for his constructive comments and suggestions.

REFERENCES

- Arneson, L. A. (1997). "The effects of pressure flow on local scour in bridge openings." PhD Thesis, Colorado State University, Fort Collins, CO.
- Arneson, L. A., and Abt, S. R. (1998). "Vertical contraction scour at bridges with water flowing under pressure conditions." *Transportation Research Record*, 1647, 10-17.
- Guo, J., Kerenyi, K., Flora, K., and Afzal, B. (2010). "Submerged-flow bridge scour under maximum clear-water conditions (II): Theory." *5th International Conference on Scour and Erosion*, San Francisco, CA.
- Lyn, D. A. (2008). "Pressure-flow scour: a re-examination of the HEC-18 equation." *J. Hydraul. Engrg.*, 134(7), 1015-1020.
- Neill, C. R. (1973). *Guide to bridge hydraulics*, University of Toronto Press, Toronto, Canada.
- Richardson, E. V., and Davis, S. R. (2001). *Evaluation Scour at bridges*. HEC-18, FHWA-NH-01-001, 4th Ed., U.S. Dept. of Transp., Washing, D.C.
- SonTek. (1997). *Acoustic Doppler velocimeter technical documentation, version 4.0*, SonTek, San Diego.
- Umbrell, E. R., Young, G. K., Stein, S. M., and Jones, J. S. (1998). "Clear-water contraction scour under bridges in pressure flow." *J. Hydraul. Engrg.*, 124(2), 236-240.

Submerged-Flow Bridge Scour under Maximum Clear-Water Conditions (II): Theory

J. Guo¹, K. Kerenyi², J. E. Pagan-Ortiz², K. Flora³, and B. Afzal¹

¹Dept. of Civil Engineering, University of Nebraska-Lincoln, PKI 204D, 1110 67th ST, Omaha, NE 68182; PH (402)-554-3873; email: jguo2@unl.edu

²Office of Infrastructure R&D, Turner-Fairbank Highway Research Center, Federal Highway Administration, 6300 Georgetown Pike, McLean, VA 22101.

³Hydraulics Branch, Structure Maintenance and Investigation, California Dept. of Transportation, P.O. Box 942873, Sacramento, CA 94273-0001.

ABSTRACT

A theoretical model for the maximum scour depth under submerged bridge flow was proposed based on the mass and energy conservation laws as well as the recent flume experimental data. It is shown that the maximum scour depth can be described by a scour number and an inundation index. In general, for submerged flow the scour number increases with the inundation index, which is equivalent to the maximum scour depth increases with deck inundation level, decreases with increasing sediment size, and is independent of bridge girders. The proposed method is expected to be applicable to prototype flows without scaling effects since it was derived from the conservation laws. An application procedure was also suggested for bridge foundation design or field scour evaluation.

INTRODUCTION

In Guo et al. (2010), a series of flume data have been collected at the FHWA J. Sterling Jones Hydraulics Laboratory. The experimental conditions and the results are summarized in Tables 1 and 2, respectively, where V_{uc} = approach velocity at upstream of bridge, Q = experimental discharge, R_h = hydraulic radius, Re = Reynolds number, Fr = Froude number, d_{50} = median sediment size, C_g = coefficient of gradation, C_u = coefficient of uniformity, h_b = bridge opening height based on the original bed, y_s = maximum scour depth, a = block depth of bridge deck, I = inundation index, and $(h_b + y_s) / (h_b + a)$ = scour number. The experimental study showed that the horizontal scour range of a submerged flow depends on the width of bridge deck, and the design of a scour profile needs the maximum scour depth y_s , which cannot be reasonably estimated by the existing methods since the Arneson and Abt (1998) method predicted an adverse tendency with the test data, the Umbrell et al. (1998) method in general overestimated the present data, and the Lyn (2008) method underestimates most of the present data.

The purpose of this paper is to propose a theoretically based method for predicting the maximum scour depth under bridge-submerged flows. Specifically, a hypothesis based on the mass and energy conservation laws is first formulated, which is then tested with the collected data in Table 2; if the hypothesis is confirmed by the collected data, an application procedure is then presented for practical design.

Table 1: Test conditions of approach flow, bridge deck and sediment

Approach flow	3-girder deck	6-girder deck
$V_{uc} = 0.41$ m/s	$d_{50} = 1.14$ mm	$d_{50} = 1.14$ mm
$Q = 64.6$ l/s	$C_g = 1.45, C_u = 1.77$	$C_g = 1.45, C_u = 1.77$
$R_h = 13.9$ cm	$h_b = (21.0, 19.5,$	$h_b = (22.0, 20.5,$
$Re = 5.7 \times 10^4$	$18.0, 16.5, 15.0,$	$19.0, 17.5, 16.0,$
$Fr = 0.17$	$13.5, 12.0, 10.5)$ cm	$14.5, 13.0, 11.5)$ cm
$Q = 83.5$ l/s		$d_{50} = 2.18$ mm
$R_h = 13.9$ cm		$C_g = 1.35, C_u = 1.59$
$V_{uc} = 0.53$ m/s		$h_b = (22.0, 20.5, 19.0,$
$Re = 7.37 \times 10^4$		$17.5, 16.0, 14.5,$
$Fr = 0.22$		$13.0, 11.5)$ cm

Note: $h_u = 0.25$ m, $Fr = V_{uc}/\sqrt{gh_u}$, $Re = R_h V_{uc}/\nu$ where $R_h =$ hydraulic radius, and, ν = kinematic viscosity of water.

HYPOTHESIS ON MAXIMUM SCOUR DEPTH

Bridge flows are divided into three cases (Picek et al. 2007): (1) the upstream low chord of a bridge is partially submerged while the downstream low chord is unsubmerged, which is not discussed here; (2) both upstream and downstream low chords are partially submerged; and (3) a bridge is totally submerged. The last two cases are analyzed in this paper.

The problem is stated with Figure 1 where a bridge is over a steady river flow with clear water, the bridge deck is modeled with a rectangular box, V_{uc} = critical velocity of approach flow at upstream of the bridge, V_{ue} = effective velocity corresponding to the flow through the bridge, h_u = depth of the flow at the upstream of the bridge before scour, h_b = bridge opening height before scour, a = effective thickness of deck blockage where the corresponding stagnation streamline divides the flow into two parts, b = physical thickness of the deck blockage, V_{bs} =

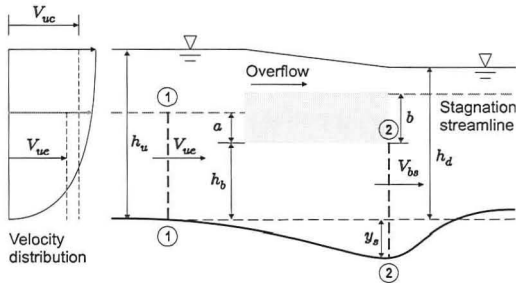


Figure 1: Sketch of definitions

Table 2: Summary of test results of maximum scour depths

Bridge opening	Measure. scour depth	Block depth	Run time	Inundate. index	Scour number	Calcul. scour depth	Error (7)-(2)
h_b , (cm)	y_s , (cm)	a , (cm)	(hrs)	I	$\frac{h_b + y_s}{h_b + a}$	y_s , (cm)	(cm)
(1)	(2)	(3)	(4)	(5)	(6)	(7)	(8)
3-girder deck with $d_{50} = 1.14$ mm, $C_g = 1.45$, $C_u = 1.77$							
21.0	2.77	4.00	36	1.53	0.95	2.76	-0.01
19.5	3.98	5.06	36	1.81	0.96	4.56	0.58
18.0	5.18	5.06	48	2.10	1.01	5.29	0.11
16.5	5.45	5.06	36	2.40	1.02	5.88	0.43
15.0	6.35	5.06	36	2.90	1.06	6.35	0.00
15.0	6.42	5.06	48	2.70	1.07	6.35	-0.07
13.5	6.41	5.06	48	3.01	1.07	6.74	0.33
12.0	6.43	5.06	48	3.33	1.08	7.03	0.60
10.5	7.31	5.06	48	3.69	1.14	7.26	-0.05
22.0	1.75	3.00	42	1.32	0.95	1.24	-0.51
6-girder deck with $d_{50} = 1.14$ mm, $C_g = 1.45$, $C_u = 1.77$							
20.5	2.99	4.02	42	1.64	0.96	3.09	0.10
20.5	2.98	4.02	42	1.64	0.96	3.09	0.11
19.0	4.23	4.02	42	1.95	1.01	3.89	-0.34
19.0	4.52	4.02	42	1.95	1.02	3.89	-0.63
17.5	4.47	4.02	42	2.26	1.02	4.54	0.07
16.0	5.55	4.02	42	2.56	1.08	5.07	-0.48
14.5	5.71	4.02	43	2.88	1.09	5.49	-0.22
13.0	5.93	4.02	48	3.21	1.11	5.82	-0.11
11.5	6.34	4.02	48	3.56	1.15	6.07	-0.27
6-girder deck with $d_{50} = 2.18$ mm, $C_g = 1.35$, $C_u = 1.59$							
20.5	1.75	4.02	42	1.27	0.91	2.16	0.41
19.0	2.83	4.02	42	1.51	0.95	2.84	0.00
17.5	3.29	4.02	42	1.74	0.97	3.44	0.15
16.0	4.14	4.02	42	1.98	1.01	3.97	-0.17
14.5	4.30	4.02	42	2.23	1.02	4.42	0.12
13.0	4.62	4.02	42	2.48	1.04	4.79	0.18
11.5	5.31	4.02	48	2.76	1.08	5.10	-0.21
7.0 ^a	6.50	4.02	48	3.78	1.23	5.64	-0.86
2.5 ^a	11.64	4.02	48	5.49	2.17	5.64	-6.00

^aExcluded in Figures 6c, 8 and 11 since the effect of the boundary layers cannot be neglected.

average velocity at equilibrium maximum scour cross-section that is close to the outlet of the bridge flow according to the present experiments, and h_d = depth of the tailwater before scour. **Find** the equilibrium submerged-flow scour depth, y_s , by considering a unit river flow.

To solve the problem, one can select a control volume consisting of cross-sections 1-1 and 2-2, the upstream stagnation streamline, the left and low faces of the bridge deck, and the scoured river bed. Applying the energy conservation law to the control volume and neglecting the friction loss (due to the short distance), one can write

$$h_u + \frac{\alpha_1 V_{ue}^2}{2g} = h_d + \frac{\alpha_2 V_{bs}^2}{2g} + K_b \frac{V_{bs}^2}{2g} \quad (1)$$

where h_u = hydraulic head at cross-section 1-1 based on the original bed, h_d = hydraulic head at cross-section 2-2, α_1 and α_2 are the energy correction factors, g = gravitational acceleration, and K_b = the bridge energy loss coefficient that is related to the difference of the upstream and downstream flow depths, $h_u - h_d$, the effective velocity, V_{ue} , and the gravitational acceleration, g . By dimensional analysis, one can assume

$$K_b = \lambda_0 \left(\frac{\sqrt{g(h_u - h_d)}}{V_{ue}} \right)^m \quad (2)$$

where λ_0 and m are two empirical parameters. Eq. (2) makes sure $K_b = 0$ when $h_u = h_d$. On the other hand, applying the mass conservation law to the control volume gives

$$(h_b + a) V_{ue} = (h_b + y_s) V_{bs} \quad (3)$$

Solving for $h_b + y_s$ from Eqs. (1)-(3) gives

$$\frac{h_b + y_s}{h_b + a} = \sqrt{\frac{\alpha_2 + \lambda_0 \left[\frac{\sqrt{g(h_u - h_d)}}{V_{ue}} \right]^m}{\alpha_1 + 2 \left[\frac{\sqrt{g(h_u - h_d)}}{V_{ue}} \right]^2}} \quad (4)$$

where the left-hand side is called a scour number. Unfortunately, the downstream flow depth h_d is usually unknown. For an approximation, it is hypothesized

$$h_u - h_d = \beta^2 (h_u - h_b) \left(\frac{h_b + a}{h_u} \right) \quad (5)$$

where β is a fitting parameter. The factor of $(h_u - h_b)$ in Eq. (5) expresses an inundation level that, take a partially submerged flow for example, increases $h_u - h_d$ (since the energy loss increases with inundation) and makes $h_u - h_d = 0$ at $h_u = h_b$. The fraction $(h_b + a)/h_u$ is introduced because $h_u - h_d$ should be independent of the upstream flow depth h_u for significant inundation while it should be 1 for partially submerged flows.

Referring to Figure 1 where the horizontal dashed line divides the approach flow into an overflow above the bridge and a pressure flow under the bridge, the unit flowrate, q_1 , under the bridge in both cases can be estimated by

$$q_1 = h_u V_{uc} \left(\frac{h_b + a}{h_u} \right)^{n+1} \quad (6)$$

where for approximately uniform flows of the present experiments $n = 0$ and for fully developed turbulent flows $n = 1/7$, and a = effective thickness of deck blockage. Theoretically, the value of a can be determined by a Bernoulli's equation in the dividing streamline if the fluid is ideal,

$$a = b - \frac{V_a^2}{2g} \quad (7)$$

where b = physical thickness of deck blockage, and V_a = approach velocity in the dividing streamline. Practically, Eq. (7) gives a small value of a because of the neglect of fluid viscosity. Nevertheless, for a thin deck with overhang shown in Figure 5 of Guo et al. (2010), the overhang forces the dividing streamline approximately at the elevation of the deck surface. Therefore, this study assumes

$$a = b \quad (8)$$

for totally submerged flow. Obviously, for partially submerged flow one has

$$a = h_u - h_b \quad (9)$$

For convenience, Eqs. (8) and (9) can be combined by

$$a = \min(h_u - h_b, b) \quad (10)$$

Considering Eq. (6), one has the effective velocity V_{ue} for cross-section 1-1

$$V_{ue} = \frac{q_1}{h_b + a} = V_{uc} \left(\frac{h_b + a}{h_u} \right)^n \quad (11)$$

Substituting Eqs. (5) and (11) into the brackets of Eq. (4) gives

$$\frac{\sqrt{g(h_u - h_d)}}{V_{ue}} = \beta \frac{\sqrt{g(h_u - h_b)}}{V_{uc}} \left(\frac{h_u}{h_b + a} \right)^{n-1/2} \quad (12)$$

Defining an inundation index

$$I = \frac{\sqrt{g(h_u - h_b)}}{V_{uc}} \left(\frac{h_u}{h_b + a} \right)^{n-1/2} \quad (13)$$

and substituting Eq. (12) into Eq. (4) gives

$$\frac{h_b + y_s}{h_b + a} = \sqrt{\frac{1 + \lambda_1 I^m}{1 + \lambda_2 I^2}} \quad (14)$$

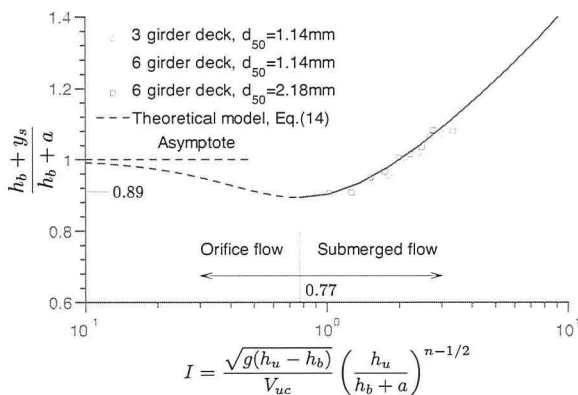


Figure 2: Test of hypothesis on maximum scour depth

which is the hypothesis of the maximum scour depth, where the energy correction factors α_1 and α_2 have been taken to be 1, the deviation due to this assumption can be combined to the model parameters $\lambda_1 (= \lambda_0 \beta^m)$, $\lambda_2 (= \lambda_0 \beta^2)$ and m , which are determined in next section.

TEST OF HYPOTHESIS

Columns 5 and 6 in Table 2 tabulate the values of the inundation index I and the scour number $(h_b + y_s) / (h_b + a)$, respectively, for the experimental data. To test Eq. (14), columns 5 and 6 are plotted in Figure 2 where the data from different sediment sizes, different girder numbers and different inundation levels almost collapse into a single curve. This means the two similarity numbers reasonably describe the submerged flow scour. Furthermore, a least-squares fitting process with MatLab gives the model parameters

$$\lambda_1 = 1.71, \lambda_2 = 2.33, \text{ and } m = 2.45 \quad (15)$$

which fit Eq. (14) to the present experimental data with a correlation coefficient $R^2 = 0.976$ and a standard deviation $\sigma_2 = 0.015$. This means with a 95% confidence interval, the estimated scour depth from Eq. (14) has an error of $\pm 3\% (h_b + a)$.

Note that Figure 2 has a minimum value at $I = 0.77$ and $(h_b + y_s) / (h_b + a) = 0.89$, which is the criterion between unsubmerged and submerged flows. At this minimum, the scour depth is $y_s = 0$ and the flow is partially submerged where $a = h_u - h_b$, which leads to

$$h_b / h_u = 0.89 \text{ or } h_u / h_b = 1.1 \quad (16)$$

This implies that submerged flow scour occurs under the conditions

$$I = \frac{\sqrt{g(h_u - h_b)}}{V_{uc}} \geq 0.77 \text{ and } h_u / h_b \geq 1.1 \quad (17)$$

The latter condition is similar to that of submerged culvert flow where $h_u/h_b \geq 1.2$ (Gupta 2008, p779). The dashed line in Figure 2 is just an extension of Eq. (14), which does not have any practical meaning since it corresponds to an orifice flow where the downstream edge of a bridge is unsubmerged. Nevertheless, it helps examine the functional structure of Eq. (14). Mathematically, when h_u approaches to h_b , or the inundation index I approaches to zero, the scour number has an asymptote $(h_b + y_s) / (h_b + a) \rightarrow 1$, which is true since $a = h_u - h_b \rightarrow 0$ and $y_s = 0$. This asymptote shows that the structure of Eq. (14) is physically reasonable. In brief, for submerged flow the scour number increases with the inundation index.

The effect of sediment size is through the upstream critical velocity V_{uc} . When sediment size increases, the upstream critical velocity V_{uc} increases, which decreases the inundation index I and then reduces the scour number $(h_b + y_s) / (h_b + a)$. In other words, scour depth decreases with increasing sediment size.

The present analysis has approximated the approach velocity distribution to be uniform, which implies the effects of the bottom and side wall boundary layers can be neglected when estimating the flowrate through a bridge. Furthermore, the deck elevation must be much higher than the bottom boundary layer. Otherwise, the estimated flowrate through a bridge is much larger than the real flowrate, which results in a large effective velocity V_{ue} in Eq. (4) or a small inundation index in Eq. (13) and, as a result, a very small scour number or depth. This explains why the last two tests in Table 2 are excluded in analyses and why the predictions of the proposed method are much smaller than the measurements where the inundation ratio $h_u/h_b = 3.57$ and 10, respectively. In practice there are seldom submerged flows with an inundation ratio $h_u/h_b > 2$. For prototype flows with fully developed turbulent boundary layers, it is suggested to use $n = 1/7$ in Eq. (6) for estimating the flowrate through a bridge and Eq. (13) for inundation index.

In briefly, the proposed theoretical model, Eq. (14), has been confirmed with the present experimental data under threshold conditions, and the model parameters are defined by Eq. (15).

APPLICATION PROCEDURE

Unlike a pure empirical method that is restricted to the range of calibrated data, the proposed method is expected to be applicable to similar prototype bridge flow without scaling effects because it is mainly derived from the mass and energy conservation laws. These laws are true within considered framework whatever are inputs, outputs or system modifications. To apply the proposed method, the following procedures are suggested.

Step 1: From the approach flow depth, h_u , and bed materials size, d_{50} , calculate the critical velocity, V_{uc} , from Eq. (2) in Guo et al. (2010).

Step 2: Check if the scour is clear water scour. If the upstream velocity, V_u , is less than or equal to the critical velocity, V_{uc} , the proposed method is used.

Step 3: Calculate the effective thickness of deck blockage, a , from Eq. (10).

Step 4: Calculate the inundation index, I , from Eq. (13) where $n = 1/7$ is

used for fully developed turbulent boundary layers.

Step 5: Check if the flow is submerged flow according to Eq. (17).

Step 6: If yes, calculate the scour number from Eq. (14), and solve for scour depth, y_s .

Step 7: Plot the design scour profile according to Eqs. (6) and (8) in Guo et al. (2010).

Column 7 in Table 2 was obtained using the above procedures, and column 8 shows the absolute errors of predictions. It is seen that except for the last two tests, all errors are less than or equal to 6.3 mm that is usually within the uncertainties of flume measurements. The large errors of the last two tests originate from the amplified upstream effective velocities in the calculations, by neglecting the effect of boundary layers. The real effective velocities were significantly smaller since the deck elevations were close to the bottom boundary layers. Without the last two tests, the correlation coefficient between the predictions and the measurements is $R^2 = 0.929$.

CONCLUSIONS

The theoretical model, Eq. (14), for the maximum scour depth has been confirmed by the experimental data in Guo et al. (2010), which shows that the maximum scour depth can be described by the scour number and the inundation index. In general, for submerged flow the scour number increases with inundation index, which is equivalent to the maximum scour depth increases with deck inundation level, decreases with increasing sediment size, and is independent of bridge girders. The proposed method is expected to be applicable to prototype flows without scaling effects, and an application procedure has been suggested for bridge foundation design or field scour evaluation.

ACKNOWLEDGMENTS

This study was financially supported by the FHWA Hydraulics R&D Program with Contract No. DTFH61-04-C-00037. The writers would like to thank Mr. Oscar Berrios for running the tests and preparing some of the figures. The writers are also thankful to Mr. Bart Bergendahl at FHWA for his constructive comments and suggestions.

REFERENCES

- Arneson, L. A., and Abt, S. R. (1998). "Vertical contraction scour at bridges with water flowing under pressure conditions." *Transportation Research Record*, 1647, 10-17.
- Guo, J., Kerenyi, K., Flora, K., and Afzal, B. (2010). "Submerged-flow bridge scour under maximum clear-water conditions (I): Experiment." *5th International Conference on Scour and Erosion*, San Francisco, CA.
- Gupta, R. S. (2008). *Hydrology and Hydraulic Systems*. 3rd ed., Waveland Press.

- Lyn, D. A. (2008). "Pressure-flow scour: a re-examination of the HEC-18 equation." *J. Hydraul. Engrg.*, 134(7), 1015-1020.
- Picek, T., Havlik, A., Mattas, D., and Mares, K. (2007). "Hydraulic calculation of bridges at high water stages." *J. Hydraul. Res.*, 45(3), 400-406.
- Richardson, E. V., and Davis, S. R. (2001). *Evaluation Scour at Bridges*. HEC-18, FHWA-NH-01-001, 4th Ed., U.S. Dept. of Transp., Washing, D.C.
- Umbrell, E. R., Young, G. K., Stein, S. M., and Jones, J. S. (1998). "Clear-water contraction scour under bridges in pressure flow." *J. Hydraul. Engrg.*, 124(2), 236-240.

Evaluation of the Structural Integrity of Bridge Pier Foundations Using Microtremors in Flood Conditions

M.Samizo¹, S.Watanabe¹, T.Sugiyama¹, K.Okada²

¹ Disaster Prevention Technology Division, Railway Technical Research Institute, 2-8-38,Hikari-cyo, Kokubunji-shi,Tokyo 185-8540.Japan;email:samizo@rtri.or.jp

² Department of Science and Engineering, Kokushikan University, 4-28-1, Setagaya, Setagaya-ku, Tokyo 154-8515.Japan

ABSTRACT

Bridge pier foundations occasionally become unstable due to scouring around piers in flood conditions, and operational restrictions imposed according to the water level are practical for maintaining safe train operation. However, when such restrictions are lifted, it is quite difficult to verify the condition of the bridge pier foundation. It is therefore necessary to develop a practical method of quantitatively evaluating and assessing the structural integrity of bridge pier foundations in flood conditions. This paper reports the results of analysis of long-term microtremor measurements made on existing bridge piers and a method to define the natural frequencies of bridges using microtremors.

1. Introduction

In Japan, most railways are subjected to severe environmental conditions such as heavy rainfall due to typhoons and the annual rainy season. Such rainfall also raises the water level of rivers, and flooding can occur in certain cases. During flood conditions, rivers scour bridge pier foundations, reducing stability and even causing collapse that may result in train accidents (Figure 1). In order to secure safe train operation against such scouring, railways have imposed stringent operational restrictions based on water levels to prevent accidents.

However, during periods when such restrictions are lifted, it is quite difficult to verify the conditions of bridge pier foundations. Impact vibration (i.e. forced vibration) testing¹⁾ is efficient as an assessment system, but it is hard to carry out tests in terms of workability and safety during flood conditions. It is therefore necessary to develop a practical method to quantitatively and easily evaluate the structural integrity of bridge pier foundations during floods.²⁾

We focused on microtremor, which is a low amplitude ambient vibration of the ground caused by man-made or atmospheric disturbances, as an effective subject of measurement to define a natural frequency of bridge piers. This paper reports the results of analysis of long-term microtremor measurements made on existing bridge piers and a method to define the natural frequencies of bridges using microtremors.



Figure 1 Destructive effect of scouring under a railway bridge (Japan).

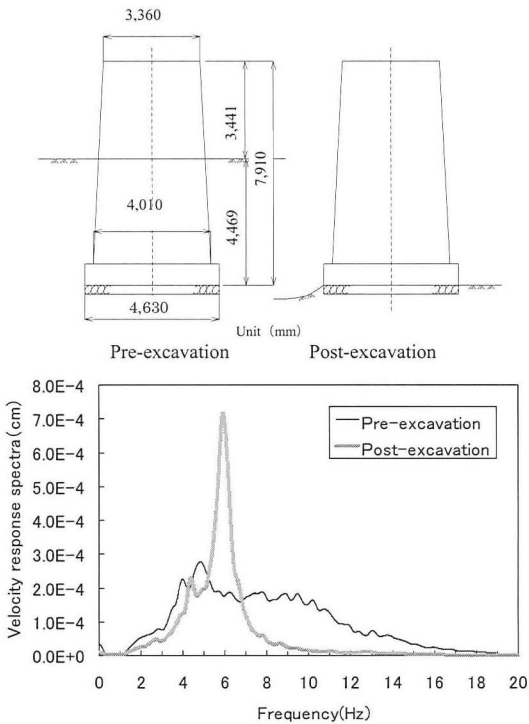


Figure 2 Schematic view of bridge pier and the Fourier spectra of the microtremors.

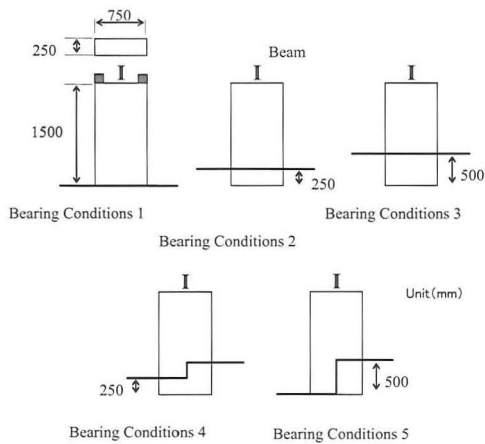


Figure 3 Schematic views of model cases.

2. Relationship between reduction in foundation soundness and natural frequency

2.1 Measurement of natural frequencies on bridge piers

2.1.1 Bridge piers with different penetration depths

We performed microtremor measurement on actual bridge piers. The vibration values were extrapolated from microtremors measured using a vibration sensor mounted on the upper surface of the pier. The subject of measurements is referred to as Bridge A, which has metal girders as a single track and concrete spread foundations. Two different penetration depths of 0m and 4m were made by excavating, and microtremors were measured without the girders because of river reparation. In order to compare natural frequencies, impact vibration tests were also conducted.

2.1.2 Results of microtremor measurement

According to the results of impact vibration testing, the initial frequencies of the bridge pier were 14.6Hz for a depth of 4m and 5.9Hz at 0m. These values indicate that the initial frequency tends to decline as depth decreases.

Figure 2 shows a schematic view of the bridge pier and the Fourier spectra of the microtremors observed at both penetration depths. As can be seen in the figure, there is a predominant spectra response around 6Hz in the case of low penetration depth, and this 6Hz value is very close to the initial frequency. In contrast, the spectra response indicates a smooth shape in the case of high penetration depth. As a result, it is probable that shallower penetration depths will allow the natural frequency of each bridge pier to be determined, enabling judgment of scouring-related failure from microtremor measurements.

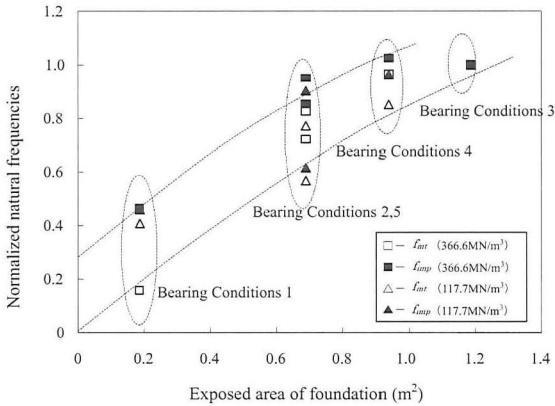


Figure 4 Relationship between exposed area of foundation and normalized values of f_{mt} and f_{imp} .

2.2 Model tests

To investigate the basic relationship between scouring shapes and foundation soundness, we carried out testing on a model concrete pier consisting of two 3,850mm H-shaped steel beams and one bridge pier. The height, width, length, and weight of the pier were 1,500mm, 250mm, 750mm and 750kg respectively. The foundation soils were made by crushed stone that is less than 20mm diameter, and the compression strength of the soils was controlled to 117.7MN/m³ and 366.6 MN/m³.

We measured three microtremors using vibration sensors, two of which were mounted on the upper surface of the pier and the other on land near the bridge foundation. The sampling rate of the sensors was 100Hz, and impact vibration testing was also conducted.

In this examination, the authors introduce the value f_{mt} to indicate the ratio of the natural frequency measured on the upper surface of the bridge to that measured on land. Additionally, the natural frequency measured by impact vibration testing is introduced as f_{imp} .

Figure 3 shows a schematic view of the models, which have different foundation shapes. Figure 4 shows the relationship between the exposed area of the foundation and the f_{mt} and f_{imp} values, with all values normalized by that of Case 3. The figure indicates that each f_{mt} and f_{imp} ratio value declines as the foundation soundness decreases, and with an exposed foundation area of 0.2m² each ratio declines by approximately 60 to 80%.

3. Changes in the natural frequency of actual bridge piers in stream flow

3.1 Measurement of river levels and microtremors in actual bridge piers

Little is known about the microtremors of actual bridge piers due to a lack of

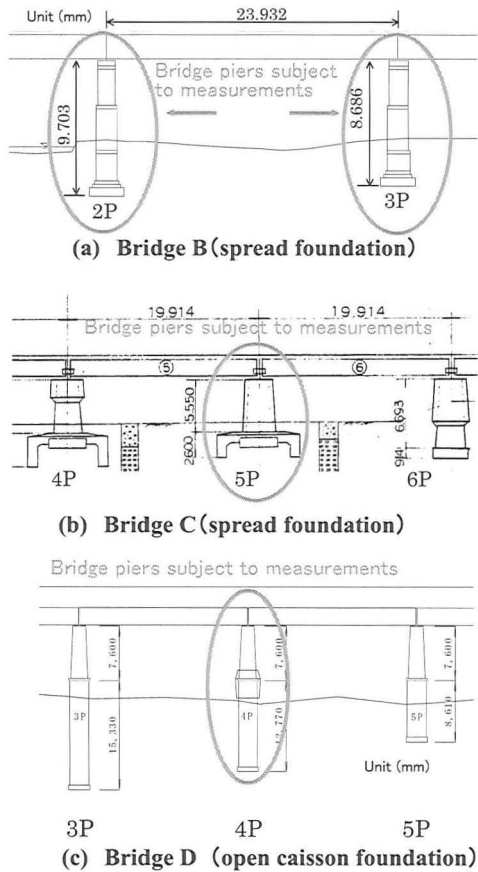


Figure 5 Schematic view of each existing bridge.

measurements made in flood conditions. In order to ascertain the characteristic frequencies found during flooding, we therefore performed continuative investigation of microtremors in actual bridge piers.

3.2 Bridge piers and the measurement period

Table 1 shows the properties of the actual bridge piers used, all of which are located on rivers that tend to experience high water levels in the rainy season or during typhoons. Table 1 also shows the measurement period and the natural frequencies obtained from impact vibration testing conducted at low water. Figure 5 shows a schematic view of each bridge.

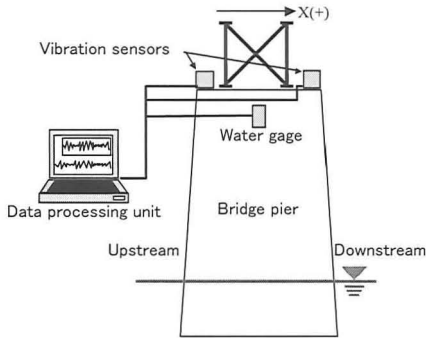


Figure 6 Schematic view of measurement system.

Table 1 Properties of the actual bridge piers.

Bridge name	Pier No.	Height of pier (m)	Width of pier (m)	Height of pier - penetration depth(m)	Penetration depth(m)	Natural frequency (Hz) [※]
Bridge B	2P	10.31	1.67	5.85	4.46	11.3
	3P	9.30	1.67	5.25	4.05	14.3
Bridge C	5P	6.95	3.66	5.20	1.75	17.4
Bridge D	4P	7.60	2.84	10.79	9.58	3.1

※ Results of impact vibration testing conducted at low water

3.3 Method of measuring microtremors

Figure 6 shows a schematic view of the measurement system. A vibration sensor was mounted on a bridge pier located on a spread foundation, and microtremors were measured at five-minute intervals at every hour with a sampling rate of 100 Hz. The sensor was able to measure three-dimensional microtremors, and horizontal dimension X was set in the direction of river flow.

3.4 Comparison of the Fourier spectra of microtremors observed at low and high water levels

Figure 7 shows the response Fourier spectra of pier No.2 on Bridge B during low and high water. The value for the low water table indicated peaks at around 3.5 Hz and 17 Hz. The former is equivalent to the natural frequency of a girder. The response spectra during high water, by contrast, indicated predominant peaks at around 7.4 Hz and 11.5 Hz. We assume that the 7.4 Hz value is the response spectra of the annex of the bridge as it also appears during low water. Figure 8 shows the relationship between the Fourier spectra measured from microtremors at high water and the values measured from impact vibration testing at low water, with the spectra normalized by the maximum value of each spectrum. As shown in Fig.8, the 11.5-Hz value was remarkably close to the pier's initial vibration frequency value of 11.3 Hz.

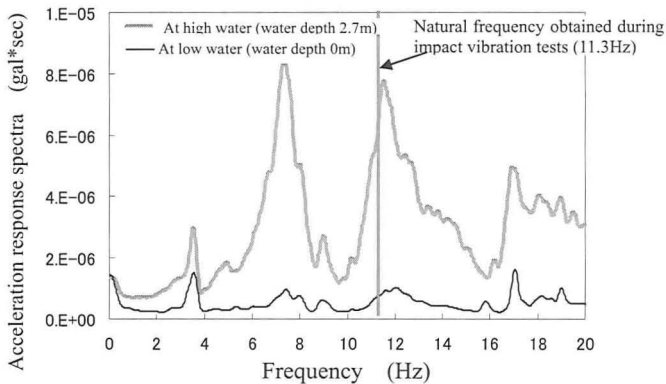


Figure 7 Response Fourier spectra of pier No.2,

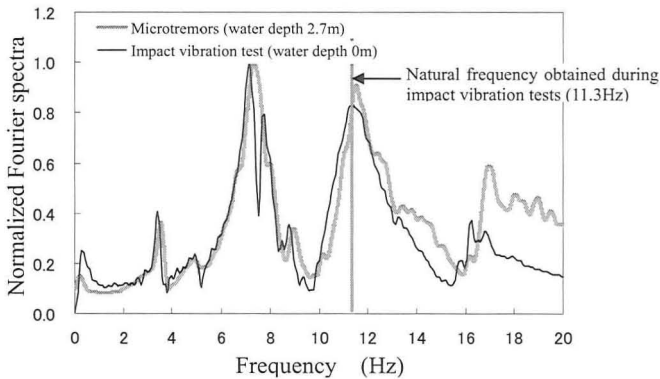


Figure 8 Relationship between Fourier spectra measured from microtremors at high water and the one measured from impact vibration testing.

From this, we could assign one predominant vibration frequency on the Fourier spectra of microtremors as a characteristic frequency for that specific pier.

4. Relationship between water level and natural frequency fluctuation

As shown in Fig.7, it has not been possible to confirm the predominant spectral response, suggesting that fluctuations in natural frequency probably differ according to the water level. These fluctuations indicate the changing range of the f_{0i} value with the passage of time involving the change in the water level. Figure 10

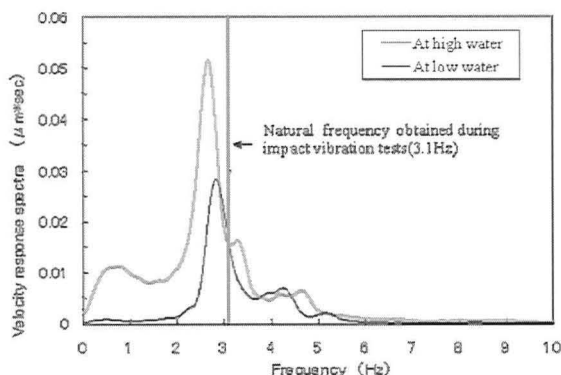


Figure 9 Response Fourier spectra for Bridge D

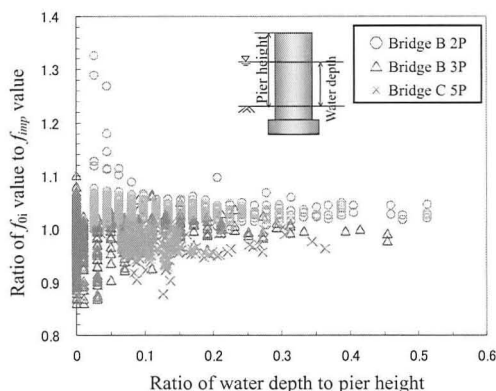


Figure 10 Relationship between the ratio of water level to pier height and the ratio of f_{0i} value to f_{imp} .

shows the relationship between the ratio of water level to pier height and the ratio of the f_{0i} value to the f_{imp} value, and also gives each ratio for the case of Bridge C. As the figure indicates, the deeper the water level, the more the natural frequencies tend to converge toward those values obtained from impact vibration testing. Thus, by comparing the frequencies obtained from impact vibration testing with the Fourier spectra of vibrations represented by microtremors, we determine that it may be possible to identify the natural frequencies of the pier at high water.

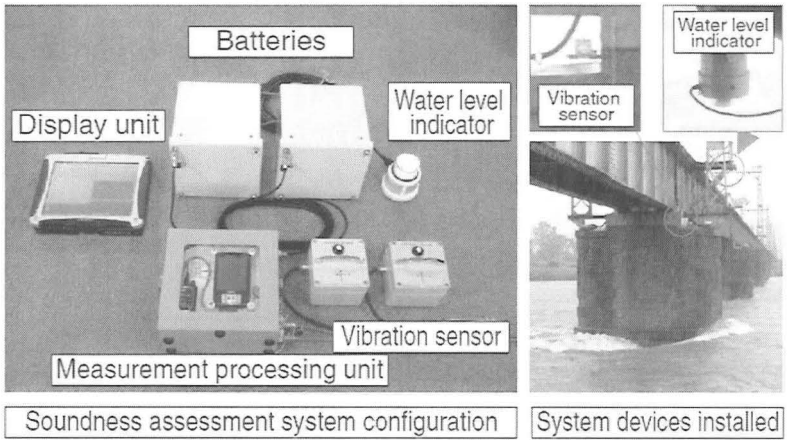


Figure 11 Soundness assessment system configuration, and installation of system devices.

5. System development

When in flood, a river may scour the riverbed around a pier, resulting in a shallower penetration depth for the pier. As a general rule, if a pier's penetration depth is sufficient, the pier will have enough resistance to withstand forces that would otherwise topple it, and the foundation will remain stable, keeping the pier sound. However, a reduction in penetration depth will diminish the soundness of the pier foundation. As the penetration depth declines, the pier's natural frequencies will tend to exhibit a corresponding decline. Focusing on the fact that natural frequencies change in this way, we developed a system that uses natural frequency values to determine the degree of soundness of pier foundations, and then provides this quantitative data to be used as one factor for deciding whether or not to suspend train operations on the bridge. Figure 11 shows the system configuration. The system is currently being tested in real-time assessments of the stability of bridge piers, with a view to improving system reliability and obtaining more data.

6. Conclusions

The conclusions of this paper can be summarized as follows:

- 1) The natural frequencies of bridge piers decline with decreasing foundation depth during periods in which the river scours the pier.
- 2) It was possible to assign one predominant vibration frequency on the Fourier spectra of microtremors as a natural frequency for that specific pier during high water.
- 3) The deeper the water, the more the natural frequencies tend to converge toward the

values previously obtained during impact vibration testing.

- 4) We developed a system that uses natural frequency to determine the soundness of pier foundations, and then provides this quantitative data to train operations.

References

- [1] Nishimura, A. et al., "A Study on the Integrity Assessment of Railway Bridge Foundations," *RTRI Report*, Vol.3, No.8, pp.41-49, 1989 (in Japanese)
- [2] Samizo, M. et al., "The Influence of Base Ground Conditions on the Vibration Properties of Spread Foundation Bridge Piers," *RTRI Report*, Vol. 18, No. 9, pp. 47-52, 2004 (in Japanese).

Evaluation of Sediment Transport Rate in Coarse-Bed Rivers

M. Yasi¹, R. Hamzepouri² and A. Yasi³

¹ Assistant Professor of River Engineering, Department of Water Engineering, Urmia University, Urmia 57153, Iran; PH (98) 441-3364520 ; m.yasi@urmia.ac.ir

² Senior Engineer, Office of Water Engineering, West-Azarbaijan Rural Water Company, Urmia 57153, Iran; PH (98) 441-3987273 ; rhamzepoury@yahoo.com

³ Postgraduate Student, Department of Civil Engineering, UTM University, Johor, Malaysia; PH (60) 10-6663496 ; aliandsquall2000@yahoo.com

ABSTRACT

The process of flow and sediment transport is different and more complex in coarse-bed rivers than in sand-bed rivers. The main aim of the present study was to evaluate different modes of sediment transport (i.e. bed, suspended and total loads) from different methods. Three river reaches were selected as representatives of coarse-bed rivers in North-West of Iran, where observed data were available. A sediment transport model (STM-CBR) was developed to calculate the bed loads from 13 methods, the suspended loads from 4 methods and the total loads from 10 methods. The effects of bed material characteristics were also examined. This paper presents the prediction results and the order of errors for different modes of the sediment loads under different flow conditions. With the inclusion of the order of predictive errors, the best-fitted relationships are recommended for the proper evaluation of different modes of sediment loads in similar coarse-bed river reaches.

INTRODUCTION

Coarse-bed Rivers are characterized by relatively high degrees of bed slope, stream power, sediment transport, particularly in the mode of bed load; and are relatively wide and shallow with potential of deposition of non-cohesive coarse sediment such as gravel and cobbles (Przedwojski, et al., 1995). The process of flow and sediment transport is different and more complex in coarse-bed rivers than in sand-bed rivers. The main characteristic of the flow in coarse-bed rivers is the development of an armor layer with coarse gravel, cobbles and boulders. While this surface layer establishes a stable and smooth boundary at low to mean flows, its mobility introduces a different mode of the flow resistance during high flows resulting in excessive bed load transport of finer sub-surface material, and channel instability (Hey, et al., 1982 ; Parker, et al., 1982).

Reliable prediction of the sediment transport capacity and determination of the different modes of transport (i.e. bed load, suspended load, and total load) in coarse-bed rivers are of major importance in river engineering.

Several relationships are available in the literature for predicting sediment transport in coarse-bed rivers, most of which are presented in Table 1. Some of these relationships evaluate the total load directly (e.g. Karim & Kennedy, 1990), a few methods calculate both the suspended and bed loads on an identical basis (e.g. Einstein, 1950), and others compute either suspended load (e.g. Englund, 1965) or bed load (e.g. Parker, 1990). There is no general guidance to select the best methods

applicable to different rivers, or different reaches of a river. The best selection among different relationships is unreliable wherever the field investigations are not involved in the river reach. The effects of bed sediment characteristics are to be considered in the adoption and reliability of the available relationships (Almedeij and Diplas, 2003; Habersack and Laronne, 2002). However, the order of 50% to 70% error is expected, even when fitting the measured data to the best predictors (van Rijn, 1993).

Table 1. Different sediment transport relationships, applicable to coarse-bed rivers

Methods	Bed Load	Suspended Load	Total Load	Application Remarks
Schoklitsch (1934)	*			D= (0.3-5) mm
Schoklitsch (1943)	*			D= (0.3-5) mm
Meyer-Peter & Muller (1948)	*			D= (0.4-30) mm
Einstein (1950)	*	*	*	Different Rivers
Laursen (1958)			*	Flume Data; D= (0.01-4.1) mm
Rottner (1959)	*			Flumes & Rivers
Engelund (1965)		*		Different Rivers
Bagnold (1966)	*	*	*	Rivers with bed form
Engelund & Hansen (1967)			*	Dune bed form rivers
Yalin (1977)	*			Sand & Gravel bed rivers
Brownlie (1981)			*	Flumes and Rivers
Parker, et al. (1982)	*			Gravel bed rivers, with armor layer
Yang (1982)			*	Different Rivers
Samaga (1985)		*		Different Rivers
Zanke (1987)	*			Coarse-bed rivers
Ackers & White (1990)			*	Different Rivers, mostly sand-bed
Karim & Kennedy (1990)			*	Different Rivers
Parker (1990)	*			Gravel bed rivers, with armor layer
Karim (1998)			*	Rivers, without armor layer
Sun & Donahue (2000)	*			Coarse-bed rivers; D= (2-10) mm
Cheng (2002)	*			Coarse-bed rivers
Wilcock & Crowe (2003)	*			Coarse-bed rivers; D= (0.5-82) mm
Yang & Lim (2003)			*	Rivers; D= (0.8-2.2) mm

Field data on suspended loads are more readily available, although lesser data are taken during high flows. Direct measurements of bed load are difficult to achieve in coarse-bed rivers, and less data is available. Therefore, the evaluation of total sediment load, and the contribution of bed load to the total load are very much

uncertain. The conventional approach suggests a small portion of suspended load is to be taken into account for the bed load (usually 5 to 25 percent). Such a fraction is generally applied to sand-bed rivers, but might be greater than 25% in coarse-bed rivers (Yang, 1996). Linsely & Franzini (1979) suggested that this ratio is to be generally between 10% to 50%, but greater percent is expected when considering the ratio of bed load to total load, and even much greater in the case of coarse-bed rivers. This ratio was found to be in the range between 0.4 and 0.8 with an average value of 0.57 (Yasi and Hamzepouri, 2008). However, the order of 40% to 50% error is expected, even in standard sediment measuring system, and in high flows.

The main aim of the present study was to evaluate the different modes of sediment transports from the best fitted hydraulic relationships to the flow conditions in three representative coarse-bed river reaches. The effects of bed material characteristics were also considered in this study.

MATERIALS AND METHODS

Three river reaches were selected as representatives of coarse-bed rivers in the North-West of Iran (Badalan reach in the Aland river, Yazdekan reach in the Ghotor river, and Baron reach in the Baron river). Presence of standard gauging station allowed for simultaneous measurements of bed and suspended loads in each of these three reaches. The Badalan reach is located in a region of $44^{\circ} 40'$ longitude and $38^{\circ} 34'$ latitude, with a length of 150 m. The average bed slope, length to width, and aspect ratios are about 0.007, 8 and 22, respectively. 407 samples of suspended load over a period of 30 years were examined. 77 out of 407 samples include simultaneous measurements of both bed and suspended loads. The Yazdekan reach is located in a region of $44^{\circ} 47'$ longitude and $38^{\circ} 29'$ latitude, with a length of 181 m. The average bed slope, length to width, and aspect ratios are about 0.011, 8 and 25, respectively. 452 samples of suspended load over a period of 15 years were examined. 87 out of 452 samples include simultaneous measurements of both bed and suspended loads. The Baron reach is located in a region of $44^{\circ} 35'$ longitude and $39^{\circ} 10'$ latitude, with a length of 212 m. The average bed slope, length to width, and aspect ratios are about 0.004, 2.3 and 120, respectively. 109 samples of suspended load over a period of 5 years were examined. 57 out of 109 samples include simultaneous measurements of both bed and suspended loads.

River survey, and bed and sediment samplings were carried out. Table 2 presents the characteristics of bed sediments from surface and subsurface layers, and from bed-load samplings in these three reaches. Sediment transport rates (i.e. suspended and bed load, thereby the total load) were evaluated from the field data in different flow conditions. Mean flow characteristics were determined from the calibrated HEC-RAS flow model under different flow conditions in these river reaches, as presented in Table 3. A sediment transport model (STM-CBR) was developed to compute sediment load from different relationships adapted to coarse-bed rivers (the bed load from 13 methods, the suspended load from 4 methods and the total load from 10 methods), as presented in Table 1. The flow characteristics in Table 3 were used as input to the STM-CBR model. As reported by van Rijn (1993), total sediment transport rate was evaluated either by using direct methods (such as: Karim & Kennedy, 1990), or indirectly by summing up the suspended and bed loads

calculated from the relationships developed on a similar basis (such as: Einstein, 1950). The effects of sediment characteristics (surface layer, subsurface layer, and bed-load material) were also examined. Relative predictive errors are calculated from the difference between the observed sediment data and corresponding estimated values divided by the observed data.

Table 2. Bed and sediment material characteristics in three river reaches

Reach (River)	Bed Material	D ₁₀ mm	D ₁₆ mm	D ₅₀ mm	D ₆₅ mm	D ₈₄ mm	D ₉₀ mm	C _u	σ_g	S _g
Badalan (Aland)	Surface	22.8	25.4	41	49.2	77.2	91	2.2	1.7	2.65
	Subsurface	0.42	.67	3.9	7.2	16.7	20.6	13.4	5.0	2.65
	Bed load	0.5	0.73	2.5	3.6	7.8	8.6	6	3.3	2.65
Yazdekan (Ghotor)	Surface	17	18.7	32.1	41.7	63.1	75	2.1	1.8	2.65
	Subsurface	0.6	0.9	3.7	6.8	14.5	22	9.2	4.0	2.65
	Bed load	0.7	0.95	3.7	6.4	13.7	20	8.5	4.8	2.65
Baron (Baron)	Surface	16	22	35	41	48.5	53	2.4	1.5	2.65
	Subsurface	0.4	0.57	3.6	8.8	24.5	29	16.1	6.5	2.65
	Bed load	0.47	0.6	1.9	2.8	4.8	7	5.3	2.8	2.65

D_s = Charact. Size; C_u = Uniformity Coeff.; σ_g = Geometric Std. Dev.; S_g = Specific Gravity

Table 3. Flow characteristics in three river reaches

Reach (River)	Water flow rate Q (m ³ /s)	Mean velocity V (m/s)	Water surface width B (m)	Hydraulic radius R (m)	Energy slope S (%)	Froude No. Fr	Shear stress τ (N/m ²)
Badalan (Aland)	14.2	1.76	15.6	0.51	0.95	0.78	47.5
	36.6	2.43	17.8	0.83	0.93	0.84	76.2
	62	2.81	20.9	1.03	0.93	0.86	94.5
Yazdekan (Ghotor)	11.7	1.57	18.8	0.40	1.12	0.71	44.4
	48.7	2.46	22.9	0.85	0.95	0.75	79.3
	80.0	2.75	24.8	1.18	0.80	0.72	90.7
Baron (Baron)	50	1.44	84.1	0.42	0.81	0.64	33.73
	100	1.82	91.9	0.61	0.68	0.67	40.16
	166	2.19	101.0	0.76	0.78	0.73	58.01

RESULTS AND DISCUSSION

Predicted sediment transport rates from the relationships in Table 1 were compared with the corresponding results from the field data, under different flow conditions at three river reaches. Typical detailed calculation of suspended loads are presented in Table 4 and compared with the range of observed data in different flow conditions, using the characteristics of surface layer, sub-surface layer and bed-load material. Similar results were provided for bed and total loads, in three river reaches.

Figures 1 shows the evaluation of suspended load from 4 relationships, in Badalan river reach, using the characteristics of bed-load sampling material.

Table 4. Detailed evaluation of suspended loads (Q_s : kg/s), Badalan River Reach

Bed Layer	Method	Water flow rate, Q : (m^3/s)						
		6	10	20	32	50	62	80
Surface layer	Einstein (1950)	0	0	4	20	32	45	66
	Engelund (1965)	0	0	0	1	2	3	5
	Bagnold (1966)	0	1	2	5	7	10	15
	Samaga (1985)	2245	2464	2700	2807	2790	2572	2413
Sub-surface layer	Einstein (1950)	4	5	11	18	30	40	58
	Engelund (1965)	3	9	38	106	219	344	580
	Bagnold (1966)	2	3	7	15	25	33	48
	Samaga (1985)	28	29	27	26	28	27	25
Bed Load Material	Einstein (1950)	3	6	13	22	34	44	63
	Engelund (1965)	8	23	95	262	546	857	1447
	Bagnold (1966)	2	4	9	18	31	41	59
	Samaga (1985)	14	12	12	10	11	11	11
Observed		7	21	96	273	718	1152	3297
Confidence Limit 90%		9	27	130	381	1026	1667	4896
		5	16	72	202	524	833	2340
Data Envelop		39	92	292	644			
		1	3	23	87			

Gray area: Uncertain range of data due to the extrapolation of field data

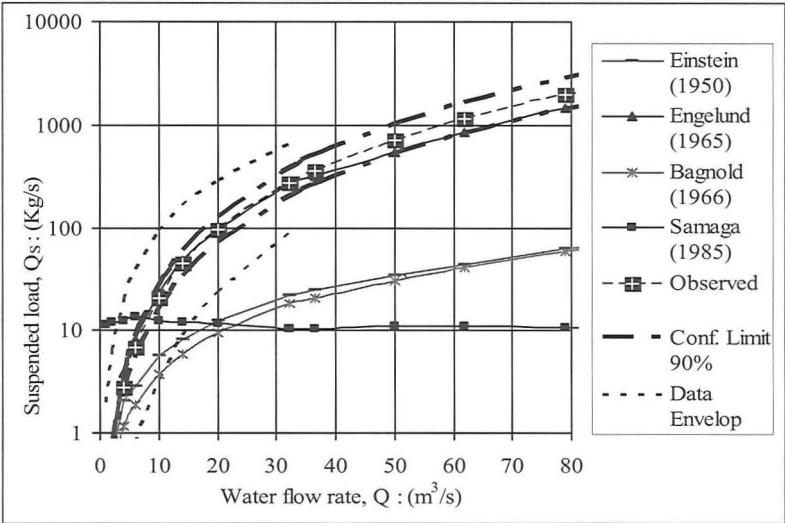


Figure 1. Evaluation of suspended load (Q_s), using bed-load material, Badalan Reach

Similarly, Figures 2 and 3 show the evaluation of bed and total loads, respectively, in Badalan river reach.

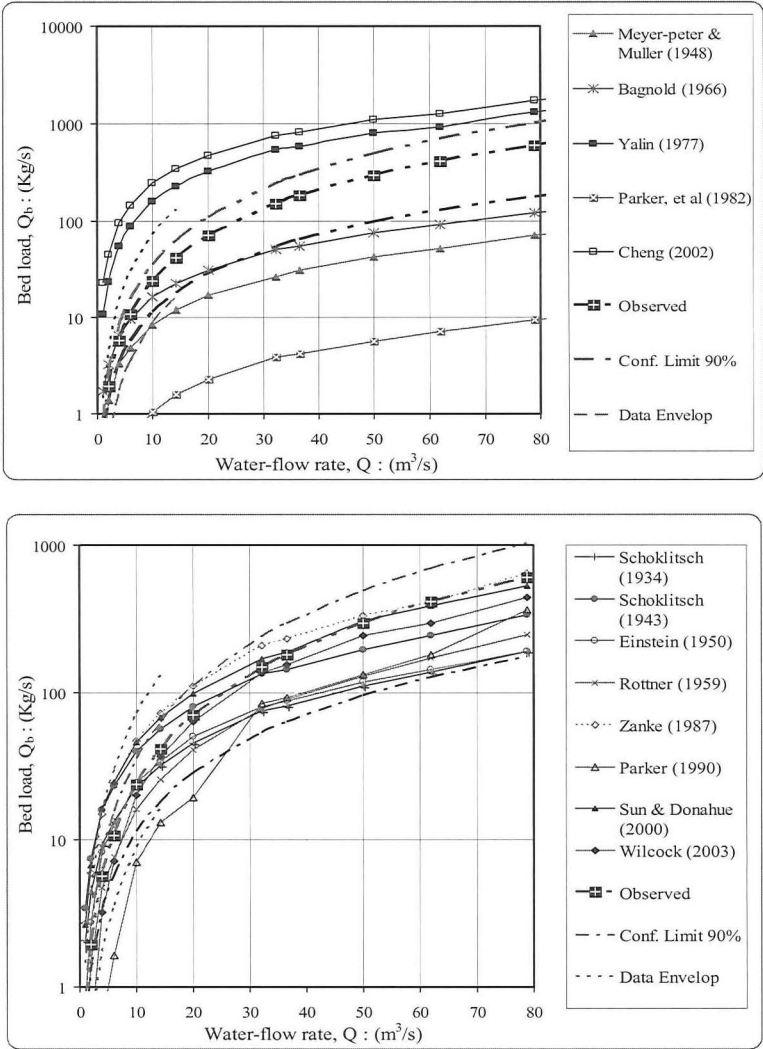


Figure 2. Evaluation of bed load (Q_b), using bed-load material, Badalan River Reach

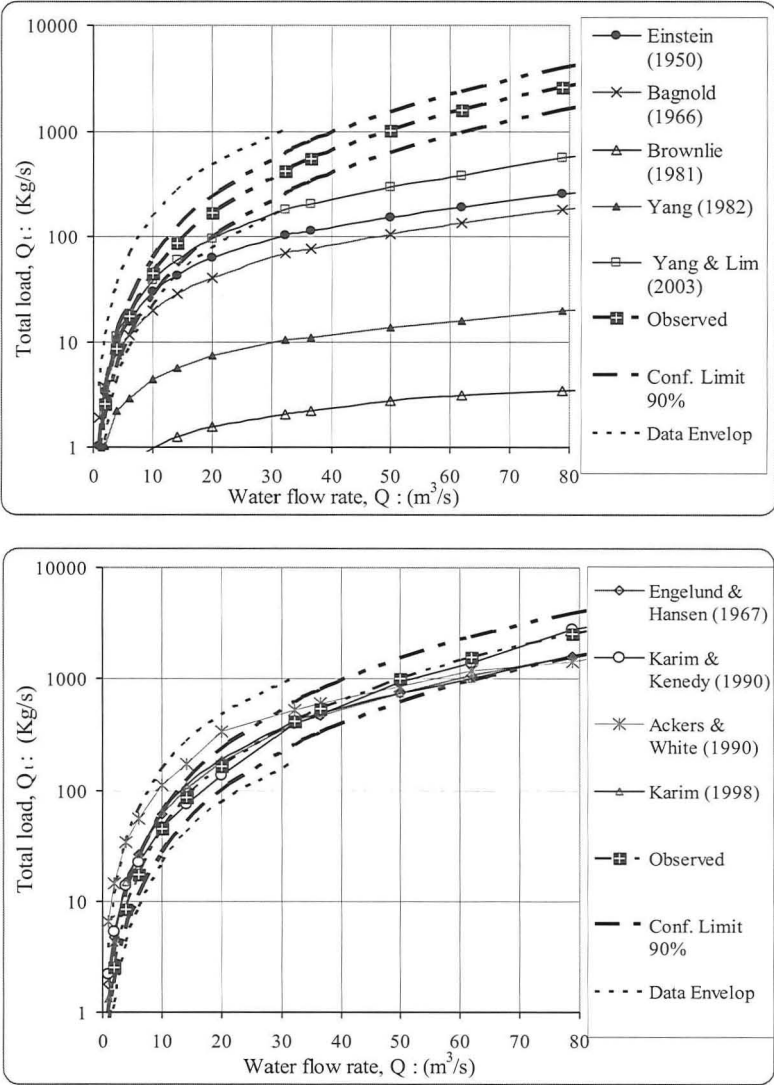


Figure 3. Evaluation of total load (Q_t), using bed-load material, Badalan River Reach

Figures 1 to 3 indicate the prediction of suspended load from 4 relationships, of bed loads from 13 relationships, and of total loads from 10 relationships; also show both the envelop curves and the 90% confidence limits for the range of field data. Similar results could be demonstrated for the inclusion of either surface layer or sub-surface layer, in the three river reaches.

The results indicated that a single relationship is impossible to detect for the prediction of each of the three modes of sediment loads (i.e. suspended, bed and total loads) in different reaches, under different flow conditions. Those relationships which are located within the range of field data (or within the general trend of envelope curves of observed data) could be considered as the best fitted predictors. An average and the range of predictive errors give more reliable estimation of sediment load with the degrees of uncertainties in such a complex problem.

Tables 5 to 7 present an average and the range of relative errors in the evaluation of bed, suspended and total loads with the best fitted relationships among different methods in Badalan river reach, using bed-load material characteristics, respectively. Similar results could be demonstrated for the inclusion of either surface layer or sub-surface layer, and for the three river reaches.

Results indicated that for most of the relationships, the sediment transport capacity is well described when the characteristics of the bed-load material are included. The inclusion of the sub-surface bed layer into the predictive relationships is considered as the second priority. This study indicated that the inclusion of surface layer is not appropriate, which is coincident with the previous studies of Almedej and Diplas (2003) and Habersack and Larone (2002).

Table 5. Suspended-load prediction error (E%) from selected relationships, using bed-load material, Badalan River Reach

Predictive Method	Einstein (1950)	Engelund (1965)	Average
Average E%	-75	-1	-38
Range E%	(0) to (-98)	(54) to (-40)	(27) to (-69)

Table 6. Bed-load prediction error (E%) from selected relationships, using bed-load material, Badalan River Reach

Predictive Method	Schk (1934)	litsch (1943)	Rottner (1959)	Zanke (1987)	Parker (1990)	Sun & Donahue (2000)	Wilcock (2003)	Average
	(1934)	(1943)	(1959)	(1987)	(1990)	(2000)	(2003)	
Average E%	18	42	-43	68	-64	62	-25	32
Range E%	(130) to (-72)	(292) to (-51)	(-62) to (-18)	(215) to (-1)	(-100) to (-37)	(253) to (-22)	(-74) to (-9)	(92) to (-42)

Table 7. Total-load prediction error (E%) from selected relationships, using bed-load, material, Badalan River Reach

Predictive Method	Laursen (1958)	Engelund & Hansen (1967)	Karim & Kenedy (1990)	Akers & White (1990)	Yang & Lim (2003)	Average
Average E%	115	10	12	104	-36	36
Range E%	(373) to (-70)	(-44) to (-88)	(109) to (-19)	(305) to (-45)	(-82) to (-43)	(152) to (-47)

CONCLUSION

The process of flow and sediment transport is different and more complex in coarse-bed rivers than in sand-bed rivers. This study indicated that the sediment transport capacity is well described when the characteristics of the bed-load material are included. With the lack of information on bed-material loads in most practical cases, the characteristics of sub-surface bed layer could be considered as input to the sediment relationships. The inclusion of surface layer is not appropriate for reliable estimation of the sediment transport capacity.

This study does not intend to introduce a single relationship for the prediction of each of the three modes of sediment loads in coarse-bed rivers (i.e. suspended, bed and total loads). The results indicated that such a relationship is impossible to achieve for different reaches, and for different flow conditions. Those relationships which are located within the range of field data could be considered as the best fitted predictors. As presented in Tables 5 to 7, the average and the range of predictive errors are to be considered for the estimation of sediment load in such a complex problem.

For the prediction of suspended load, the overall results indicated that the relationship of Engelund (1965) gives better predictions in the three coarse-bed river reaches. With the inclusion of bed-load material, the predictive error was estimated to be in the range of -97% to -48% with an average of -77%. When sub-surface layer is included, the calculated suspended loads are reduced in half (by 200%), in average.

For the prediction of bed load, the methods of Schoklitsch (1934, 1943), Rottner (1959), Parker (1990), Zanke (1987), Wilcock (2003) and Sun & Donahue (2000) are more reliable than the others. The predictive error was estimated to be in the range of -58% to +193% with an average of +37%. With the inclusion of sub-surface layer, the calculated bed loads are reduced by 10%, in average.

For the evaluation of total sediment load, the relationships of Ackers & White (1990) Engelund & Hansen (1967), Yang & Lim (2003), and Karim & Kenedy (1990) resulted in better predictions in the river reaches under different flow conditions. The predictive error was estimated to be in the range of -95% to -48% with an average of -74%. With the inclusion of sub-surface layer, the total sediment loads are reduced by 50% in average.

The previous study in these three coarse-bed rivers indicated that the ratios of bed load to total load are in the order of 40% to 80%, which are significantly much higher than that in sand-bed rivers (Yasi and Hamzepouri, 2008).

The evident discrepancies in the prediction of the sediment loads are considered to be largely as the results of uncertainties in: (1) the present state of the hydraulic relationships; (2) the contribution of wash load; (3) the lack of field sediment data for the range of high flows, and (4) the unavoidable order of errors in the state of the art of the field measuring devices and techniques. These are major challenges in coarse-bed river engineering

REFERENCES

- Almedeij, J. H. and Diplas, P. (2003). "Bed load transport in gravel bed streams with unimodal sediment." *J. Hydr. Eng., ASCE*, 129 (11): 896-904.
- ASCE Task Committee (1971). "Sediment transportation mechanics: Sediment discharge formulas." *J. Hydr. Div., ASCE*, 97 (HY4): 523-567.
- Fisher, K. R. (1995). "Manual of sediment transport in rivers." Report No. SR359, HR Wallingford, UK, 75 p.
- Hamzepouri, R. (2005). "Evaluation of sediment transport rate in coarse-bed rivers in the Aras River-Western Basin." M. Sc. Thesis, Dept. of Water Engineering, Urmia University, Urmia. Iran, 220 p., in Persian.
- Habersack, H. M., Laronne, J. B. (2002). "Evaluation and improvement of bed load discharge formulas based on Helly-Smith sampling in an alpine gravel bed rivers." *J. Hydr. Eng., ASCE*, 128 (5): 484-499.
- Hey, R.D., Bathurst, J.C., and Thorne, C.R. (1982) "Gravel-bed rivers: Fluvial processes, engineering and management." John Wiley and Sons Ltd., N.Y., 875 p.
- Linsley, R.K. and Franzini, J.B. (1979) "Water resources engineering." Mc. Graw-Hill Book Co., N.Y., 716 p.
- Parker, G., Klingeman, P.C., and McLean, D.G. (1982). "Bed load and size distribution in paved gravel-bed streams." *J. Hydr. Div., ASCE*, 108 (4): 544-571.
- Przedwojski, B., Blazjewski, R., and Pilarczyk, K.W. (1985). "River training techniques: Fundamental, design and application." A.A. Balkema, Rotterdam, N.L., 625 p.
- van Rijn, L.C. (1993). "Principles of sediment transport in rivers, estuaries and coastal seas." AQUA Publication, N.L., 360 p.
- Yang, C. T. (1986). "Sediment transport: theory and practice." Mc. Graw-Hill Book Co., N.Y., 263 p.
- Yasi, M. and Hamzepouri, R. (2008). "Ratio of bed load to total sediment load in coarse-bed rivers." Proc., Fourth International Conference on Scour and Erosion, ICSE-4 Tokyo, 5-7 November 2008 (CD-ROM), Tokyo, Japan.

Prediction Of Localized Scour Hole On Natural Mobile Bed At Culvert Outlets

Soleyman Emami¹ and Anton J. Schleiss²

¹ Mahab Ghodss consulting engineering, Tehran – Iran;

Email: Soleyman_emami@yahoo.com

² Laboratory of Hydraulic Constructions (LCH), Swiss Federal Institute of Technology of Lausanne (EPFL); Anton.Schleiss@epfl.ch

Abstract

Systematic physical tests were conducted to evaluate the natural mobile bed erosion without any protection measure. The experiments were performed using a hydraulic model built at the Laboratory of Hydraulic Constructions of the Swiss Federal Institute of Technology in Lausanne. In the preliminary tests, the principal parameters were found to be the discharge, tailwater depth, pipe diameter, and the bed material properties.

Upon the completion of scour tests, an empirical analysis was conducted to correlate the maximum depth, length, width and distance of maximum depth from the outlet, tailwater depth and downstream bed characteristics. The maximum depth, length and width of the scour hole were presented in dimensionless relationships for various of discharges and tailwater depths. Based on the tests results, general applicable design charts and formulas for defining the local scour hole have been developed. The results of present experimental study have compared with some results of other authors.

1 Experimental work

1.1 Experimental facility

The experiments were conducted using a hydraulic model with 7 m length, 2.5 m wide and consist of different parts:

- A horizontal pipe with 10 cm diameter and 1.0 m length, which was connected to the pump. Water flow was controlled upstream of the pipe using a hand operated valve.
- Alluvial bed with 3.2 m length, 2.2 m width and 3% slope. The height of the bed was 0.7 m at the pipe outlet.
- Hand operated tailwater flip gate situated at 3.2 m from the pipe outlet to control the tailwater level.
- Basin with dimension of 1.2 m length and 1.5 m width at the end of the model which was equipped with a rectangular sharp-crest weir to measure the discharge.
- Outlet channel.

In all tests an almost uniform graded non-cohesive sediment $\sigma_g = \sqrt{(d_{84} / d_{16})} = 3.16$ were used in the downstream area of the pipe. At the beginning of each test, the sediment bed was levelled using guide rails on the side of the channel with a longitudinal slope of 3% (Figure 1, left). A hand operated tailwater flip gate was used downstream of the sediment bed to change the tailwater depth and a point gage for measuring the tailwater depth which was situated upstream of the gate (Figure 1, right).

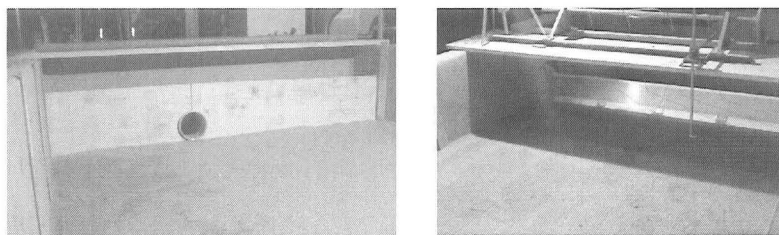


Figure 1: Alluvial bed; view towards upstream (left), view towards downstream, tailwater flip gate and point gage (right)

1.2 Scope of tests

In the preliminary tests, the principal parameters were found to be the discharge rate, the tailwater depth, the diameter of the pipe, and the bed material properties. The systematic tests investigated the effect of these principal parameters on the scour hole characteristics. Test conditions of these experimental studies are summarized in Table 1.

Table 1: Experimental conditions

Tests	Natural bed
Discharge (l/s)	$5.0 < Q < 12.5$
Tailwater variable ($D=10$ cm)	$0.1 < h_{TW}/D < 0.2$ $1.0 < h_{TW}/D < 1.1$
Discharge Intensity	$0.9 < Q/(g^{0.5} \cdot D^{2.5}) < 1.3$
Densimetric Froude number	$7.5 < F_0 < 14.5$
Geometric standard deviation of the bed, $\sigma_g = \sqrt{(d_{84} / d_{16})}$	3.16
d_{50} / D	0.008

1.3 Experimental procedure

To start each test, flow was introduced slowly to avoid initial local scouring of the bed. When the tailwater depth was reached to the desired level, the flow rate was increased to desired discharge and then remained constant throughout the test period. The water surface was read with a point gage situated upstream of the tailgate and discharge was measured using a rectangular sharp-crest weir in the downstream basin of the hydraulic model. Each tests was allowed to continue for 2.5 hours in order to achieve almost equilibrium conditions. The rate of change of the scour profile between 75 minutes and 150 minutes was less than a few millimetres.

2 Analysis of the results

The results of tests in natural mobile bed were analysed in order to compare the local scour development in different conditions. The scour hole geometry for each series of tests was presented in dimensionless form and discussed.

Upon the completion of 40 scour tests, an empirical analysis was conducted to correlate the maximum depth (d_{sc}), length (L), width (W) and distance of maximum depth from the pipe outlet (X) to the discharge, tailwater depth and downstream bed characteristics. Analysis of the results was performed using high and low tailwater depths.

2.1 Dimensional analysis

Scour hole geometry depends on many variables that characterize the conduit, the bed material and the flow. These parameters are:

- velocity u_0
- tailwater depth, h_{TW}
- pipe diameter, D
- pipe slope, S
- pipe roughness coefficient, n
- particle size of the bed material, d_{50}
- density of the bed material, ρ_s
- water density, ρ
- dynamic viscosity of the water, μ
- acceleration due to gravity, g

Thus, if "y" represents any dimension of the scour hole, then

$$y = f(u_0, h_{TW}, D, S, n, d_{50}, \rho_s, \rho, \mu, g) \quad (1)$$

However, for the purpose of this study some of these variables can be disregarded, and only the more significant ones are preserved. First, $S = 0$ since the pipe was horizontal. Furthermore the water viscosity μ was assumed to be constant. The pipe roughness coefficient n was also eliminated, because the same pipe was used during all the tests. Thus the equation (1) simplifies to:

$$y = f(u_0, h_{TW}, D, d_{50}, \rho_s, \rho, g) \quad (2)$$

Upon performing dimensional analysis, the following non-dimensional function was obtained:

$$y = f(F_0, h_{TW}/D) \quad (3)$$

In the equation (5.3), F_0 represents the densimetric Froude number expressed as $u_0 / \sqrt{(\rho_s / \rho - 1) \cdot g \cdot d_{50}}$.

2.2 Definition of the scour hole geometry

The different parameters of the scour hole geometry are described in Figure 2.

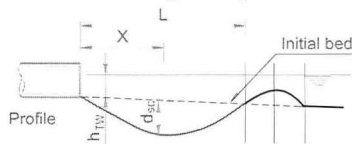


Figure 2: Definition sketch for scour hole geometry

2.3 Tailwater effect

The results of the scour hole for high and low tailwater depths are shown in Figure 3.

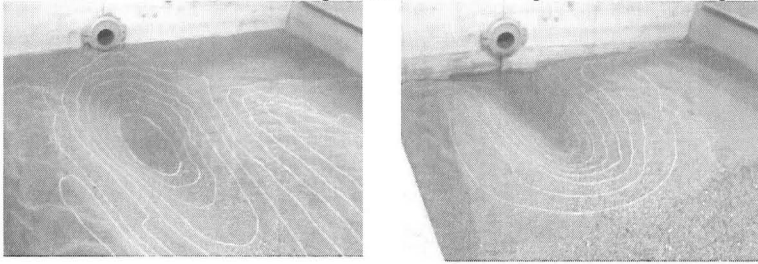


Figure 3: high tailwater depth (left), low tailwater (right) – $Q=12.5$ l/s

2.4 Equilibrium scour profile

Figure 4 represents the equilibrium scour profiles during experimental tests under a variety of discharge and tailwater conditions.

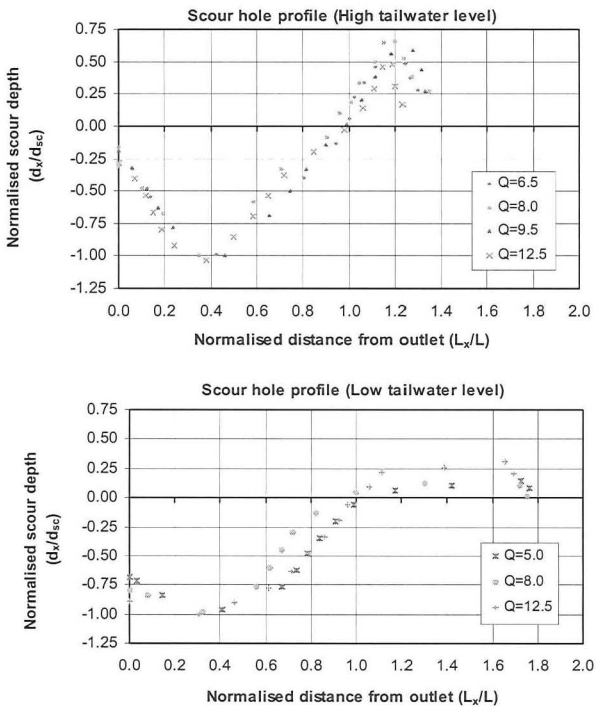


Figure 4: Equilibrium scour profile with different discharges and tailwater conditions

According to the equilibrium scour profile, it is observed that:

- The maximum erosion depth is located about 40% of the maximum scour length from the pipe outlet in case of high tailwater depth ($1.0 < h_{TW}/D < 1.1$),
- For low tailwater depth ($0.1 < h_{TW}/D < 0.2$), the maximum erosion depth is located about 30% of the maximum scour length from the pipe outlet,
- Scour depth at the pipe outlet for high and low tailwater depth is 25% and 75% of the maximum scour depth respectively.

2.5 Graphical representation of the experimental data

According to the dimensional analysis, the parameters of the scour hole geometry were correlated to the densimetric Froude number, F_0 , as:

$$F_0 = u_0 / \sqrt{(\rho_s / \rho - 1) \cdot g \cdot d_{50}}$$

Logarithmic regression lines were compiled correlating the scour hole depth for different tailwater conditions to the densimetric Froude number as presented in Figure 5. This type of line had the highest Correlation coefficient, r^2 , comparing than the other types.

Similar plots were compiled for the scour length, the distance of maximum scour depth from the pipe outlet and the scour width. These results are presented in Figures 6 – 7 respectively.

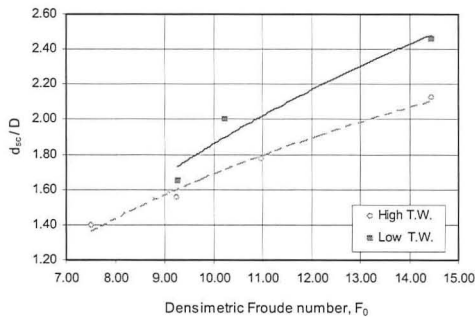


Figure 5: Variation of the scour hole depth with the densimetric Froude number

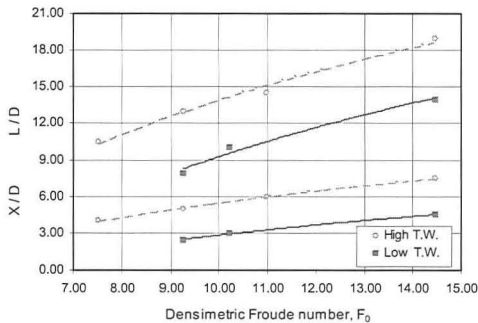


Figure 6: Variation of the scour hole length and the distance of maximum scour depth from pipe outlet with densimetric Froude number

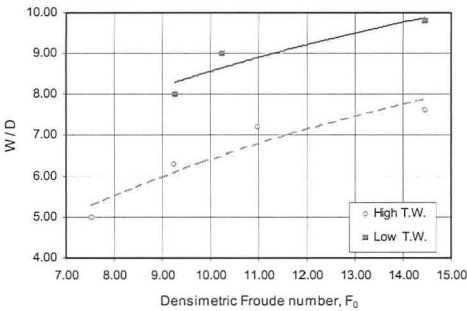


Figure 7: Variation of the scour width with the densimetric Froude number

- Graphical representation of data indicates that for $7.5 < F_0 < 14.5$:
- For similar values of the densimetric Froude number, the maximum depth of scour hole; d_{sc} , is approximately 10 - 25% more in case of low tailwater depth.
 - The value of L/D and X/D are less than the corresponding value for the case with high tailwater depth.
 - The scour hole width; W , is approximately 30% more in case of low tailwater depth.

2.6 Formula for evaluation of the scour hole on mobile riverbed

According to the analysis of the experimental data, the non-dimensional relationships of scour hole geometry for each tailwater depth can be written as:

$d_{sc}/D, L/D, X/D$ and $W/D = f(F_0)$

In order to find the highest Correlation coefficient, r^2 , different regression lines were fitted through the data. The best result was a logarithmic regression as an equation with the form of $y = a \cdot \ln(x) + b$ (4)

where;

y = dimensionless parameter of the scour hole, a, b = constant

x = the densimetric Froude number defined $u_0 / \sqrt{(\rho_s/\rho - 1) \cdot g \cdot d_{50}}$

The parameters and coefficients of the equation (4) summarized in Table 2.

Table 2: Summary of equation coefficients

Scour hole characteristics	y	a	b	Tailwater condition	Correlation coefficient, r^2
Maximum scour depth	d_{sc}/D	1.14	-0.93	1.05·D	0.99
		1.69	-2.04	0.15·D	0.95
Maximum scour length	L/D	12.81	-15.55	1.05·D	0.99
		13.15	-21.02	0.15·D	0.98
Distance of d_{sc} from pipe outlet	X/D	5.39	-6.92	1.05·D	0.99
		4.62	-7.82	0.15·D	0.99
Maximum scour width	W/D	3.97	-2.72	1.05·D	0.91
		3.59	0.28	0.15·D	0.87

In Figure 8, the values of the coefficients “a” and “b” are presented versus h_{TW}/D for each dimensionless parameter of the scour hole.

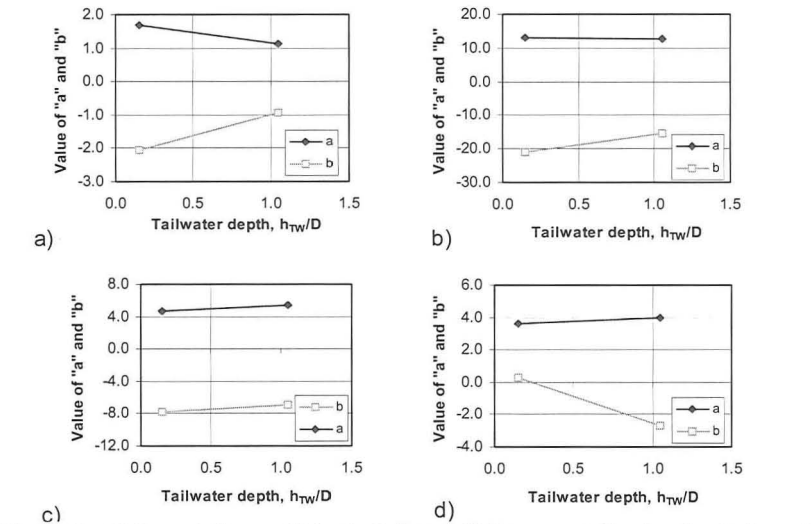


Figure 8: Values of the coefficients “a” and “b” versus tailwater depth for; a) maximum scour depth, b) maximum scour length, c) distance of maximum scour depth from the pipe outlet, d) maximum width of scour

The values of “a” and “b” with function of h_{TW}/D are presented in Table 3. Scour hole characteristics could be calculated using these values in the equation 4, $y = a \cdot \ln(x) + b$.

$$x = u_0 / \sqrt{(\rho_s / \rho - 1) \cdot g \cdot d_{50}}$$

Table 3: Summary of equation coefficients, scour hole on natural mobile bed function of tailwater depth

Dependent variable of scour hole geometry, y	a	b
d_{sc} / D	$-0.60 \cdot (\frac{h_{TW}}{D}) + 1.80$	$1.23 \cdot (\frac{h_{TW}}{D}) - 2.25$
L / D	$-0.38 \cdot (\frac{h_{TW}}{D}) + 13.20$	$6.08 \cdot (\frac{h_{TW}}{D}) - 21.95$
X / D	$0.86 \cdot (\frac{h_{TW}}{D}) + 4.49$	$1.00 \cdot (\frac{h_{TW}}{D}) - 7.97$
W / D	$-0.42 \cdot (\frac{h_{TW}}{D}) + 3.53$	$-3.33 \cdot (\frac{h_{TW}}{D}) + 0.78$

3 Comparison of the results

Formulas proposed for calculating scour hole characteristics by different authors have been presented in Table 4. It is established that scour hole is calculable using tailwater depth, culvert outflow velocity and particle size of the bed material. In this chapter, the results of present experimental study for scour hole on natural mobile bed have compared with some other authors results.

Table 4: Comparison of different formulas conditions

Researchers	Vertical dimension of the jet (mm)	Densimetric Froude F_0	Discharge intensity	Submerged ratio h_{TW}/D	Maximum scour depth formulas
Present study	100	7.5 – 14.5	0.9 – 1.3	0.15, 1.05	$d_{sc}/D = a \cdot \ln(x) + b$ $a = -0.60 \cdot (\frac{h_{TW}}{D}) + 1.80$ $b = 1.23 \cdot (\frac{h_{TW}}{D}) - 2.25$ $x = u_0 / \sqrt{(\rho_s / \rho - 1) \cdot g \cdot d_{50}}$
Lim (1995)	15, 26	1.91 – 24.6		0.47	$d_{sc}/D = (\frac{3.68}{\sigma_g}) \cdot F_0^{0.57} \cdot (\frac{d_{50}}{D})^{0.4}$
Abt et al. (1987)	102	7.2 – 21.81	0.9 – 3.14 (circular)	0.45 (± 0.05)	$d_{sc}/R_H = 7.84 \cdot (Q / (A \cdot g^{0.5} \cdot R_H^{0.5}))^{0.28}$
Abt, Kloverdanz, Mendoza (1984)	102, 254	2.0 – 24.4	0.3 – 3.1	0.45	$d_{sc}/D = 1.77 \cdot (\frac{Q}{g^{0.5} \cdot D^{2.5}})^{0.63}$
Abt, Ruff, Mendoza (1983)	102		0.4 – 3.0	0.45	$d_{sc}/D = 2.08 \cdot (\frac{Q}{g^{0.5} \cdot D^{2.5}})^{0.37}$
Ruff et al. (1982)	100.7, 260, 345, 446	7.3 – 33.7		0.00, 0.25, 0.45	$d_{sc}/D = 2.07 \cdot (\frac{Q}{g^{0.5} \cdot D^{2.5}})^{0.45}$
Abt and Ruff (1982)	273, 356, 457		0.5 – 2.0	0.45 (± 0.05)	$d_{sc}/D = 0.86 \cdot (\frac{\rho \cdot u_0^2}{\tau_c})^{0.18}$

Graphical comparison of the present experimental results and six other scour formulas are shown in Figure 9. The tests conditions of these six formulas indicate that all have concentrated on flow depth downstream of culverts less than half of the diameter, $h_{TW}/D = 0.45$.

In order to investigate the variation of the scour hole due to tailwater depth, the results of scouring for two other tailwater depths below and over the mentioned ratio have been presented by the present study.

The “hidden line” represents the mean values of the six scour formulas results and two other lines below and over show the present experimental results for submergence ratio of 1.05D and 0.15D respectively.

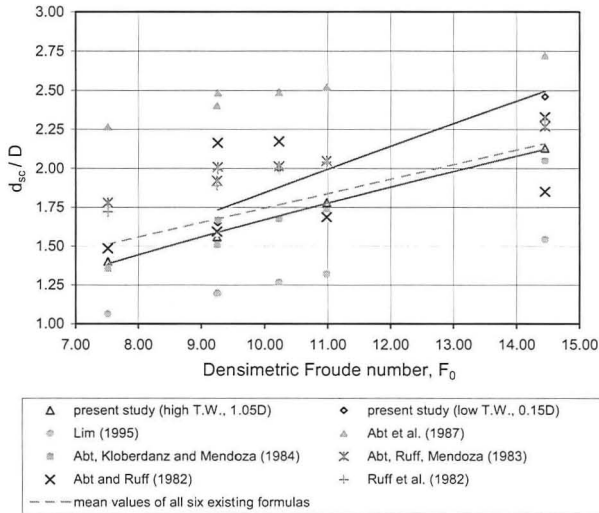


Figure 9: Comparison of the maximum scour depth results between the present study and other authors

On the six selected equations, only three equations defined the length and width of the scour hole. They consist of Abt et al. (1987), Abt, Kloverdanz, Mendoza (1984), and Abt and Ruff (1982).

It should be noted that the results of Abt et al. (1987) for the length of the scour hole has been eliminated because the scour length from square culverts deviated as much as 40% from the scour length of the circular culverts.

4 Conclusions

The experimental study for non-cohesive bed material led to the following conclusions:

- For low and high tailwater depths, the maximum erosion depth was located about 30% and 40% of the maximum scour length from the pipe outlet respectively.
- Scour depth immediately at the pipe outlet was 25% and 75% of the maximum scour depth for high and low tailwater depths respectively.
- For similar values of the densimetric Froude number, the maximum depth of scour hole was approximately 10 - 25% deeper in case of low tailwater depth.
- The scour hole length increased and the scour hole width decreased while increasing the tailwater level.
- The mean values of all investigated existing formulas were found to be close to the present study. The closer results were identified by the formulas of Abt, Kloverdanz & Mendoza (1984) and Abt & Ruff (1982), which had almost similar test conditions as the present study.
- Results of Lim (1995) and Abt et al. (1987) were found below and above the other experimental results. Lim (1995) used rather small culvert diameters and Abt et al. (1987) used different culvert shapes.

REFERENCES

- Abida, H. & Townsend, R.D. (1991). Local scour downstream of box-culverts. *Journal of Irrigation and Drainage Engineering*. Vol. 117, No. 1. pp. 425 – 440.
- Abt, S.R. & Ruff, F. (1982). Estimating culvert scour in cohesive material. *Journal of Hydraulic Division*, Proceeding of the American Society of Civil Engineering, ASCE, Vol. 108, No. 1. pp. 25 – 34.
- Abt, S.R., Kloverdanz, R.L. & Mendoza, C. (1984). Unified culvert scour determination. *Journal of Hydraulic Engineering*, Vol. 110, No. 10. pp. 475 – 479.
- Abt, S.R., Ruff, J.F., Doehring, F.K. & Donnell, C.A. (1987). Influence of culvert shape on outlet scour. *Journal of Hydraulic Engineering*, ASCE, Vol. 113. pp. 475 – 479.
- Bohan, J.P. (1970). Erosion and riprap requirements at culvert and storm-drain outlets. US Army Engineers Waterways Experiment Station, Vicksburg, Mississippi, Report No. H-70-2.
- Breusers, H.N.C. & Raudkivi, A.J. (1991). Scouring. IAHR, Hydraulic Structures Design Manual. No. 2.
- Chiew, Y. & Lim, S.Y. (1996). Local scour by a deeply submerged horizontal circular jet. *Journal of Hydraulic Engineering*, Vol. 122, No. 9. pp. 529 – 532.
- Day, R.A., Liriano, S.L. & White, W.R. (2001). Effect of tailwater depth and model scale on scour at culvert outlet. *Proceedings of the Institution of Civil Engineering, Water & Maritime Engineering* 148.
- Hoffmans, G.J.C.M. & Verheij, H.J. (1997). Scour Manual. Balkema: Rotterdam.
- Mendoza, C. (1980). Headwall influence on scour at culvert outlets. Thesis presented to Colorado State University, at Fort Collin, Colo.
- Mendoza, C., Abt, S.R. & Ruff, F. (1983). Headwall influence on scour at culvert outlets. *Journal of Hydraulic Engineering*, Vol. 109, No. 7. pp. 1056 – 1060.
- Oliveto, G. & Hager, W.H. (2002). Temporal evolution of clear-water pier and abutment scour. *Journal of Hydraulic Engineering*, Vol. 128, No. 9. pp. 811 – 820.
- Opie, T.R. (1967). Scour at culvert outlets. MSc Thesis, Colorado State University, Fort Collin, Colorado.
- Rajaratnam, N. & Berry, B. (1977). Erosion by circular turbulent wall jets. *Journal of Hydraulic Research. IAHR*. No. 3, pp. 277 – 289.
- Rajaratnam, N. & Diebel, M. (1981). Erosion Below Culvert-like Structures, Sixth Canadian Hydrotechnical Conference, pp. 469 – 484.
- Rajaratnam, N. (1998). Generalized study of erosion by circular horizontal turbulent jets. *Journal of Hydraulic Research*, Vol. 36, No.4. pp. 613 – 635.
- Stevens, M. A., and Simons, D. B. (1971). Stability analysis for coarse granular material on slopes. *River Mechanics*, H. W. Shen, Ed., Fort Collins, Colorado, 1, 17 - 1 Straub, L.G. Dredge fill closure of Missouri River at Fort Randall. *Proceeding of Minnesota International Hydraulics Convention*, Minneapolis, Minnesota. pp 61 – 75.
- Valentin, F. (1967). Consideration concerning scour in case of flow under gates. Proceeding, 12th Congress, IAHR, Vol. 3, Colorado State University, Fort Collins, Colorado.
- Whittaker, J.G. & Schleiss, A. (1984). Scour related to energy dissipaters for high head structures. ETHZ - VAW Report No. 73, Zürich.

Impacts of Debris on Bridge Pier Scour

P.F. Lagasse¹, F.ASCE, L.W. Zevenbergen², M.ASCE, and P.E. Clopper³, M.ASCE

^{1,2,3}Ayres Associates Inc, 3665 JFK Parkway, Building 2, Suite 200,
Fort Collins, CO 80525; PH (970) 223-5556; FAX (970) 223-5578; e-mail:
lagassep@ayresassociates.com, lylez@ayresassociates.com,
clopperp@ayresassociates.com

ABSTRACT

Waterborne debris (or drift) often accumulates on bridges during flood events. The effects can vary from minor flow constrictions to severe flow contraction resulting in significant bridge foundation scour. The results of National Cooperative Highway Research Program (NCHRP) Project 24-26, "Impacts of Debris on Bridge Pier Scour" represent a significant advance to predicting debris scour considering the variable geometry of debris clusters observed at bridge piers in the field. The study produced results on two related problems: predicting the accumulation characteristics of debris from widely varying source areas, and developing improved methods for quantifying the depth of scour at bridge piers. This paper highlights the observations from laboratory testing and the development of improved algorithms for predicting the depth of scour at debris-laden bridge piers.

INTRODUCTION

Waterborne debris (or drift), composed primarily of tree trunks and limbs, often accumulates on bridges during flood events. Debris accumulations can obstruct, constrict, or redirect flow through bridge openings resulting in flooding, damaging loads, or excessive scour at bridge foundations. The size and shape of debris accumulations vary widely, ranging from a small cluster of debris on a bridge pier to a near complete blockage of a bridge waterway opening. Debris accumulation geometry is dependent on the characteristics and supply of debris transported to bridges, on flow conditions, and on bridge and channel geometry. The effects of debris accumulation can vary from minor flow constrictions to severe flow contraction resulting in significant bridge foundation scour.

At the outset of NCHRP Project 24-26 in June 2004 there was a pressing need for State Departments of Transportation (DOTs) and other bridge owners to have improved prediction methods for the geometry (size and shape) of typical debris accumulations, and the conditions under which debris can be expected to develop. In addition, there was a need for accurate methods of quantifying the effects of debris on scour at bridge-pier foundations for use by DOTs and other agencies in the design, operation, and maintenance of highway bridges.

The objectives of NCHRP Project 24-26 were to produce results on two related problems: (1) predicting the accumulation characteristics of debris from potentially widely varying source areas, in rivers with different geomorphic characteristics, and on bridges with a variety of substructure geometries, and (2) developing improved methods for quantifying the depth and extent of scour at bridge

piers considering both the accumulation variables and the range of hydraulic factors involved (Lagasse et al. 2010). This paper highlights the observations from laboratory testing and the development of improved algorithms for predicting the depth of scour at debris-prone bridges.

OVERVIEW OF RESEARCH APPROACH

As an extension of the original work by Diehl (1997) for the Federal Highway Administration (FHWA), guidelines and flow charts were developed for estimating the potential for debris production and delivery from the contributing watershed of a selected bridge, and the potential for accumulation on individual bridge elements. The application of the guidelines was illustrated by a case study of a debris-prone bridge on the South Platte River in Colorado. The case study introduces and illustrates the use of Field Reconnaissance Data Sheets for evaluating the potential for debris production and delivery from a given watershed.

As a basis for laboratory testing, an extensive photographic archive of debris accumulations at bridges nationwide was assembled. This archive includes 1079 photos at 142 sites in 31 states. The archive together with a field pilot study of debris sites in Kansas, and the South Platte River case study were examined to develop a limited number of debris shapes that would represent the maximum number of configurations found in the field. Simplified, yet realistic, shapes that could be constructed and replicated with a reasonable range of geometric variables were needed for laboratory testing. Rectangular and triangular shapes with varying planform and profile dimensions were selected to represent prototype debris accumulations. To account for additional variables thought to be relevant to debris clusters in the field, a method to simulate both the porosity and roughness of the clusters was developed.

The laboratory testing program included the use of a large indoor flume at Colorado State University and model bridge pier shapes, development of state-of-the-art instrumentation for data acquisition, and a wide range of materials to fabricate the debris clusters. Baseline tests were conducted and results were compared with several pier scour prediction equations. A series of tests under clear-water conditions with the various debris shapes were completed. The following sections highlight the laboratory testing and analytical phases of the project.

LABORATORY TESTING OF DEBRIS

Testing Requirements

The objective of laboratory testing was to provide sufficient data for a range of debris accumulations to develop adjustment factors to FHWA's HEC-18 pier scour equation (Richardson and Davis 2001). The laboratory plan was designed to develop a series of tests for a wide range of debris configurations that could be run quickly and efficiently. The tests were performed for single debris clusters at individual piers, which was the most prevalent type of debris accumulation identified for all physiographic regions in the U.S. The majority of the testing was performed for clear-water sediment transport conditions (approach flow velocity (V) less than the critical

velocity to initiate sediment transport (V_c) for durations much less than would be required to achieve ultimate scour. The duration was, however, sufficient to achieve at least 60% of ultimate scour.

Debris Dimensions

All of the physical modeling was conducted in the 2.4 m (8 ft) wide flume at Colorado State University under clear-water flow conditions. Square piers 10.2 cm (4 inches) in width were used for most runs, although slender wall-type piers and multiple-column piers were also tested. All of the dimensions were normalized by the pier width so the field conditions could be used to develop a realistic range of laboratory runs. The range of debris dimensions was selected to encompass the range observed in the field \pm one standard deviation around the mean.

The testing considered a range of debris characteristics including debris accumulation shape, thickness, width, and length. The range of debris accumulation size tested in the laboratory was related to actual debris accumulations observed in the field or from the photographic archive. Figures 1 and 2 illustrate typical debris shapes (rectangular and conical in profile and either rectangular or triangular in planform) that were modeled and define the dimensions for the various shapes.

Figure 3 shows a 1.22 m (4 ft) wide by 0.9 m (3 ft) long by 0.3 m (1 ft) high triangular debris configuration incorporating roughness and porosity before testing. Figure 4 shows the results of testing the debris configuration after 8 hours of testing at $1.0 V_c$. The upper segment of the pier has been removed for data collection purposes. Ambient bed elevation is represented by the top of the lower segment of the pier.

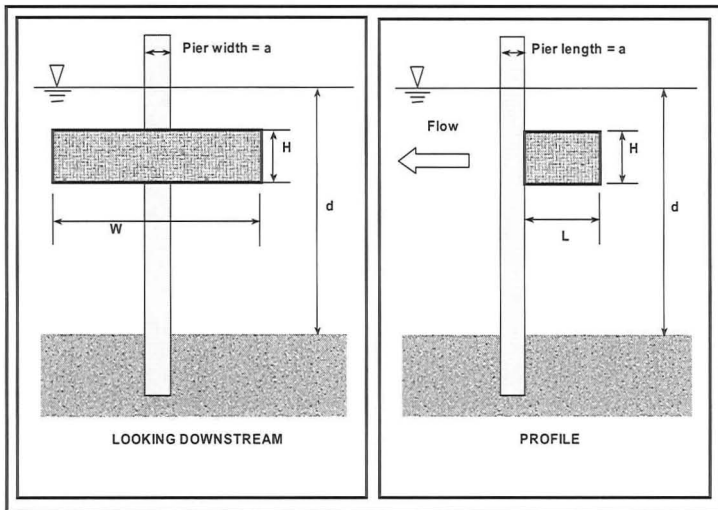


Figure 1. Rectangular shape definition sketch.

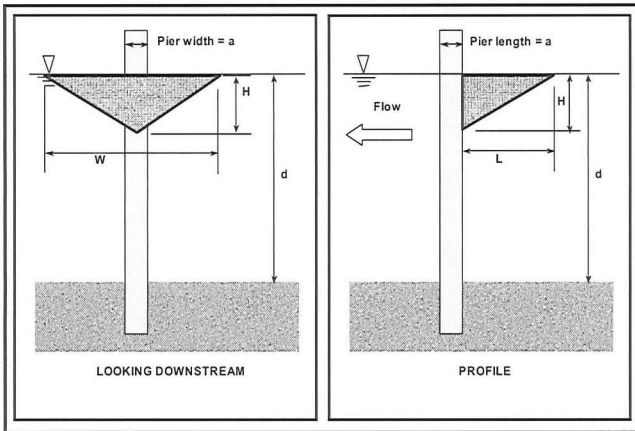


Figure 2. Triangular/conical shape definition sketch.

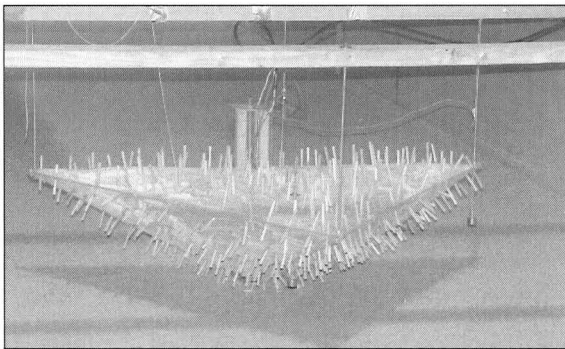


Figure 3. Triangular/conical debris cluster before Test 007_02A, mounted such that the top surface of the debris was located at the water surface.

SCOUR PREDICTION AT BRIDGE PIERS WITH DEBRIS LOADING

Introduction

The laboratory testing program was conducted to develop information on a variety of factors related to debris accumulations at piers including:

- Shape: Rectangular or triangular
- Size: Width, length, and thickness
- Location: Surface (floating), mid-depth, or bed (partially buried)
- Roughness: Smooth or roughened
- Porosity: Impermeable or 25% porosity
- Approach velocity: V/V_c ratios of 0.70 and 1.0



Figure 4. Scour hole resulting from Test 007_02A after 8 hours of testing at $1.0 V_c$.

Selected combinations of these factors were also tested; for example, a particular debris shape might be tested as (1) a smooth impermeable body, (2) a smooth porous body, (3) a rough impermeable body, and (4) a rough porous body. Factors not considered in the test program include the effect of bed material grain size, flow depth, live-bed conditions, and contraction scour. Fifty-three tests of debris-laden piers were run under clear-water scour conditions. Most of the tests (35) were conducted with the top surface of the debris at the water surface, forming a "raft." Selected tests were also performed with the debris located in the center of the water column, resting on the bed, or buried into the bed.

Equivalent Pier Width

All pier scour prediction equations use pier width as a factor that contributes to the estimated scour depth. Intuitively, the accumulation of debris on a pier causes the pier to appear larger in the flow field, thereby increasing the total area blocked by obstruction. HEC-18 (Richardson and Davis 2001) uses the width W of the debris perpendicular to the flow direction to estimate the additional obstruction.

Melville and Dongol (1992) provide an equation to calculate the "equivalent width," b_e , of a bridge pier that is loaded with debris. The equation uses both the width W and thickness T of the debris, and is based on scour data from a limited number of tests (17 tests) in a laboratory flume. Only floating (surface) debris at cylindrical piers was tested, with the debris wrapped around the pier in all directions. The effect of the vertical location of the debris mass within the water column was not investigated. Their equation to calculate equivalent pier width is:

$$b_e = \frac{K_{d1}(TW) + (y - K_{d1}T)a}{y} \quad (1)$$

where:

- b_e = Effective width of the pier, m (ft)
- K_{d1} = Dimensionless coefficient equal to 0.52 from lab tests (Dongol 1989)
- T = Thickness of debris, m (ft)
- W = Width of debris normal to flow, m (ft)
- a = Pier width (without debris) normal to flow, m (ft)
- y = Depth of approach flow, m (ft)

Comparing a calculated effective pier width (b_e) with an observed effective width indicates that the Melville-Dongol equation tends to overestimate the effective width of the pier when debris is present, particularly for triangular shapes. The Melville-Dongol equation does not take into account the shape of the debris mass (e.g., rectangular vs. triangular), nor does it consider the length L of the debris extending upstream from the pier.

A modification to the equivalent width equation was, therefore, proposed and tested against the laboratory data. The proposed modification is denoted as " a_d^* " to distinguish it from the Melville and Dongol " b_e ," and is given as:

$$a_d^* = \frac{K_{d1}(TW)(L/y)^{K_{d2}} + (y - K_{d1}T)a}{y} \quad (2)$$

where:

- K_{d1} = Dimensionless coefficient optimized from lab test data
 - K_{d2} = Dimensionless exponent optimized from lab test data
 - L = Length of debris upstream from pier face, m (ft)
- Other terms are as defined previously.

Optimizing the coefficient K_{d1} and exponent K_{d2} to the observed laboratory data revealed that the shape and upstream extent of the debris do affect the resulting scour at the pier face. For rectangular debris shapes, K_{d1} and K_{d2} were found to be 0.39 and -0.79, respectively, whereas for triangular shapes, K_{d1} and K_{d2} were 0.14 and -0.17, respectively. **The coefficient K_{d1} is thus seen to be a shape factor, while the exponent K_{d2} is a factor that describes the intensity of the plunging flow created by the debris blockage.**

A relationship better suited to design should tend towards conservatism; that is, underestimation of the observed (i.e., actual) scour should be relatively rare. Based on the laboratory data developed for an approach velocity of $1.0 V_{crit}$, the shape coefficient K_{d1} that provides overestimation 90% of the time (underestimating 10% of the observations) is 0.79 for rectangular debris shapes, and 0.21 for triangular shapes.

The recommended design equations for estimating an equivalent pier width for use with the HEC-18 pier scour equation are, therefore:

$$a_d^* = \frac{K_{d1}(TW)(L/y)^{K_{d2}} + (y - K_{d1}T)a}{y} \quad \text{for } L/y > 1.0 \quad (3)$$

and

$$a_d^* = \frac{K_{d1}(TW) + (y - K_{d1}T)a}{y} \quad \text{for } L/y \leq 1.0 \quad (4)$$

where:

- K_{d1} = 0.79 for rectangular debris, 0.21 for triangular debris
 - K_{d2} = -0.79 for rectangular debris, -0.17 for triangular debris
 - L = Length of debris upstream from pier face, m (ft)
 - y = Depth of approach flow, m (ft)
- Other terms are as defined previously.

The design or "envelope" values using the recommended equations are shown in Figure 5 for all runs with debris at the water surface and an approach velocity of $1.0 V_{crit}$. In this figure, the HEC-18 pier scour equation is used to predict ultimate clear-water scour at the pier face, using the equivalent pier width calculated by Equations 3 and 4 and the recommended K_{d1} and K_{d2} values presented above.

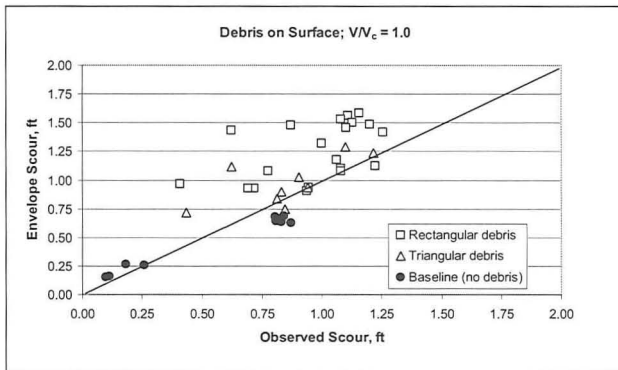


Figure 5. Comparison of observed scour to the recommended design equation using 90% envelope values.

CONCLUSIONS

Observations From Laboratory Testing

The scour processes observed in the laboratory can be visualized by comparing idealized flow lines at a pier with no debris to those at a pier with rectangular and triangular debris clusters. In Figure 6, the flow lines at an unobstructed pier are essentially uniform in the approach section. At the pier, the flow dives down the front face and spirals past the pier in the classic "horseshoe vortex" pattern.

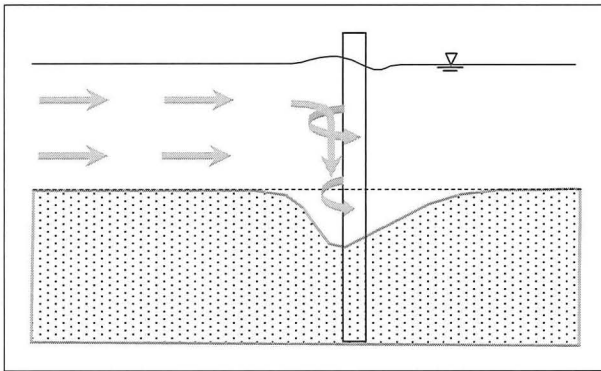


Figure 6. Idealized flow pattern at an unobstructed pier.

In contrast, flow at a pier with a rectangular debris cluster is significantly obstructed and forced to plunge beneath the upstream face of the debris as shown in Figure 7. **The plunging flow creates the upstream scour trough that was observed consistently during the laboratory testing program.**

Because of the blockage created by the debris, some flow is forced around the sides as well. As the flow beneath the debris approaches the pier, the diving and spiral horseshoe patterns are still observed. Depending on the degree of blockage compared to the entire channel (flume) cross section, the relative strengths of the diving flow and horseshoe vortex may be greater or less than the unobstructed case.

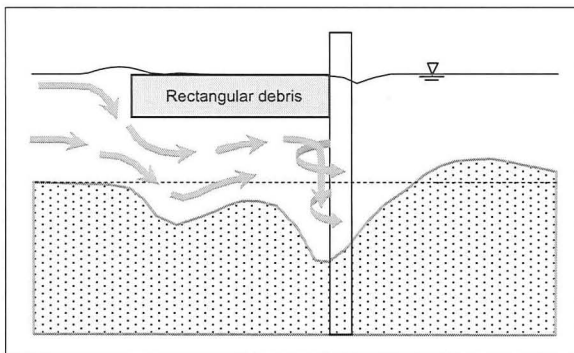


Figure 7. Idealized flow pattern at a rectangular debris cluster.

Rectangular, blocky debris masses tended to produce the greatest scour at the pier when the extent ("length" dimension) of the debris upstream of the pier was on the order of one flow depth. This condition produced plunging flow that was directed toward the channel bed in the immediate vicinity of the pier face, resulting in a worst-case scour condition (i.e., when the upstream trough coincides with scour generated

by the pier). Total scour at the pier was also significantly increased when the total frontal area of flow blockage (as a percent of the cross-sectional area of the approach channel) was large. In that case, the debris-induced scour appeared to be similar to that created by pressure flow and contraction effects, for example, pressure flow beneath bridge decks that are submerged during floods.

Triangular-shaped debris clusters were also investigated, because the debris photo archive revealed that this is another very common shape that can be produced in the field as drift accumulates at a pier. In a triangular configuration, the thickness of the debris is greater at the pier face, tapering upward and thinning toward the leading (upstream) point. The scour pattern created by triangular debris clusters (Figure 8) was markedly different from that exhibited by the rectangular clusters. **No scour troughs upstream of the pier were observed with any of the triangular debris clusters.**

The portion of the flow that plunges beneath a triangular/conical blockage is seen to be funneled towards the pier face, creating additional scour at the pier compared to the baseline condition. The scour at the pier face was found to be related to the thickness of the debris blockage at the pier face; i.e., a greater thickness of debris lodged directly against the pier created more scour at the pier face, with the triangular debris shapes.

As with the rectangular debris tests, lateral extent of scour created by triangular debris clusters was directly related to the width of the cluster. However, the lateral extent of scour caused by a triangular debris cluster was shown to be greater than that of a rectangular one. This appears to be caused by the shedding of flow around the triangular shaped debris, and has implications regarding the effect of this shape at adjacent piers or abutments.

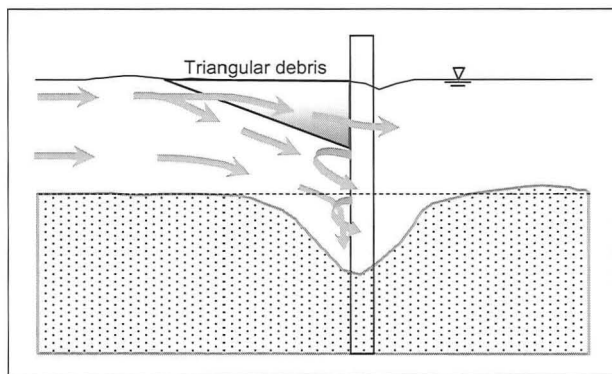


Figure 8. Idealized flow pattern at a triangular debris cluster.

The laboratory studies revealed that the roughness and porosity of a debris mass do not significantly affect the pattern of scour or the magnitude of the scour depth at the pier face. For the range of these properties examined, debris roughness and porosity can be considered, at most, second-order variables that are not significant compared to the size, shape, and location of the debris mass.

Scour Prediction at Bridge Piers with Debris Loading

Building on the algorithm originally proposed by Melville and Dongol and using an equivalent pier width, a_d^* , an improved predictive equation is now available. Considering the most common shapes of debris clusters (rectangular in planform and profile, and triangular in planform but conical in profile) length, width, and thickness of the debris accumulation upstream of a bridge pier can now be considered. Different coefficients and exponents based on more extensive laboratory testing are recommended, but the basic form of the effective width equation is retained. The recommended equation is stable, can be adapted to most conditions found at bridge piers in the field, and complements the approach to estimating pier scour currently recommended in FHWA's HEC-18.

The end results of NCHRP Project 24-26 are practical, implementable guidelines for bridge owners that enhance their ability to predict debris-related hazards at bridges and design, operate, inspect, and maintain bridges considering those hazards. The results of this research were published by the Transportation Research Board as NCHRP Report 653 in June 2010.

REFERENCES

- Diehl, T.H. (1997). "Potential Drift Accumulation at Bridges," Report FHWA-RD-97-28, U.S. Department of Transportation, Federal Highway Administration Research and Development, Turner-Fairbank Highway Research Center, McLean, VA.
- Dongol, M.S. (1989). "Effect of Debris Rafting on Local Scour at Bridge Piers," Report No. 473, School of Engineering, University of Auckland, Auckland, New Zealand.
- Lagasse, P.F., Clopper, P.E., Zevenbergen, L.W. (2010). "Effects of Debris on Bridge Pier Scour," NCHRP Report 653, Transportation Research Board, National Academies of Science, Washington, D.C.
- Melville, B.W. and Dongol, D.M. (1992). "Bridge Pier Scour with Debris Accumulation," *Journal of Hydraulic Engineering*, Vol. 118, No. 9, pp. 1306-1310.
- Richardson, E.V. and Davis, S.R. (2001). "Evaluating Scour at Bridges," Fourth Edition, *Hydraulic Engineering Circular No. 18*, Federal Highways Administration Publication No. FHWA NHI 01-001, Washington, D.C.

From Auwaiakeakua to Weoweopilau: Assessing Scour Critical Bridges in Hawaii (It's a Tough Job, But Someone Has To Do It)

Christine Warren¹, P.E., Jake Gusman², P.E., Martin J. Teal³, P.E., P.H.,
Mike Hunnemann⁴, P.E., Curtis Matsuda⁵, P.E.

¹WEST Consultants, Inc., Senior Hydraulic Engineer, 11440 W. Bernardo Court, Suite 360, San Diego, CA 92127. Email: cwarren@westconsultants.com

²WEST Consultants, Inc., Project Manager, 11440 W. Bernardo Court, Suite 360, San Diego, CA 92127.

³WEST Consultants, Inc., Vice President, 11440 W. Bernardo Court, Suite 360, San Diego, CA 92127.

⁴KAI Hawaii, Inc., Vice President, 31 N. Pauahi Street, 2nd Floor, Honolulu, HI 96817.

⁵Hawaii DOT, Hydraulic Design Engineer, Highways Division, 601 Kamokila Blvd, Room 636, Kapolei, HI 96707.

ABSTRACT: In the State of Hawaii, nearly 60 bridges have been identified as potentially scour critical based on observed or anticipated conditions at the bridges. The Hawaii Department of Transportation (DOT) is preparing a Plan of Action (POA) for each bridge that will outline procedures for Hawaii DOT personnel to follow during high flow events to help ensure public safety. Each POA will include a scour vulnerability assessment, recommended actions including hydraulic/structural countermeasures, increased inspections, and/or flood monitoring, and a bridge closure plan. Waterways involved range from large, sand-bed rivers along the coastline of Oahu to the steep, rocky Hamakua Coast on the Big Island. A number of bridges on the historic Hana Highway on Maui are also included. Drainage areas range from less than 0.5 km² to nearly 650 km². Flows were developed for each bridge based on available data along with a detailed hydraulic analysis. Scour vulnerability was determined based on contraction and pier scour depths using HEC-18 guidelines.

INTRODUCTION

The Federal Highway Administration (FHWA) has collected information on nearly 600,000 of the nation's bridges and created the National Bridge Inventory (NBI) database. This database includes the number, location, and general condition of bridges in each state. Item 113 in the database is used to indicate the status of each bridge regarding scour vulnerability. A bridge is identified as *scour critical* if the value for Item 113 is between 0 and 3, with a value of 3 indicating that the bridge foundations were determined to be unstable based on a calculated or assessed scour depth being at or below the footing base or pile tips, and a value of 0 indicating the bridge has failed and is closed to traffic (FHWA, 1995). In the State of Hawaii, 57 bridges have been identified as *scour critical* on the NBI database. These bridges are spread throughout the five major islands and include those on Oahu (22), Kauai (10), Hawaii (13), Maui (10), and Molokai (2). A summary is provided below of the bridges located on each of the islands.

Island of Oahu

The Island of Oahu is the most populated of the Hawaiian Islands and also has the most developed highway system. Twenty-two bridges were determined to be scour critical and their locations are shown in Figure 1. The bridges encompass the entire island and they cover a wide variety of hydraulic and hydrologic characteristics. Drainage areas range from 0.4 km² for Kapalaau Stream to 100 km² for Kaukonahua Stream, both located on the northwest side of the island on State Highway 930 near Waialua. There are bridges that cross steep, gravel bed streams on the east coast of the island near Kaneohe Bay and those that cross relatively flat, sand bed streams near Waimea Bay along the scenic and popular North Shore. The Manoa-Palolo and Kalihi Stream bridges are located in the urbanized city of Honolulu, while a large number of bridges are in more rural areas. The majority of the bridges are located on the coastal highway loop that consists of the Kamehameha and Farrington highways. Only six bridges are located more than 500 feet from the Pacific Ocean.

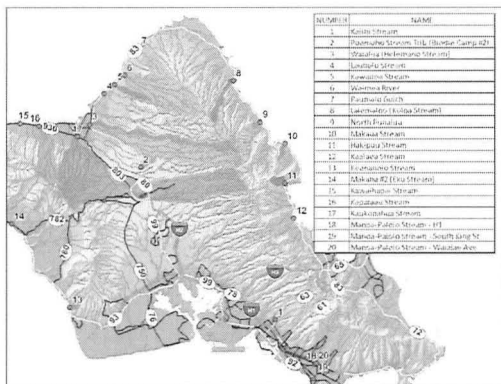


Figure 1. Oahu Scour Critical Bridges

Island of Kauai

The Island of Kauai is the oldest of the Hawaiian Islands and is nicknamed the *Garden Isle* because of its lush vegetation. Ten bridges were identified as scour critical and their locations are shown in Figure 2. All the bridges are along the Kaumuali and Kuhio Highways that circle the island. The Waimea River bridge has a drainage area of 222 km² and is home to the spectacular Waimea Canyon, which is over a mile wide and is the deepest non-submarine canyon in the Pacific with depths up to 3,000 feet. At the center of the island is Mount Waialeale which is considered the "wettest place on earth". The watersheds for all 10 bridges extend from the slopes of Mount Waialeale to the Pacific Ocean.

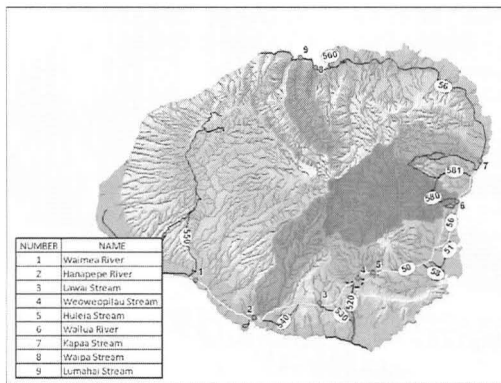


Figure 2. Kauai Scour Critical Bridges

Island of Hawaii

The Island of Hawaii is the largest of the Hawaiian Islands and is commonly called the *Big Island* with its area being twice the size as all the other islands combined. Regardless of its size, only thirteen bridges were identified as scour critical and they are all located on the northern side of the island as shown in Figure 3. Twelve of the bridges are located along the Hawaii Belt Road (H-19) that follows the coastline around the northern half of the island and eleven of these are within a 20 mile stretch on the northeastern side referred to as Hamakua Coast. This stretch of coast is comprised of steep, rocky streams and high cliffs that drop to the ocean. Drainage areas range in size with the largest at 641 km² for Wailuku River. The headwaters for Wailuku River begin at the peaks of Mauna Loa and Mauna Kea volcanoes and the river enters the Pacific Ocean in the City of Hilo. Due to its size and proximity to the ocean, the Wailuku Bridge will not only be subject to riverine scour, but also scour from a tsunami-generated tidal bore.

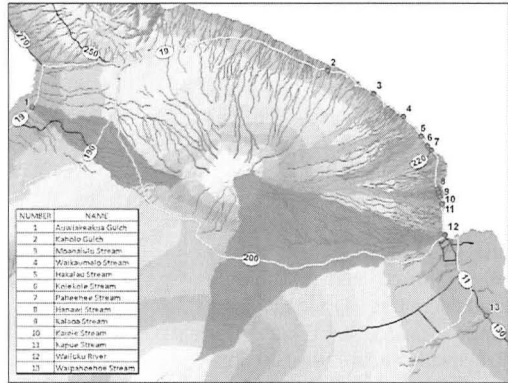


Figure 3. Hawaii Scour Critical Bridges

Island of Maui

The Island of Maui is often called the *Valley Isle* for its beauty and is the second most visited of the Hawaiian Islands, only second to Oahu. Ten bridges were identified as scour critical and their locations are shown in Figure 4. Four of the bridges are located along Highway 30 which circles the northwestern part of the island. Four bridges are located on the historic Hana Highway on the northern coastline and have construction dating as far back as 1912. The remaining three bridges are further inland and lie on the western slope of Haleakala volcano. Drainage areas range from as small as 1.4 km² for Oopuola Stream to 35.2 km² for Maliko Stream.

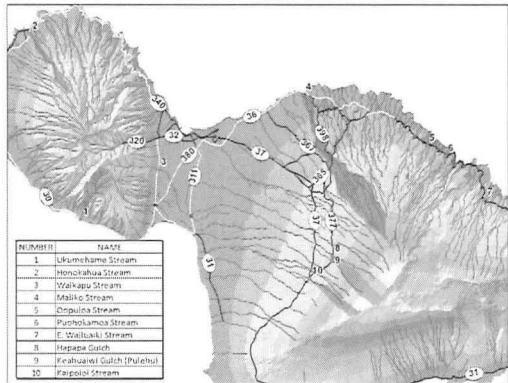


Figure 4. Maui Scour Critical Bridges

Island of Molokai

Although the Island of Molokai has the smallest population of the five major Hawaiian Islands, it has the largest population of native Hawaiians and is often referred to as the *Friendly Isle* or the *Most Hawaiian Island*. Only two bridges were identified as scour critical and their locations are shown in Figure 5. Both bridges are located along Highway 450 on the southern coastline of the eastern half of the island. Both bridges drain the southern side of Kamakou Volcano which can receive up to 300 inches of rain annually. The watersheds are heavily forested and have drainage areas of 1.1 km² for Kupeke Stream and 11.9 km² for Kamalo Stream.

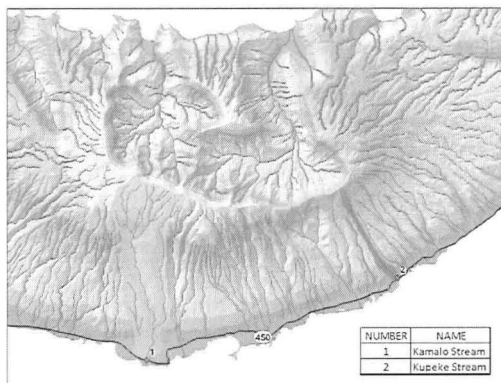


Figure 5. Molokai Scour Critical Bridges

HYDROLOGY

The Islands of Hawaii are subject to prevailing winds that blow from the northeast to the southwest, which splits the islands into two very distinct hydrologic regions. The northern and eastern sides of each island are considered the *windward sides* and are subject to higher amounts of precipitation and tend to have a lush, green landscape. The southern and western sides of each island are considered the *leeward sides* and are protected from the wind and precipitation by high elevations on the interior of each island. The *leeward sides* generally have a more arid or semi-arid landscape. The scour critical bridges are comprised of watersheds that are located on both the windward and leeward sides of the islands and will in turn have a variety of hydrologic properties.

Peak flows for each scour critical bridge were determined from a number of available sources including published flows derived from FEMA Flood Insurance Studies (FIS), USGS streamgage data, or published regional regression equations. FIS reports were obtained for communities that included any of the scour critical bridge reaches as flooding sources. In some instances, peak flows from the FIS reports were discarded due to outdated hydrologic techniques or the location on the stream where the flow was defined. In these instances, further analysis was required to estimate peak flows using flood frequency analysis or regional regression equations.

Flood Frequency Analysis

Annual peak discharges were retrieved from the USGS's national streamflow database (USGS, 2009) for streamgages located on study reaches. Peak flows were estimated for the 100-year and 500-year events using the U.S. Army Corps of

Engineers Statistical Software Package HEC-SSP (USACE, 2009). The software package follows the guidelines in Bulletin 17B (Interagency Advisory Committee on Water Data, 1982), which recommend the use of the Log Pearson Type III distribution as a base method for flood frequency studies.

If a bridge was located on a stream with a gage, but is downstream or upstream of the streamgage, a drainage area comparison was performed to determine whether the gage could be used to calculate peak flows at the bridge. If the drainage area at the bridge was within 0.5 to 1.5 times the drainage area at the streamgage, peak flows at the bridge could be calculated based on the peak flows at the gage using the area weighing procedure below (USGS, 2007).

$$Q_u = \left[\frac{A_u}{A_g} \right]^b Q_g$$

where Q_u is the weighted peak flow estimate for the ungaged bridge site, A_u is the drainage area for the ungaged bridge site, A_g is the drainage area for the streamgage, b is the drainage area exponent from regional regression equations (or 1 if regression equations are not available), and Q_g is the peak flow estimate for the streamgage. If the bridge drainage area is less than 0.5 or greater than 1.5 times the streamgage drainage area, regression equations were obtained or developed to determine peak flow estimates at the bridge.

Regional Regression Equations

For streams with no available FIS report or USGS streamgage data, regional regression equations were used to estimate peak flows. The USGS has recently published regional regression equations for the Islands of Kauai, Oahu, Molokai, Maui, and Hawaii (USGS, 2010) for recurrence intervals ranging from 2 to 500 years. For the regression analysis, the islands were divided into hydrologic regions with peak flow equations developed for each region. An example of the regression equations for the 100-year peak flow for the two Oahu regions is shown below.

$$\begin{aligned} (\text{Region 3} - \text{Oahu Leeward}) \quad Q_{100} &= 24.9 DA^{0.65} P^{0.33} \\ (\text{Region 4} - \text{Oahu Windward}) \quad Q_{100} &= 516.7 DA^{0.726} \end{aligned}$$

where Q_{100} is the calculated 100-year peak flow (m^3/s), DA is the drainage area at the bridge (km^2), and P is the median annual precipitation (mm). Values of P were obtained from the Hawaii Rainfall Atlas (HDLNR, 1986). The USGS regional regression equations were used to calculate the 100-year and 500-year peak flows for the scour critical bridges using the appropriate equations.

HYDRAULIC MODELING

A hydraulic model was developed for the majority of the bridges on the scour critical list using the HEC-RAS (River Analysis System) program, version 4.0 (USACE, 2008). A small number of bridges did not require a hydraulic model because the bridge foundations were on solid bedrock with no exposed footings or signs of scour or there was a limited amount of flow that reached the bridge. The HEC-RAS models were developed to obtain hydraulic characteristics at each bridge to use in the scour calculations and countermeasure design, if applicable.

An area of interest (AOI) was delineated for each bridge and included the bridge and extended upstream and downstream several hundred feet. The AOI's provided the limits for obtaining aerial imagery and topographic data for each bridge. Aerial imagery was downloaded from a range of sources including the National Oceanic and Atmospheric Administration (NOAA), Hawaii Coastal Geology Group (<http://www.soest.hawaii.edu/coasts/>), and the U.S. Department of Agriculture (USDA) Geospatial Data Gateway (<http://datagateway.nrcs.usda.gov/>). Topographic data was obtained in the format of an InterMap v1.5 digital terrain model (DTM) for each bridge and contours were created from the DTM's. Although the InterMap data proved to be good for many of the bridges, some bridges with dense vegetation rendered the InterMap data unusable and surveyed cross sectional data was required.

For each bridge, the following procedure was used to create the hydraulic model. The ArcGIS program, version 9.1 (ESRI, 2005), with the HEC-GeoRAS extension, was used to extract cross section profiles in the vicinity of the bridge from the DTM. Bridge data was extracted from as-built plans and field measurements and added to the HEC-RAS model. Manning's n values were estimated based on aerial imagery and field observations and contraction and expansion coefficients were increased to 0.3 and 0.5, respectively, in the vicinity of the bridge. A subcritical flow regime was assumed for the majority of the scour critical bridges; however, there were several steep streams in the study that may require a mixed flow regime. Because the purpose of the study is scour vulnerability, a mixed flow regime will provide the most conservative results and was used where suitable.

SCOUR VULNERABILITY

The scour vulnerability of each bridge was determined by calculating the scour depth based on the developed HEC-RAS model results and comparing the scour depth to elevations of the existing bridge foundation. The scour depth at each bridge was calculated based on the 100-year flow. However, if the 100-year flow overtopped the bridge, the incipient overtopping flow was determined and used to calculate the scour depth. If the 100-year flow does not overtop the bridge, the 500-year flow was analyzed and if it did not overtop, it was used to calculate the scour depth.

Scour Calculations

The total scour depth at each bridge was estimated based on the sum of contraction scour and pier scour (where applicable). Contraction scour occurs when a bridge structure and its embankments cause a constriction to the natural flow area and as a result, velocities increase through the bridge opening. Piers cause scour due to

the vortex created around the front and sides of the pier. The resulting scour depth is a function of hydraulic characteristics, pier geometry, and bed material size.

Two types of contraction scour can occur in a channel, live-bed or clear-water. Live-bed contraction scour occurs when bed material is transported from the upstream reach into the bridge and clear-water contraction scour occurs when there is no bed material transport. For each bridge, the critical velocity in the approach section was calculated using Laursen's equation (FHWA, 2001) to determine whether live-bed or clear-water scour would occur at the bridge. If the velocity in the approach section exceeded the calculated critical velocity, this indicates the transport of bed material and Laursen's *live-bed scour equation* (FHWA, 2001) was used to compute contraction scour. If the velocity in the approach section was less than the calculated critical velocity, this indicates no transport of bed material and Laursen's *clear-water scour equation* (FHWA, 2001) was used to compute contraction scour.

If the bridge structure includes piers, the pier scour depth was calculated using the Colorado State University (CSU) equation (FHWA, 2001). The calculated pier scour depth was then added to the calculated contraction scour depth to obtain the total scour depth at each bridge.

Several of the scour critical bridges have foundations that are constructed on bedrock. Historically, limited guidance has been available to determine scour vulnerability for bridges founded on rock; however, a study recently conducted by the National Cooperative Highway Research Program should provide a methodology for estimating scour vulnerability for these bridges. When this publication is released, it will be used to estimate the scour at the bridges with foundations on bedrock.

Foundations

Two types of foundations were found at the scour critical bridges, spread footings and pile supported footings. A spread footing is a wide, shallow footing typically made of reinforced concrete. Pile supported footings consist of piles driven through the soil to bedrock or a depth where the soil friction prevents any movement of the pile. Pile footings are common when soil conditions are unable to support bridge loads or in soils that are hard to excavate. For scour vulnerability, spread footings are a higher concern due to the shallow nature of their design.

As-built plans were provided for many of the bridges and the majority included information on the type and depth of the bridge foundation. However, some of the older bridges do not have as-built plans available or the plans did not include details on the foundation. Without this information, a comparison could not be made between the calculated scour depth and foundation elevations. In these scenarios, if the calculated scour depth was of concern, further investigation was necessary to determine the extents of the foundation. Critical elevations of a foundation from a scour vulnerability standpoint are (1) bottom of spread footing, (2) bottom of pile supported footing, and (3) bottom of a pile bent. These are common trigger elevations for streambed monitoring at a bridge (described below).

RECOMMENDED ACTIONS

Once the scour assessment was completed, the next component of a Plan of Action (POA) was to provide recommended actions for a bridge specific to that

bridge's scour vulnerability. Recommended actions include one or more of the following: (1) increased inspections, (2) hydraulic and/or structural countermeasures, and (3) flood monitoring. The POA for each bridge outlines the recommended actions to be taken to prevent and/or monitor further scour at the bridge.

Increased Inspections

Every bridge on the scour critical list for the State of Hawaii currently undergoes an inspection every 24 months. The purpose of a bridge inspection is not only to rate the condition of the bridge superstructure, but also to rate the condition of the abutments, piers, foundations, and note any observed scour or debris build-up. Observing these items on a regular basis can provide insight to whether scour is increasing at a bridge. If a bridge was determined to be scour critical from this study, one recommended action could be to increase the frequency of inspections to a shorter time interval, such as every 12 months. In addition, a single storm event has the potential to produce a large amount of scour; therefore it is imperative to perform inspections after large storms for scour critical bridges.

Hydraulic and/or Structural Countermeasures

Hydraulic and/or structural countermeasures can be specified as a recommended action in the POA for a bridge. These countermeasures are designed specifically to prevent further scour from occurring while also being cost effective. For bridge abutment protection, countermeasures could include bank and/or bed hardening designs such as riprap, grouted surfaces, gabions, etc., or redirection of flow designs including spur dikes, barbs, bendway weirs, etc. Inline weirs are another countermeasure option that can provide grade control at a bridge. Countermeasures for pier scour mainly consist of hardening the bed around the pier with riprap, gabions, articulated concrete blocks, etc.

Design of the scour countermeasures is based on the results from the HEC-RAS model for the 100-year flow. Structural retrofitting of a bridge is a structural countermeasure option for the bridge owner; however, it was not a part of this study.

Flood Monitoring

Each POA specifies when flood monitoring should be initiated based on one or more of the following triggers: (1) water surface elevation reaches a predetermined level on the bridge, (2) discharge or stage at a gaging station reaches a predetermined flow rate or stage, (3) water surface elevation surpasses bankfull and is rising rapidly, (4) an official flood warning for the stream, and (5) predicted rainfall depth to exceed a predetermined amount. Each bridge will have a different set of triggers depending on the presence of a gage station, accessibility to the bridge, etc.

Once flood monitoring is initiated, the POA outlines what type of monitoring should follow, water surface elevation monitoring and/or streambed elevation monitoring. Streambed monitoring is more useful for bridges with high scour vulnerability because it provides a clearer picture of the scour that may be occurring at the abutments and/or piers, whereas water surface monitoring can only provide an estimate of the scour occurring at that corresponding water surface elevation.

However, streambed monitoring is not always possible because of lack of accessibility, velocities in the channel during a flood event, cost, etc.

Bridge Closure

During flood monitoring, bridge closure will be initiated based on a list of criteria in the POA, which is specific to each bridge based on the results of the scour vulnerability assessment. The POA will specify bridge closure if one or more of the following criteria are met (1) water surface elevation reaches a critical elevation, (2) streambed elevation reaches a critical scour elevation (i.e., at or below the bottom of a spread footing), (3) debris buildup causes a significant obstruction of the bridge opening, and (4) any movement of the substructure.

In the case of a bridge closure, each POA includes a contact list that provides a list of personnel that should be notified. Each POA also includes a detour route which may be necessary during a bridge closure. In some remote areas of the islands, a detour route is not feasible and a temporary bridge design may be required instead. This decision is ultimately the choice of the Hawaii DOT.

Once a flood event has subsided and the water surface recedes to an accessible elevation, an inspection should be performed to determine whether the bridge is suitable for reopening. The criteria for reopening can include one or more of the following: (1) assess the post-flood streambed elevations, (2) confirm that no damage has occurred to the substructure, (3) remove any excess debris from the channel that may have accumulated during the flood, and (4) verify the condition of any existing scour countermeasure. The bridge should not be reopened until the required criteria listed on the POA are met.

EXAMPLE PLAN OF ACTION

Paumalu Gulch is located on the northeastern tip of Oahu (Figure 1) and the drainage area at the bridge is 7.6 km². Grouted rock has been placed along the abutments and piers as well as loose rock ($\sim D_{50} = 15$ cm) at the piers as a scour countermeasure; however, the grouted rock is being undermined. The bridge was identified as scour critical and a Plan of Action (POA) was completed and the results are summarized below.

A flood frequency analysis was performed on USGS gage #16318000, which is located approximately 640 meters upstream of the bridge on Paumalu Gulch. The drainage area ratio between the bridge and gage is equal to 1.1; therefore, the 100-year peak flow of 42.2 m³/s was calculated based on the area weighting procedure of the estimated flows at the gage.

An HEC-RAS model was created for the bridge based on the DTM, bridge as-built plans, and field measurements/observations. Because the 100-year flow did not overtop the bridge, the 500-year flow was modeled and determined to also not overtop and was therefore used for scour calculations. The bed material was determined to be sand with silt and gravel and has a D_{50} of 0.6 mm. Based on this and results from the HEC-RAS model, contraction and pier scour were calculated to be 0.0 and 2.0 m, respectively, for the 500-year flow. Bridge as-built plans showed the foundation of the Paumalu Gulch Bridge to be wooden piles capped with concrete

socket piles. Pile tip elevations are unknown and further investigation is required to determine these.

Based on the scour calculations, the POA for Paumalu Gulch Bridge listed recommended actions for the bridge. Placement of riprap with a minimum D_{50} of 0.5 m (based on the 100-year flow) at the base of the piers was recommended. Inspection frequencies should be increased to every 12 months, specifically to observe the stability of the grouted riprap and riprap placed at piers. During periods of intense rainfall or flooding, the bridge should be inspected periodically. A 100-year water surface elevation mark (4.8 meters below the top of rail on upstream side) should be installed and will act as the trigger elevation to initiate constant flood monitoring. Criteria for closure of Paumalu Gulch Bridge were determined to be when one or more of the following occurs: (1) pressure flow and/or overtopping of the bridge or approach roadways, (2) significant debris buildup in the channel, and (3) any movement of the bridge structure. If bridge closure occurs, the steps to be taken prior to reopening of the bridge are to compare the post-flood streambed elevation to baseline bed elevation, removal of debris accumulated during the high flow, and verify the condition of scour countermeasures.

The preparation of a Plan of Action for each of the 57 scour critical bridges in the State of Hawaii is currently underway and will ultimately outline procedures for Hawaii DOT personnel to follow during high flow events to help ensure public safety.

REFERENCES

- ESRI (2005). *ArcGIS Software. Version 9.1*, 2005.
- FHWA (1995). "Recording and Coding Guide for the Structure Inventory and Appraisal of the Nation's Bridges". U.S. Department of Transportation, Federal Highway Administration, FHWA-PD-96-001, Reston, VA.
- FHWA (2001). "Hydraulic Engineering Circular No. 18, Evaluating Scour at Bridges, Fourth Edition". U.S. Department of Transportation, Federal Highway Administration, FHWA-NHI-01-001, Arlington, VA.
- HDLNR (1986). "Rainfall Atlas of Hawaii". Hawaii Department of Land and Natural Resources, Division of Water and Land Development, Honolulu, HI.
- Interagency Advisory Committee on Water Data (1982). "Guidelines for Determining Flood Flow Frequency: Bulletin 17B". U.S. Geological Survey, Office of Water Data Coordination, Reston, VA.
- USACE (2008). *HEC-RAS, River Analysis System. Version 4.0*, Hydrologic Engineering Center, Davis, CA.
- USACE (2009). *HEC-SSP Statistical Software Package. Version 1.1*, CPD-86. Davis, CA.
- USGS (2007). "The National Streamflow Statistics Program: A Computer Program for Estimating Streamflow Statistics for Ungaged Sites". U.S. Geological Survey, Reston, VA.
- USGS (2010). "Flood-Frequency Estimates for Streams on Kauai, Oahu, Molokai, Maui, and Hawaii, State of Hawaii". Scientific Investigations Report 2010-5035, U.S. Geological Survey, Reston, VA.
- USGS (2009). *Surface-Water Data for Hawaii, National Water Information System: Web Interface*. waterdata.usgs.gov/ne/nwis/sw.

The Observational Method for Scour and the Schoharie Creek Bridge Failure

A.V. Govindasamy¹, J.-B. Briaud² and D. Kim³

¹Staff Engineer, Geocomp Corporation, 1145 Massachusetts Avenue, Boxborough, MA 01719; PH (978) 621-8106; email: agovindasamy@geocomp.com

²Professor and Holder of the Buchanan Chair, Zachry Dept. Of Civil Engineering, Texas A&M University, College Station, TX 77840; PH (979) 845-3795; email: briaud@tamu.edu

³GIS Developer, Dewberry, 8401 Arlington Boulevard, Fairfax, VA 22031; PH (703) 206-0847; email: dokim@dewberry.com

ABSTRACT

The observational method for estimating the future scour depth at existing bridges was introduced by Briaud et al. (2009) and Govindasamy (2009). The method utilizes measured scour data and observed or estimated flow parameters at a bridge to evaluate the future scour depth at an existing bridge. It provides more realistic scour risk estimates due to the fact that it utilizes measured data and accounts for time dependent scour depth in clays. Other important features of the method are its ability to recognize and efficiently filter scour depths exceeding foundation allowable values and also account for scour in multilayered soil deposits. The Schoharie Creek bridge failure of 1987 was selected as a case history to illustrate the how the observational method would have identified the bridge as requiring immediate attention if it was used to evaluate the bridge prior to its collapse, hence preventing the serious consequences of the disaster.

Introduction

The observational method for estimating the future scour depth at existing bridges was introduced by Briaud et al. (2009) and Govindasamy (2009). The method utilizes measured scour data and observed or estimated flow parameters to evaluate the future scour depth at an existing bridge. The observational method provides more realistic scour risk estimates due to the fact that it utilizes measured data and accounts for time dependent scour depth in clays. The method also does not require site specific erosion testing and therefore reduces the effort and cost associated with evaluating a bridge for scour. The features of the observational method that form the crux of this study are its ability to recognize and efficiently filter scour depths exceeding allowable (threshold) values for foundations (more specifically in this case, footings) and also account for multilayered deposits, namely the presence of a strong layer overlying a weak layer. A case history was selected to highlight the importance of these features in bridge scour predictions. The case history is the Schoharie Creek bridge failure of 1987 (Figure 1).

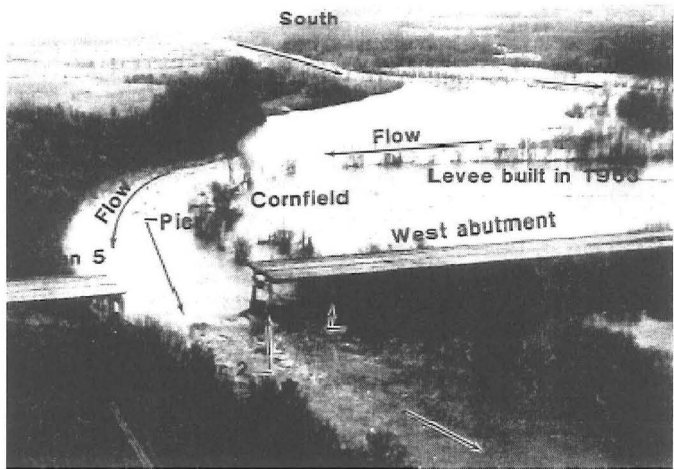


Figure 1. The 1987 Schoharie Creek Bridge Failure (NTSB 1987).

The Observational Method for Scour

The observational method is the first phase of a three-phase bridge scour assessment procedure. The main idea behind the method is to obtain the scour depth corresponding to a specified future flood event using scour depth observations at the site and from charts that relate the scour depth ratio ($Z_{\text{fut}}/Z_{\text{mo}}$) to the velocity ratio ($V_{\text{fut}}/V_{\text{mo}}$). Z_{fut} is the scour depth corresponding to a specified future flood, Z_{mo} is the maximum observed scour at the bridge, V_{fut} is the velocity corresponding to the specified future flood, and V_{mo} is the maximum velocity observed at the bridge until the time Z_{mo} is measured. These charts are termed the Z-Future Charts (Briaud et al. 2009 and Govindasamy 2009). The velocity ratio, $V_{\text{fut}}/V_{\text{mo}}$ is obtained through a simplified hydrologic analysis. The general steps in the observational method are outlined in Table 1.

Table 1. General Steps in the Observational Method for Scour

Step 1	Observe the maximum scour at the bridge Z_{mo}
Step 2	Determine the velocity ratio $V_{\text{fut}}/V_{\text{mo}}$
Step 3	Extrapolate/interpolate field measurements to predict future scour depth using the Z-Future Charts. This is represented by $Z_{\text{fut}}/Z_{\text{mo}} = f(V_{\text{fut}}/V_{\text{mo}})$.
Step 4	Compare the future scour depth Z_{fut} to the allowable (threshold) scour depth of the foundation Z_{thresh}

As mentioned previously, the observational method can account for scour in a uniform soil deposit as well as in a multilayered soil deposit. For the latter, the

procedure for obtaining hydraulic information is extended to obtain explicit values of V_{fit} and V_{mo} . The reader is referred to Briaud et al. (2009) for a detailed description of this procedure.

Overview of the Schoharie Creek Bridge Failure

The bridge was a five-span, 540-ft long highway bridge over the Schoharie Creek in Montgomery County near Amsterdam, New York (National Transportation Safety Board 1987). The bridge was built in 1954 and was founded on spread footings that were approximately 19 ft wide and 5 ft thick. On April 5, 1987, one of the piers of the bridge (Pier 3) collapsed, causing two spans of the bridge to plunge into the creek (Figure 2). This was followed by the collapse of an adjacent pier (Pier 2). The failure of this bridge caused the deaths of 10 people. The cause of the failure was attributed to scour (National Transportation Safety Board 1987; Resource Consultants, Inc., and Colorado State University 1987; Wiss, Janney, Elstner Associates, Inc., and Mueser Rutledge Consulting Engineers 1987).

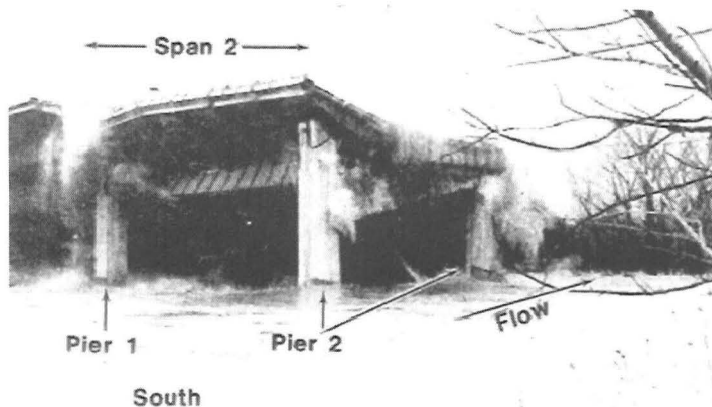


Figure 2. One of the Schoharie Creek Bridge Spans Plunging into the River (NTSB 1987).

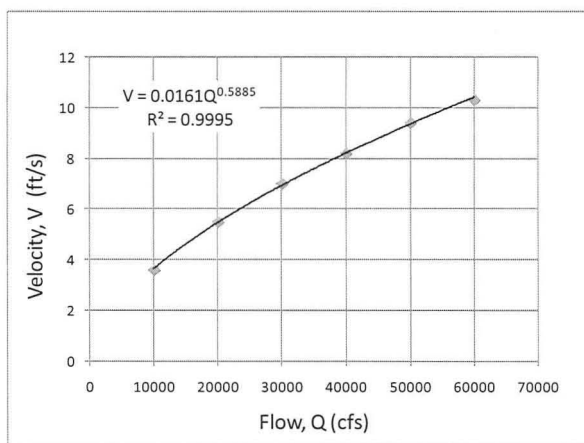
Flow History at the Schoharie Creek Bridge

The bridge experienced its largest flood in 1955. The second largest flood was the flood that took place in 1987 during the failure of the bridge. According to the National Transportation Safety Board (NTSB) (1987), the magnitudes of both floods (peak) were $Q_{peak,1955} = 2084 \text{ m}^3/\text{s}$ (73,600 cfs) and $Q_{peak,1987} = 1758 \text{ m}^3/\text{s}$ (62,100 cfs), respectively. The flow velocities at Pier 3 were obtained from the one-dimensional flow computer model, Water-Surface Profile Computations or WSPRO (FHWA 1986). The computer simulations were carried out by Resource Consultants, Inc., and presented by NTSB (1987) (Table 2).

Table 2. Peak Discharge versus WSPRO Mean Velocity at Schoharie Creek Pier 3 (after NTSB 1987).

Peak Discharge (cfs)	WSPRO Mean Velocity (ft/s)
10,000	3.6
20,000	5.5
30,000	7.0
40,000	8.2
50,000	9.4
60,000	10.3

The flow-velocity data shown in Table 2 were plotted and shown in Figure 3. A regression was performed on the data to obtain the flow-velocity relationship. The regression produced an R^2 value of 0.99. Using the relationship shown in Figure 3, the flow values $Q_{\text{peak},1955} = 2084 \text{ m}^3/\text{s}$ (73,600 cfs) and $Q_{\text{peak},1987} = 1758 \text{ m}^3/\text{s}$ (62,100 cfs) translate into velocities $V_{\text{peak},1955} = 3.6 \text{ m/s}$ (11.8 ft/s) and $V_{\text{peak},1987} = 3.2 \text{ m/s}$ (10.5 ft/s), respectively.

**Figure 3. Flow-Velocity Relationship for Schoharie Creek Pier 3.**

Previous and Current Investigations into the Failure

Prior investigations into the failure revealed that riprap was placed at the bridge piers prior to 1955 as protection against scour. NTSB (1987) states, "At Piers 2 and 3, riprap was installed from bottom of footing (elevation 270 ft) sloping to elevation 279.5 ft prior to the 1955 flood. Therefore, at Pier 3 the thickness of the riprap was approximately 9.5 ft (Figure 4). Photos taken on October 30th 1956 showed riprap movement at Piers 2 and 3. Various photographs taken from 1954 to 1977 during low water showed that some of the rocks had moved northward (downstream) during that time. Photographic analysis of Pier 2 (aided by computers)

confirms the downstream movement of rock at Pier 2 from 1954 to 1977.” Figure 5 shows Pier 3 in 1956. Figure 6 shows Pier 2 in 1977.

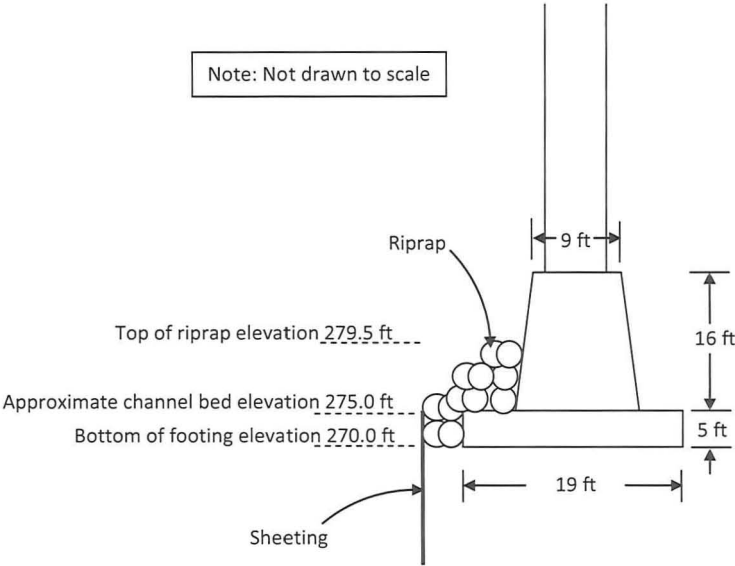


Figure 4. Schoharie Creek Pier 3 (after NTSB 1987).

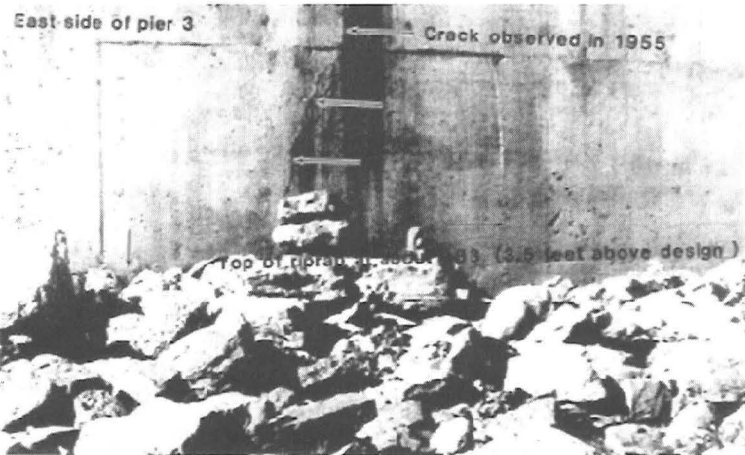


Figure 5. Photo of Pier 3 Taken in 1956 (NTSB 1987).

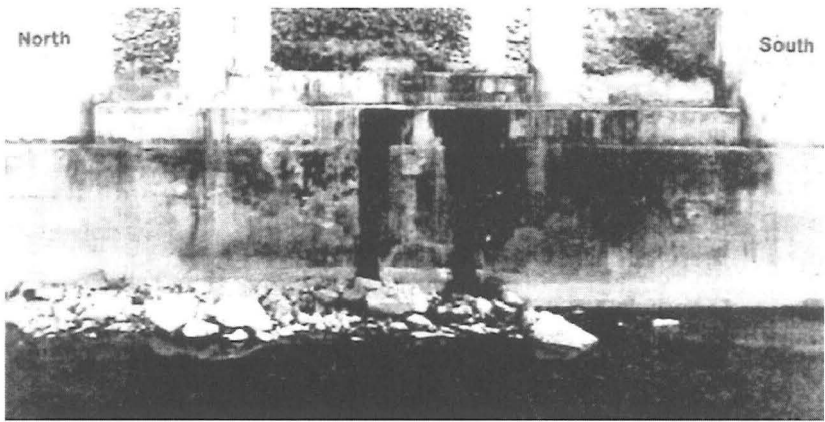


Figure 6. Photo of Pier 2 Taken in 1977 (NTSB 1987).

With reference to the riprap placed at the bridge prior to the 1955 flood, NTSB (1987) states, “The only riprap dimensions specified in the bridge plans should be a minimum thickness of 8 inches and a maximum thickness of 15 inches. The plans also call for the riprap to be an Item 80 riprap according to the New York Department of Public Works (DPW) specifications. An Item 80 riprap should have at least 50% of the stones weighing in excess of 300 lbs each.”

In order to obtain the critical velocity of the riprap, the Erosion Threshold Chart (Briaud et al. 2009, Govindasamy 2009) is used (Figure 7) This chart relates the mean particle diameter D_{50} to the critical velocity V_c . For $D_{50} = 8$ inches = 203 mm:

$$V_c \text{ (m/s)} = 0.35[D_{50}(\text{mm})]^{0.45}$$

$$V_c = 0.35(203)^{0.45} = 3.8 \text{ m/s (12.5 ft/s)}$$

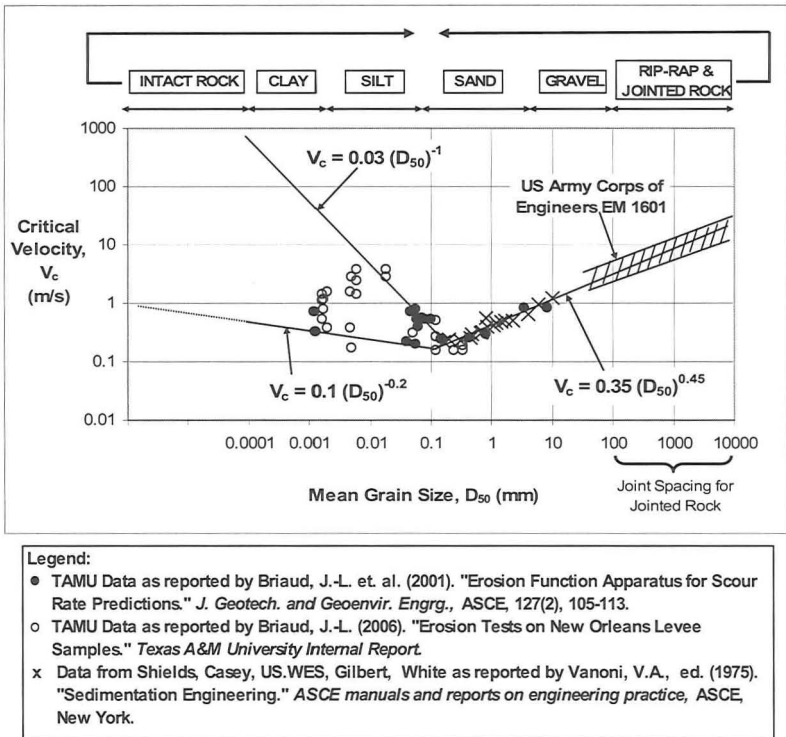


Figure 7. The Z-Threshold Chart (Govindasamy 2009)

For a DPW Item 80 riprap, assuming a spherical piece of riprap weighing 136 kg (300 lb) and with a specific gravity $S_g=2.65$, results in a diameter of 460 mm (1.5 ft).

Again from the Figure 7:

$$V_c \text{ (m/s)} = 0.35[D_{50}(\text{mm})]^{0.45}$$

$$V_c = 0.35(460)^{0.45} = 5.5 \text{ m/s (18.1 ft/s)}$$

It should be noted that the critical velocity of 5.5 m/s (18.1 ft/s) is for a non-porous spherical boulder.

However, NTSB (1987) states, "field observations and photographs indeed showed movement of riprap between 1954 and 1977, the critical velocity, V_c of the riprap should be less than 3.6 m/s, which is the largest flood velocity experienced at the Schoharie Creek bridge." It goes on to state, "it is evident that there was riprap movement between 1956 and 1977." The maximum flow between 1956 and 1977 was 1144 m³/s (40,400 cfs) (National Transportation Safety Board 1987), which corresponds to an approach velocity of 2.5 m/s (8.3 ft/s). Therefore, it is reasonable to

assume that the critical velocity of the riprap should be below 1.5 times the approach velocity, 3.75 m/s. This is the local velocity at the pier. In order to illustrate the erodibility of the riprap, the Erosion Function Chart (Briaud et al. 2009, Govindasamy 2009), which relates the erosion rate to velocity is used (Figure 8). Approximating V_c of the riprap as 3.5 m/s (below 3.75 m/s), the upper boundary of a Category V material (very low erodibility) in Figure 8 can be taken as the approximate erosion function of the riprap. According to Resource Consultants, Inc., and Colorado State University (1987), V_c of the glacial till = 1.5 m/s (4.9 f/s). The upper boundary of a Category IV material (low erodibility) is translated to the right so that the critical velocity corresponds to the critical velocity of the glacial till (Figure 8).

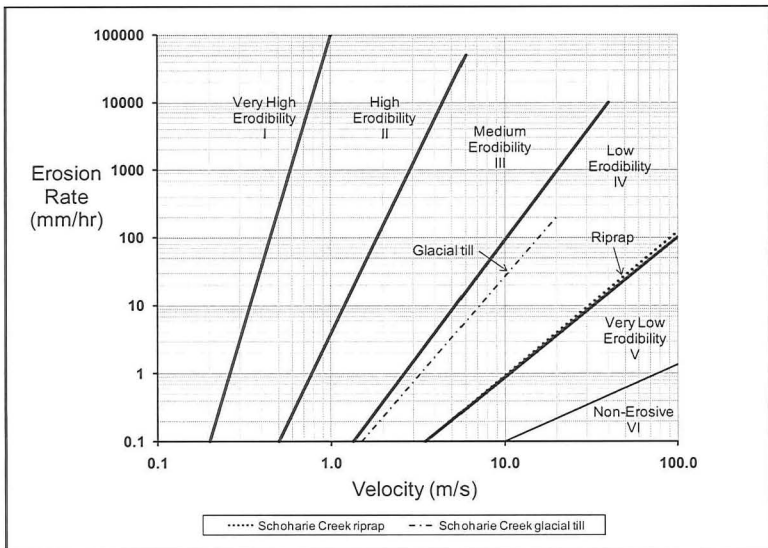


Figure 8. Estimated Erosion Functions for the Schoharie Creek Riprap and Glacial Till.

Through prior investigations into the Schoharie Creek bridge failure, it was found that the 1955 flood and following smaller floods caused the riprap to move between 1955 and prior to the 1987 collapse. Since the riprap was placed down to the bottom level of the footing, it is believed that there was still some remaining riprap just prior to the 1987 flood. Otherwise, the erosion would have undermined the footing before the 1987 flood. Since the velocity of the 1987 flood is believed to have been greater than V_c of the riprap (although the previous sections of this paper approximate $V_{\text{peak},1987}$ to be slightly smaller than V_c based on D_{50}), it is highly likely that the 1987 flood moved the remaining riprap, thus exposing the more erodible glacial till beneath. As shown in Figure 8, the till was more erodible than the riprap.

Once the till was exposed, the footing was undermined, very rapidly causing the bridge to fail.

Therefore, the reason for the Schoharie Creek Bridge failure under a lesser flood in 1987 than the flood of 1955 is a multilayer deposit response and not a uniform deposit response. Indeed, during the 1955 event, the scour hole remained in the riprap, while in 1987 it eroded what was left of the riprap (strong layer) and rapidly advanced in the glacial till below (weak layer).

Conclusion

If the observational method for scour presented by Briaud et al. (2009) and Govindasamy (2009) was used to evaluate the Schoharie Creek bridge prior to its collapse, it would have identified the bridge as requiring immediate attention. This is because Z_{thresh} would have been exceeded (for footings, Z_{thresh} is normally taken as the length between the original as-built channel level and the top of the footing). In the case of the Schoharie Creek bridge, the riprap below the top of footing level had moved prior to the 1987 collapse. Moreover, the method also has provisions to account for multilayer deposit response and would have accounted for the rapid erosion in the more erodible glacial till underlying the riprap.

Acknowledgements

This paper is an outcome of a bridge scour project funded by the Texas Department of Transportation (Grant No. 0-5505). The authors are grateful for this support.

References

1. Briaud, J.-L., F.C.K. Ting, H.-C. Chen, Y. Cao, S.W. Han, and K.W. Kwak (2001a). "Erosion Function Apparatus for scour rate predictions." *Journal of Geotechnical and Geoenvironmental Engineering*, ASCE, Vol. 127, No. 2, pp. 105-113.
2. Briaud, J.-L. (2006). "Erosion Tests on New Orleans Levee Samples," Internal Report, Zachry Department of Civil Engineering, Texas A&M University, College Station, Texas.
3. Briaud J.-L., A.V. Govindasamy, D. Kim, P. Gardoni, F. Olivera, H. C. Chen, C. Mathewson, and K. Elsbury (2009). "Simplified Method for Estimating Scour at Bridges," Report 0 5505-1, Texas Department of Transportation, Austin, Texas.
4. Federal Highway Administration (1986). "Bridge Waterways Analysis Model (WSPRO) User's Manual," Report No. FHWA-IP-87-3 Draft Report.
5. Govindasamy, A.V. (2009). "Simplified Method for Estimating Future Scour Depth at Existing Bridges," Ph.D. Dissertation, Texas A&M University, College Station, Texas.

6. National Transportation Safety Board (1987). "Collapse of the New York Thruway (I-90) Bridge over the Schoharie Creek, near Amsterdam, New York, April 5, 1987." Highway Accident Reports, NTSB/HAR-88/02, United States Government, Washington, D.C.
7. Resource Consultants, Inc., and Colorado State University (1987). "Hydraulic, erosion, and channel stability analysis of the Schoharie Creek Bridge failure, New York." Report for the National Transportation Safety Board, Washington, D.C., and the New York State Thruway Authority, Albany, New York.
8. Vanoni, V. (1975). "Sedimentation Engineering," ASCE Manual and Report on Engineering Practice, American Society of Civil Engineers, New York.
9. Wiss, Janney, Elstner Associates, Inc., and Mueser Rutledge Consulting Engineers (1987). "Collapse of the Thruway Bridge at Schoharie Creek for New York State Thruway Authority, Albany, NY."

Scour Evaluation of Bridge Foundations Using Vibration Measurement

Y. Y. Ko¹, Ph.D., W. F. Lee², Ph.D., W. K. Chang³, Ph.D., H. T. Mei⁴, M.Eng., and C. H. Chen⁵, Ph.D.

¹National Center for Research on Earthquake Engineering, No. 200, Sec. 3, Hsinhai Rd., Taipei 10668, Taiwan; +886-2-6630-0872; email: yyko@ncree.org.tw

²National Taiwan University of Science and Technology, No. 43, Sec.4, Keelung Rd., Taipei 10607, Taiwan; +886-2-2737-3243; email: weilee@mail.ntust.edu.tw

³National Taiwan University, No. 1, Sec. 4, Roosevelt Rd., Taipei 10617, Taiwan; +886-2-2362-3356; email: d90521008@ntu.edu.tw

⁴National Taiwan University, No. 1, Sec. 4, Roosevelt Rd., Taipei 10617, Taiwan; +886-2-2362-3356; email: travismeil107@gmail.com

⁵National Taiwan University, No. 1, Sec. 4, Roosevelt Rd., Taipei 10617, Taiwan; +886-2-3366-4246; email: chchen2@ntu.edu.tw

ABSTRACT

The exposure of bridge foundations due to scouring has been recognized as the most critical cause for highway bridge failures in Taiwan, yet difficulties have been found to identify its risk level. In an effort to develop an efficient measure for the detection and estimation of the scour of bridge foundations, a series of field vibration measurements were conducted on selected highway bridges of which the foundations had been suffered different levels of scouring. In this paper, theoretical background of utilizing vibration measurement to estimate the exposure of bridge foundation is introduced. The setup of vibration measurement on bridges and schemes of data processing are described. Results of the mentioned field tests on bridges are presented, and the feasibility of using vibration measurement to evaluate the scour of bridge foundations is thus verified. The findings of this study are helpful in developing the inspection and monitoring technology for bridge scouring.

INTRODUCTION

Several major highway bridge failures occurred in Taiwan in recent years, leading to considerable casualties and property losses. Most of them were due to the exposure of the pier foundation due to scouring, which reduced the bearing capacity of foundation. These disasters can be prevented if the damage or the insufficient capacity of the foundation can be detected in advance, and the repair and retrofit works, or the restraint of use is timely executed. However, the exposure of pier foundation can not be directly observed visually if the water table is above the foundation level. Although it is possible to inspect the exposure in a contact manner by using instruments directly installed on the foundation, the flow-induced loading and the impact of the flow carryovers may destroy the instruments. Consequently, it is necessary to develop reliable non-destructive and indirectly scour evaluation techniques for bridge foundations.

The structural vibration response of a soil-structure system shows the characteristics of the system itself, and reflects the boundary conditions as well. Therefore, the vibration measurement has been extensively applied to the system

identification and the damage detection of structures. Similarly, the measurement of structural vibration can be used to evaluate the foundation exposure due to scouring. It is easy to perform and ensures the durability of sensors since they are not installed on the foundation. Moreover, the vibration analysis methods are well-developed, and many criteria for damage evaluation were proposed and have been widely used.

In this study, the influence of foundation exposure on the vibration characteristics of the bridge superstructures was firstly investigated. The setup of field vibration measurements on bridges and the schemes of data processing were accordingly proposed. Field measurements on two highway bridges in Taiwan of which the foundations had been suffered scouring were then presented to actually examine how the foundation exposure affects the vibration behavior of bridge. Thus, the vibration measurement on the bridge can be applied to the scour evaluation of bridge foundations. It meets the requirements of regular inspection and long-term monitoring, and is therefore helpful to bridge management and disaster mitigation.

DAMAGE EVALUATION USING VIBRATION MEASUREMENT

Vibration characteristics for damage evaluation

The vibration characteristics of a structure system, *e.g.* the natural frequency, the modal shape, and the damping ratio, are related to the stiffness and the integrity of the system. When the structure is damaged, its natural frequency will be lowered because of the decrease of overall stiffness; the modal shape will be changed because of the stiffness redistribution due to the defects; and, the damping will be increased because of the development of the cracks. Hence, if the changes in the vibration characteristics of the structure can be identified experimentally, the structural damage can be thus detected (Doebeling *et al.*, 1996). In the vibration measurement tests, the obtained vibration time history is often transformed into the frequency domain by spectrum analysis (*e.g.* fast Fourier transformation) to show its frequency content, and accordingly the structure can be characterized.

For the detection of the structural damage, instinctively the variation of the natural frequency is used. However, some random errors might be produced in the measurement due to the electrical noise, the environmental effects, and the variations in test conditions. Although the uncertainty level of the natural frequency is usually less than on other structural vibration characteristics (Farrar *et al.*, 2000), its variation is sometimes not sensitive enough to reveal the damage level, especially for the local component damage in a complex structure. Therefore, the precision of measurement must be high enough and the damage must be not too slight so that the damage can be detected merely by the variation of the structural natural frequency.

The natural frequency and the modal shape can be adopted simultaneously for a better estimation of structural damages (*e.g.* Kim *et al.*, 2003). Nakamura (1997) used both the natural frequency and the amplification amplitude of a system estimated from microtremors and proposed the vulnerability indices for the ground, the embankment, the viaduct, and the derailment/overturn of trains.

As for the applications of vibration measurement to scour evaluation of bridges, Samizo *et al.* (2007) utilized the decline of the natural frequency of the bridge pier identified from microtremors and impact tests to evaluate the exposure of

the foundation due to scouring. In their study, a data dividing and averaging analysis scheme was introduced to eliminate the dispersion of the predominant frequencies identified from long-term microtremor measurement.

Vibration measurement tests

Vibration measurement tests usually adopted for system identification include:

1. Ambient Vibration Measurement: The ambient vibration is randomly generated by man-made or natural disturbances in the environment and has a wide frequency content, and is therefore useful for the identification of structural dynamic properties. By measuring the input ambient vibration and the excited response of the structure simultaneously, the transfer function can be deduced for the identification of structural dynamic properties. For example, Ivanovic *et al.* (2000) extracted the natural frequency and the corresponding modal shape of a severely damaged RC building from the transfer function obtained from the ambient vibration data. For the case that the input motion is unavailable, it is still possible to characterize the structure merely by its excited response based on the assumption that the ambient vibration can be regarded as a white noise, that is, a random process with a constant power spectral density, *e.g.* Samizo *et al.* (2007).
2. Forced Vibration Test: The artificial vibration sources such as moving vehicles, the harmonic vibrator, and the hammer impact are utilized to cause the structure to vibrate. It helps to recognize the vibration characteristics of the structure for a specific vibration source or under a larger strain level. Ko and Chen (2009) derived the natural frequency and the corresponding modal shape of a full-scale school building specimen from the results of the forced vibration test using the harmonic vibrator. Samizo *et al.* (2007) conducted the impact test on the bridge for the natural frequency of the bridge pier. Chen *et al.* (2009) characterized the attenuation of ground vibration using the field measurement of the high-speed train induced vibrations and the falling weight test.

VIBRATION MEASUREMENT FOR SCOUR EVALUATION OF BRIDGE

Influence of scour on structural vibration of bridge

For a pier-soil system, when the ground level is lowered by scouring, the free length of the column is increased, leading to the decline of its lateral stiffness. If the scour is getting more severe and the foundation is exposed, the foundation stiffness is degraded so that the total stiffness of the system is further reduced. The stiffness reduction can be reflected by the variation of the structural vibration characteristics.

In order to investigate the influence of foundation exposure due to scouring on the vibration characteristics of the bridge superstructures, a FE model of a typical single-span simple supported bridge unit was established using SAP 2000 software, as shown in the top of Figure 1. It was composed of two piers with caisson foundation and a deck with girders. The structure configurations are based on the Wulin Bridge in Taiwan. The column, cap beam, and girder were modeled by beam element, the deck was modeled by shell element, and the caisson was regarded as a rigid body with the mass of infillings added. The support condition between the cap beam and the girder was regarded as a hinge since the small-strain vibration was

considered here. The mass of the deck of the neighboring span is considered yet the confinement is ignored. The supporting soil is modeled by spring elements, and the foundation exposure is simulated by removing the soil springs.

Firstly, the modal analysis was performed, as shown in the bottom of Figure 1. The 1st mode is the local bending of the deck, with a corresponding fundamental frequency of 3.15 Hz; the 2nd mode is the coupled translation-rocking responses of the two piers in the horizontal longitudinal (HL) direction, with a fundamental frequency of 3.24 Hz; and, the 3rd mode is the coupled translation-rocking responses in the horizontal transverse (HT) direction accompanied by some local twist of the deck, with a fundamental frequency of 4.40 Hz. Since the local mode of the deck is hardly influenced by the foundation exposure, the focus will be on the HL and HT vibrations of the pier top hereafter.

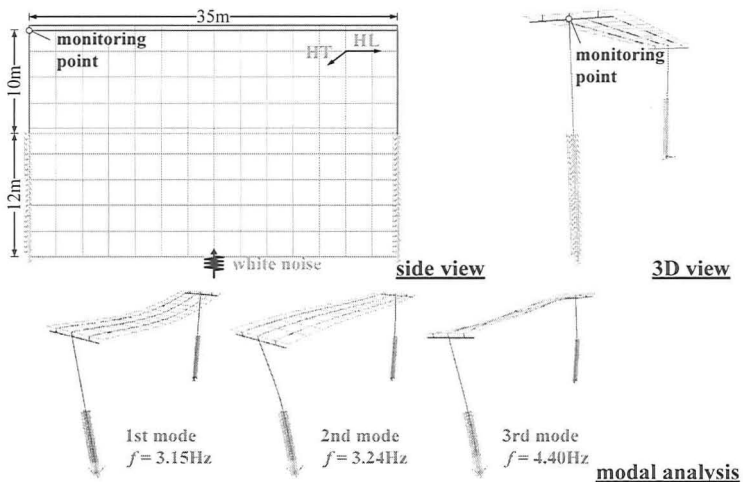


Figure 1. FE model and modal analysis of a simple-supported bridge unit.

Then, the dynamic time history analyses were conducted by using white noise as the input motion at the foundation. Three foundation exposure conditions were adopted, including no exposure, 2.5m exposure, and 5m exposure. The Fourier spectra of the excited HL and HT responses at the top of pier in each case are shown in Figure 2. The predominant frequencies for the HL and HT vibrations in the no-exposure case are confirming to the fundamental frequencies of the 1st and 2nd modes just mentioned, and are lowered as the exposure gets more severe. It is noticed that the decline of the predominant frequency for the HT vibration is more obvious, and the increase of the peak amplitude with respect to the exposure level is also observed.

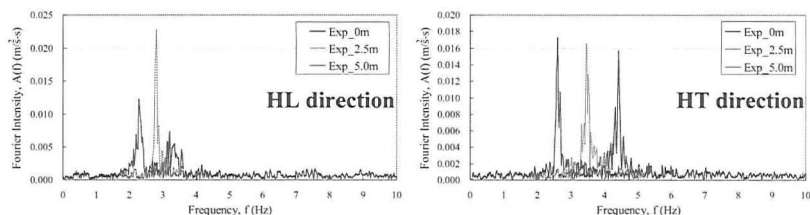


Figure 2. Fourier spectra of excited responses of the bridge unit model.

Setup and data processing of vibration measurement on the bridge

1. Vibration sources

- (a) **Vehicle induced vibrations:** Dynamic loads from the moving vehicles is directly applied on the deck and is the main vibration source of the bridge. Nevertheless, when the weight of the vehicle is too small or the speed is too low, it might merely induce the local vibration of the deck instead of the vibration the entire pier-soil system. In this case, the vibration response can characterize only the superstructure of the bridge or the vehicle mechanical properties rather than the pier-soil system, and in this case the foundation exposure can not be reflected.
- (b) **Ambient vibrations:** If the ambient vibration is input from the ground into the bridge foundation and propagates up to the superstructure, it can be used to characterize the pier-soil system. However, the amplitude is usually small and is easy to be concealed by the vehicle induced vibration unless no vehicle passing.

2. Test configurations

In the vibration measurement, the velocity sensors were used. Sensors were deployed on the cap beam of the tested pier or on the deck right above the tested pier, as shown in Figure 3, where the vibration responses showed the characteristics of the pier-soil system. The vibrations in the HL direction and in the HT direction were continuously recorded for 10–20 minute at off-peak traffic flow condition with a sampling rate of 200 Hz.

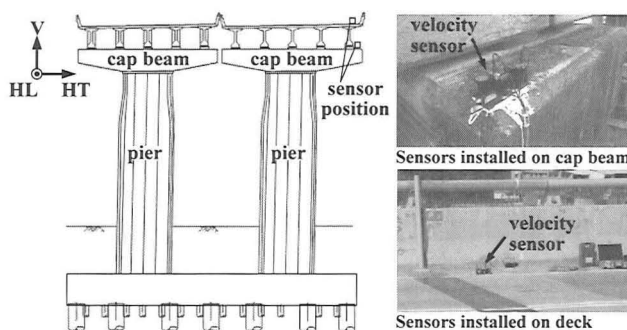


Figure 3. Sensor positions in vibration measurement on the bridge.

3. Data processing scheme

When a long-term field vibration measurement is performed, the vibration characteristics at different moments show some dispersion since the environment and the vibration source are not constant. In order to eliminate the dispersion, Samizo *et al.* (2007) used a concept that sections with a fixed duration are extracted from the overall record, and each section is partially overlapped with the next. The Fourier spectrum is calculated in each section, and the structural natural frequency is identified accordingly. Finally, all these natural frequencies are averaged to obtain a representative one. Based on this idea, an averaged Fourier spectrum is deduced in this study, as shown in Figure 4. Thus, the structural characteristics can be better described, while the time-dependent variance can still be reduced.

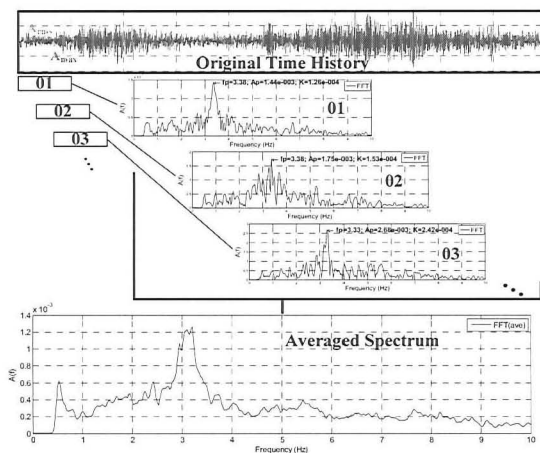


Figure 4. Processing scheme of averaged spectrum analysis.

FIELD VIBRATION MEASUREMENTS OF BRIDGES

Case study I- Wensui Bridge

The Wensui Bridge of Provincial Highway No. 3 in Taiwan had suffered the exposure of the caisson foundations of the piers located on the riverbed due to scouring, and the reconstruction using the pile group to replace the caisson was started in late 2008 and has been finished in late 2009. During the reconstruction, the riverbed level beside the pier P3 was lowered for the work space below the deck, causing the caisson to be exposed around 6~7m, as shown in Figure 5. In order to investigate the difference of the vibration characteristics of the bridge superstructures at different levels of foundation exposure, the field vibration measurements were made simultaneously at the pier P3, of which the foundation was severely exposed, and at the neighboring pier P2, of which the foundation was slightly exposed and had been reinforced by gabions. In this case, the sensors were deployed on the deck right above P2 and P3 respectively since there was no access to the cap beam.

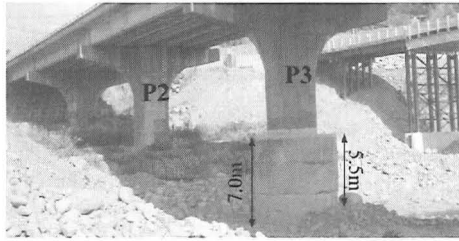


Figure 5. Foundation exposure of Wensui Bridge at the field measurement.

The previous mentioned average spectrum analysis scheme is adopted here to reduce the time-dependent variability of the field measurement. Figure 6 shows the averaged Fourier spectrum of the vibrations at P2 and P3. For the HL direction, the spectral curves of P2 and P3 are similar, with a main peak at the frequency of about 3.5 Hz. It might be the constraint in the HL direction provided by the deck and girders to make the characteristics of the HL vibration of the two piers close to each other. Hence, the vibration in HL direction can not reflect the foundation exposure very well in this case. As for the HT direction, the averaged Fourier spectrum of P2 has two peaks, located at 1.7 Hz and 2.1 Hz, respectively; while only a major peak at 1.7 Hz shows for P3, with a larger amplitude than the peak at 1.7 Hz for P2.

For a better interpretation of the peaks in these averaged Fourier spectra of HT vibrations, the FE model of the unit P2-P3 of the Wensui Bridge was generated for the modal analysis. The model is similar to that one in the previous section, yet the degree of freedom in the HL direction is restrained for simplification. The modal shapes obtained are given in Figure 7. The 1st mode shows the in-phase coupled translation-rocking responses in the HT direction of P2 and P3 with a fundamental frequency of 1.72 Hz, in which the modal displacement of P3 is larger than that of P2. The 2nd mode represents the out-of-phase coupled translation-rocking responses in the HT direction of P2 and P3 with a fundamental frequency of 2.09 Hz, in which the modal displacement of P2 is larger. Consequently, the peak at 2.1 Hz in the averaged Fourier spectrum of the HT vibration of P2 characterizes the structural behavior of P2, while the peaks at 1.7 Hz in both the spectra of the HT vibration of P2 and P3 characterize P3. Since the severe foundation exposure of P3 reduced its lateral stiffness, the lower predominant frequency and the larger amplitude of the vibration of P3 exhibited, which even influenced the vibration response of P2.

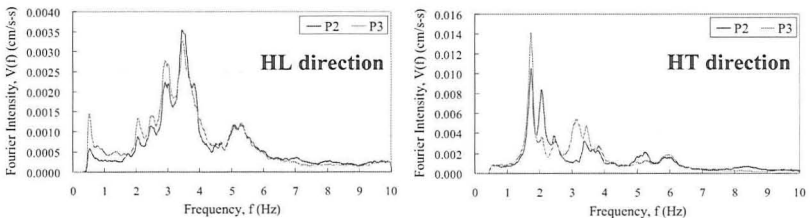


Figure 6. Averaged Fourier spectra of vibration at P2 and P3 of Wensui Bridge.

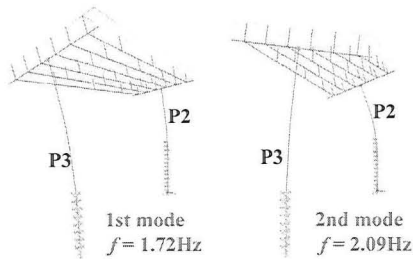


Figure 7. Results of modal analysis of Wensui Bridge unit model.

Case study II- Hsichou Bridge

The Hsichou Bridge of Provincial Highway No. 1 in Taiwan also had suffered the scour of its group-pile foundation and the piles had been severely exposed. The retrofit work of foundations by lowering the foundation level, adding piles and enlarging the pile cap was started in May 2009 and is expected to be finished in September 2010. The pier P36 was adopted for study. Before the retrofit (April 2009) the piles of P36 were about 4.5m exposed, while during the retrofit work (July 2009) the riverbed level beside the P36 was lowered for the work space, causing the piles to be exposed around 7.5m, as shown in Figure 8. Field vibration measurements were made at P36 under the two mentioned foundation exposure conditions respectively. In this case, the sensors were installed on the cap beam.

Figure 9 depicts the averaged Fourier spectra of the vibrations at P36 at 4.5m exposure and at 7.5m exposure. For the HL vibration, the predominant vibration frequency is about 3.6 Hz at 4.5m exposure and is 3.4 Hz at 7.5m exposure. The later is slight lower yet the difference is small. It might be also due to the constraint in the HL direction from the superstructure. As for the HT vibration, the averaged Fourier spectrum of the 4.5m exposure case has two peaks, located at 2.0 Hz and 3.7 Hz, respectively, and the averaged Fourier spectrum of the 7.5m exposure case also has two peaks located at 1.5 Hz and 3.5 Hz. Assuming that the peaks around 1.5~2 Hz and around 3~4 Hz are corresponding to two different vibration modes, then the former one reflects the foundation exposure better. The corresponding predominant frequency at 7.5m exposure is 20% lower than at 4.5m exposure. It should be noted that though the amplitude of the averaged Fourier spectrum is larger for the 7.5m exposure case in both direction, it is not appropriate to attribute this to the foundation exposure since the test conditions (especially the vibration source) were not the same.

Similar to the previous case study, the FE model of the unit P35-P36 of the Hsichou Bridge was established to perform the modal analysis for a better interpretation. The model is similar to the previous models except the pile was modeled by beam element. The modal shapes of the model with an exposure of 4.5m are given in Figure 10. The 1st mode is the in-phase coupled translation-rocking responses in the HT direction of P35 and P36 with a fundamental frequency of 1.97 Hz, close to the first predominant frequency from the field vibration measurement in the 4.5m exposure case. The 2nd mode is the out-of-phase coupled translation-rocking responses in the HT direction of P35 and P36 with a fundamental frequency

of 2.29 Hz. The 3rd and 4th modes are the local bending and twist of the deck, with the fundamental frequencies of 3.49 Hz and 3.83 Hz. For the case of 7.5m exposure, the modal shapes of the first four modes are similar. The fundamental frequencies for the 1st and 2nd modes are 1.54 Hz and 1.74 Hz, which dropped significantly, while those of the 3rd and 4th modes are 3.42 Hz and 3.60 Hz, only slightly lowered. Thus, it can be concluded that the predominant frequencies of the HT vibration around 1.5~2 Hz from the field measurements were corresponding to the in-phase coupled translation-rocking mode in the HT direction of the two piers, and were lowered significantly when the foundation was more severely exposed. While those around 3~4Hz were related to the local mode of the superstructure and therefore were close in the two foundation exposure condition.



April 2009 (piles exposed around 4.5m)



July 2009 (piles exposed around 7.5m)

Figure 8. Foundation exposure of Hsichou Bridge at the field measurement.

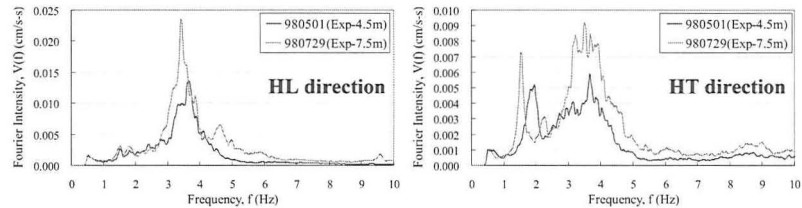


Figure 9. Averaged Fourier spectra of vibration at P36 of Hsichou Bridge.

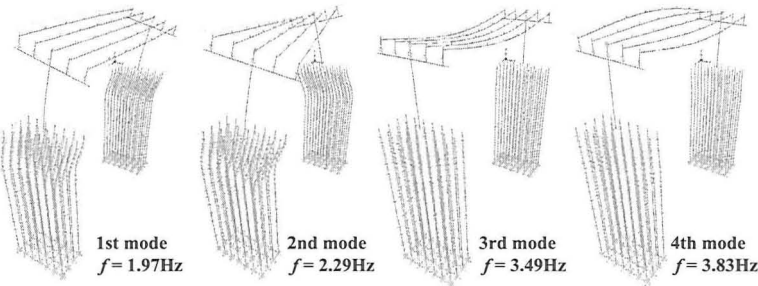


Figure 10. Results of modal analysis of Hsichou Bridge unit model.

CONCLUSION AND FUTURE APPLICATIONS

According to the results of the numerical analyses and field vibration measurements presented, several conclusions can be drawn as follows:

1. By the dynamic analysis of the bridge unit FE model, it is shown that the foundation exposure will decrease the overall stiffness of the bridge-soil system and lower the predominant frequency of the vibration of the superstructure, especially in the HT direction.
2. According to the results of field vibration measurements, the influence of the foundation exposure on the vibration behavior of the superstructure of the bridge is actually verified.
3. The vibration measurement on the superstructure of the bridge gives a reasonable assessment of the foundation exposure due to scouring. In addition, since the real bridge is a complex soil-structure system, it is recommended that a numerical model should be established for a better interpretation of the vibration response.

REFERENCES

- Doebling, S.W., Farrar, C.R., Prime, M.B., and Shevitz, D.W. (1996). Damage identification and health monitoring of structural and mechanical systems from changes in their vibration characteristics: a literature review. *Report LA-13070-MS*. Los Alamos National Laboratory, Los Alamos, NM.
- Farrar, C.R., Cornwell, P.J., Doebling, S.W., Prime, M.B., and *et al.* (2000). Structural health monitoring studies of the Alamosa Canyon and I-40 bridges. *Report LA-13635-MS*. Los Alamos National Laboratory, Los Alamos, NM.
- Kim J.T., Ryu Y.S., Cho H.M., and Stubbs, N. (2003). "Damage identification in beam-type structures: frequency-based method vs mode-shape-based method." *Engineering Structures* 25(1): 57-67.
- Nakamura, Y. (1997). "Seismic vulnerability indices for ground and structures using microtremor." *Proceedings of World Congress on Railway Research*, Florence, Italy.
- Samizo, M., Watanabe, S., Fuchiwaki, A., and Sugiyama, T. (2007). "Evaluation of the structural integrity of bridge pier foundations using microtremors in flood conditions." *Quarterly Report of the Railway Technical Research Institute* 48(3): 153-157.
- Ivanovic, S.S., Trifunac, M.D., Novikova, E.I., Gladkov, A.A., and Todorovska, M.I. (2000). "Ambient vibration tests of a seven-story reinforced concrete building in Van Nuys, California, damaged by the 1994 Northridge Earthquake." *Soil Dynamics and Earthquake Engineering* 19(6): 391-411.
- Ko, Y.Y. and Chen, C.H. (2009). "Soil-structure interaction effects observed in the in situ forced vibration and pushover tests of school buildings in Taiwan and their modeling considering the foundation flexibility." *Earthquake Engineering and Structural Dynamics* (accepted).
- Chen, C.H., Huang, T.C., and Ko, Y.Y. (2009). "In-situ ground vibration tests in Southern Taiwan Science Park." *Journal of Vibration and Control* (accepted).

Tidal Bridge Scour in a Coastal River Environment: Case Study

Serkan Mahmutoglu, P.E.

AECOM, 500 Southborough Drive South Portland, ME 04106 PH: (207) 775-2800

ABSTRACT

As part of an innovative design/build project a data-rich hydraulics and scour analysis was performed for the proposed 5 kilometer long Washington Bypass Bridge over the Tar River in Washington, NC. This analysis featured: 1) a current and stage monitoring program, 2) historical aerial photograph analysis, 3) extensive long term bed elevation study, 4) debris scour evaluation, 5) variable skew angles due to spatial and temporal changes in flow characteristics, 6) complex pier analysis, and 7) use of a two-dimensional (2D) hydrodynamic model (TABS RMA-2) to evaluate riverine flooding and hurricane surge hydraulics causing extensive wetting-and-drying.

The model was subjected to a comprehensive two-step model calibration/verification process. Low-flow conditions were calibrated and verified using project-collected Acoustic Doppler Current Profiling (ADCP) and tidal gage monitoring. Boat-mounted ADCP measurements collected by USGS during hurricane surge (Hurricane Dennis) and rain-induced flooding (Hurricane Floyd) were used for high-flow calibration and verification. This was a rare opportunity for a bridge designer to be able to evaluate scour using a sophisticated hydrodynamic model that was calibrated with field data collected during an event that represented the design conditions.

Two-dimensional hydrodynamic modeling was used to simulate complex hydraulics of the project site located at the end of the 8,300 square kilometer watershed which is tidally influenced. Due to the size of the upstream drainage area and the proximity to the open ocean both rain-induced-flow and storm-surge scenarios were considered.

INTRODUCTION

AECOM was hired by Flat Iron – United Joint Venture (FLUNJV) to perform engineering services relating to the hydraulics and scour analysis for the Washington Bypass Bridge (BIN 353-US17 over the Tar River) in Washington, NC (Figure 1). Under this agreement, AECOM developed a 2-dimensional hydrodynamic model (RMA-2) to evaluate the flow depth and velocity for the 100-, and 500-year storm events. The predicted velocity and depth information from these events were used to calculate scour depths at the bridge and assist in designing the bridge substructure units to withstand scour.

As part of this study, AECOM designed and oversaw the required data collection performed by Ocean Surveys, Inc. (OSI) which was used for the calibration and verification of the hydrodynamic model. The data collection occurred during a Spring Tide and involved three (3) tide gages, one (1) “upward looking” Acoustic Doppler Current Profiler (ADCP), and ADCP transects of cross sections at and either side of the bridge.

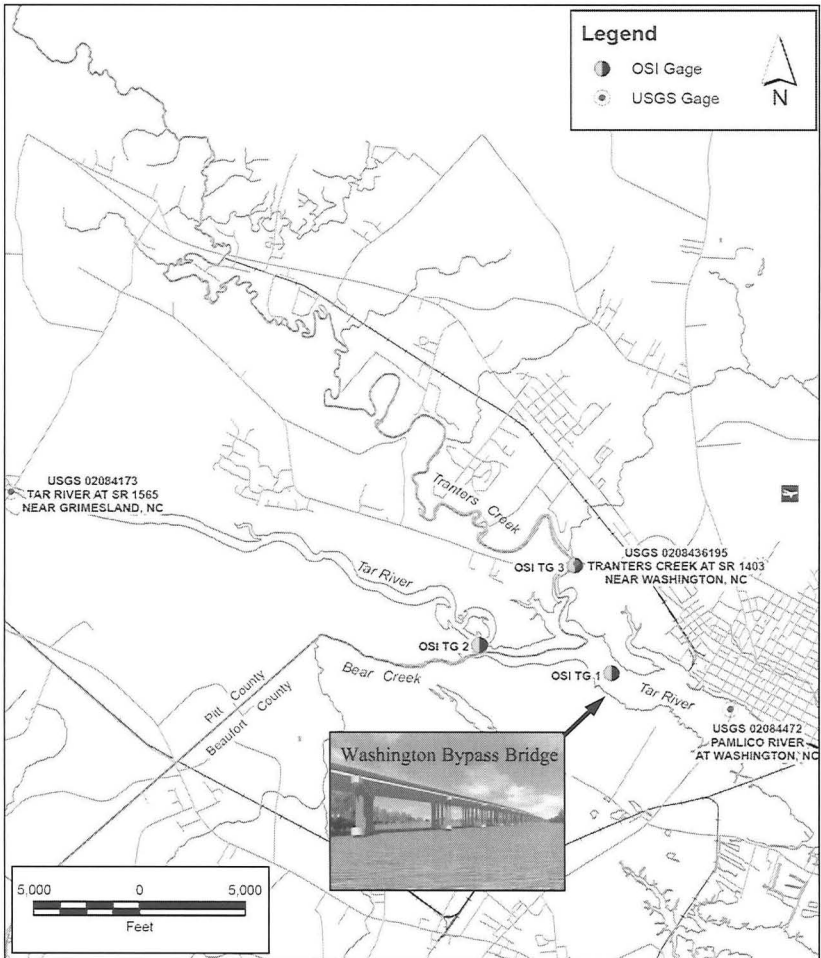


Figure 1. Project location.

Due to the size of the upstream drainage area (8,300 sq. km) and the proximity to the open ocean (i.e. to Atlantic Ocean through Pamlico River and Pamlico Sound), both rain-induced-flow and storm-surge scenarios were considered separately as indicated by HEC-25 (1st Edition, Section 2.8 Page 2.31).

Local pier scour was calculated for each of the 127 pile bents (piers) for 8 different conditions: 2 (rain/surge) x 2 (100-year/500-year) x 2 (debris/no-debris) = 8. Upon evaluating the results, scour calculations were determined to be sensitive to debris. Therefore, a debris accumulation potential evaluation per HEC-9 3rd Edition

(Debris Control Structures – Evaluation and Countermeasures) was performed for each bridge component. Contraction scour caused by the proposed bridge, which is scour due to contraction of the flow's conveyance area caused by the bridge structure and its approaches, was also calculated.

In addition to local and contraction scour, long-term bed elevation change was analyzed. The analysis consisted of three subtasks. The first subtask utilized historical aerial photographs of the area to digitize the shoreline and then to observe the evolution of the shoreline changes in time. The second subtask was obtaining various historical bathymetric surveys conducted at the US 17 Bridge crossing, located about 1.6 km downstream of the Washington Bypass Bridge, and calculating the vertical changes of the river bottom. The third subtask was the channel stability assessment performed by geomorphologist Prof. Stanley Riggs of Eastern Carolina University, who is an expert on the riverine geomorphology for this site.

METHODOLOGY

In order to estimate the site-specific detailed hydrodynamic characteristics at the Washington Bypass Bridge it was necessary to construct a 2-dimensional hydrodynamic model. Hydrodynamic modeling was accomplished using the Surface Water Modeling System (SMS) in conjunction with RMA-2.

Model Domain

The model domain was defined considering the area of interest, location of available data sources, and the limitation on computational resources. The area of interest was confined to the vicinity of the bridge crossing. In order to obtain an adequate solution at the area of interest, model boundaries were established distant from the area of interest and where USGS station locations were available as data sources.

For the storm surge scenario the downstream model boundary needed to be moved further downstream (35 km downstream of Pamlico USGS gage) to utilize available data stations.

The model domain was meshed using triangular and rectangular elements. The approximate number of elements in the meshes used ranges from 9,000 to 23,000.

Calibration and Verification

The RMA-2 model is calibrated primarily with two (2) parameters: the Peclet Number (Pe) and the Manning Roughness Coefficient (n), and was performed in two stages. In the first stage, the detailed information collected by project survey team was used to calibrate only the model cells representing the channel. Calibration with this detailed data was limited to the channel because during the data collection period, water was confined to the channel. In the second stage, an extreme event was used to calibrate the overbank areas (i.e. wetlands and other floodplain areas) while they are exposed to flow. The data records collected at the US 17 crossing by USGS during Hurricane Dennis in 1999 were used for this purpose.

The channel calibration of the model was performed with the available data and the data sets collected during the project's monitoring period. The point in-situ

ADCP and the project's Tide Gage No. 1 (TG 1) were used to compare the actual data with the model results.

Overbank calibration of the model was performed using data collected by the USGS at the Pamlico Gage. Input variables for the model included WSE from the Pamlico Gage and model elements account for storage in watershed (which were used beyond the Tranter's Creek and Grimesland boundaries). Calibrated channel properties were kept the same and the overbank depth varying Manning's n roughness was used for calibration.

Verification of the model was performed in two (2) ways. First, for low flow conditions flow measurements at Pamlico gage were compared to model results. Second, for high flow conditions USGS ADCP velocity transects data at the maximum velocity conditions during Hurricane Floyd at 45 meters upstream of US 17 were compared to model predictions.

Calibrated model prediction of Hurricane Dennis compared to flow measurements taken at the USGS Pamlico Gage is shown in Figure 2.

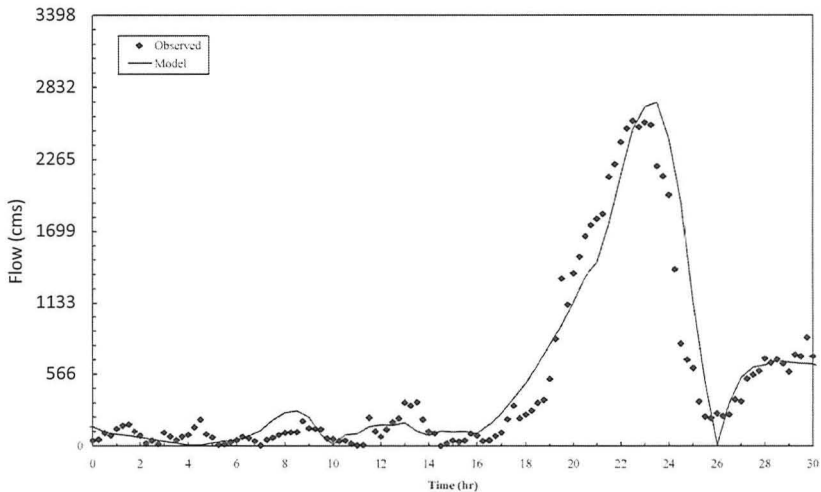


Figure 2. Calibrated model simulation of Hurricane Dennis.

RESULTS

Once the model was calibrated and verified, two different scenarios and two different return intervals totaling four (4) flow cases were developed: a rain-induced-flow scenario and a storm-surge scenario, for 100- and 500-year storms.

Rain Induced Flow Scenario

As seen during Hurricane Floyd, a hurricane causing significant rainfall over an already saturated ground can cause significant flooding in Tar/Pamlico watershed. Another observation made during Floyd was the duration of the peak flow. Unlike the tidal surge, which has a peak that passes within a few hours (i.e. dynamic), Hurricane

Floyd's peak was sustained for days (i.e. steady). The duration is important for scour in cohesive sediment (such as this case), as equilibrium scour conditions require time to develop. FEMA FIS (Reference 2) was used to determine peak flow values for the model boundaries. Tar River peak flows were estimated using the flows represented in the FIS immediately downstream of the Bear Creek confluence, and the Tranter's Creek boundary flows were also read from the FIS upstream of the confluence with Tar River. Table 1 shows the peak flow values used for the rain induced flow cases (i.e. Case 1 and 2).

Table 1. Upstream Boundary Peak Flow Conditions in Cubic Meters per Second (cms)

	Tar River	Tranter's Creek
Case 1 (100-year)	1,550	310
Case 2 (500-year)	2,200	485

The downstream boundary condition was the WSE at the USGS Pamlico gage. The WSE for both cases was calculated using a stage-flow relationship developed from the data collected at the gage. Only high flows (i.e. >283 cms) in ebb direction were considered while generating the relationship.

In general, velocities are lower on the overbanks and higher in the channel and highest around the thalweg as expected.

Hurricane Surge Scenario

Upon establishment of the typical tide, design hurricane surges were developed using the Pooled Fund Study (Reference 5) that was coordinated by the SCDOT and Boundary Conditions for Bridge Scour Analysis (Reference 6) by the NCDOT. From the latter study, a peak storm surge value (S_p) of 3.4 meters was obtained for the 100-year case at Station No. 3. In order to utilize the data from the Station No. 3, the downstream model boundary was moved to the location (latitude 35.4, longitude 76.72) that corresponds to the Station No. 3. The same data sources used to create the calibrated model (i.e. shoreline, bathymetry, topography, etc.) were also used to extend the model. Roughness and turbulence properties developed for the calibrated model were also applied to the extended section.

Similar wetting/drying issues that were encountered during the NCDOT Study (Reference 6) were also applicable to the 2D model used during this analysis. Due to the large floodplain-to-channel ratio in the area (>8), most of the numerical model cells were dry except for a short duration during the entire simulation. The abrupt wetting/drying due to the dynamic surge causes numerical instability in the 2D model. Therefore, the marsh porosity approach, available through RMA2, was utilized. Marsh porosity gradually decreases the conveyance capacity when the WSE drops below the average ground elevation, providing a smooth transition between wetting and drying, which increases the numerical stability of the model.

Storm surge scenario events, both 100-year and 500-year, were simulated using the extended model. Both synthetic storm surges (100-year 6,500 cms and 500-year 12,900 cms) are significantly greater than the observed 2,600 cms peak flow magnitude of Hurricane Dennis.

The direction of the flow for the storm-surge scenario deviated from the average direction (observed from the field data collection) as the velocities increased. The deviation was observed to be 8 degrees during ebb times (i.e. rain-induced-flow scenario) and 20 degrees during flood times (flood periods produce peak velocity/depth combinations).

Figure 3 shows peak velocity magnitude and direction for the 100-year storm-surge scenario. Color-coding indicates velocity magnitude and the vectors are scaled to magnitude. In general, velocities are lower on the overbanks and higher in the channel and highest around the thalweg as expected. One exception to that is the bents located adjacent to Kennedy Creek experience increased velocities compared to other overbank bents due to the relatively lower friction path provided by Kennedy Creek during flood stages of the surge.

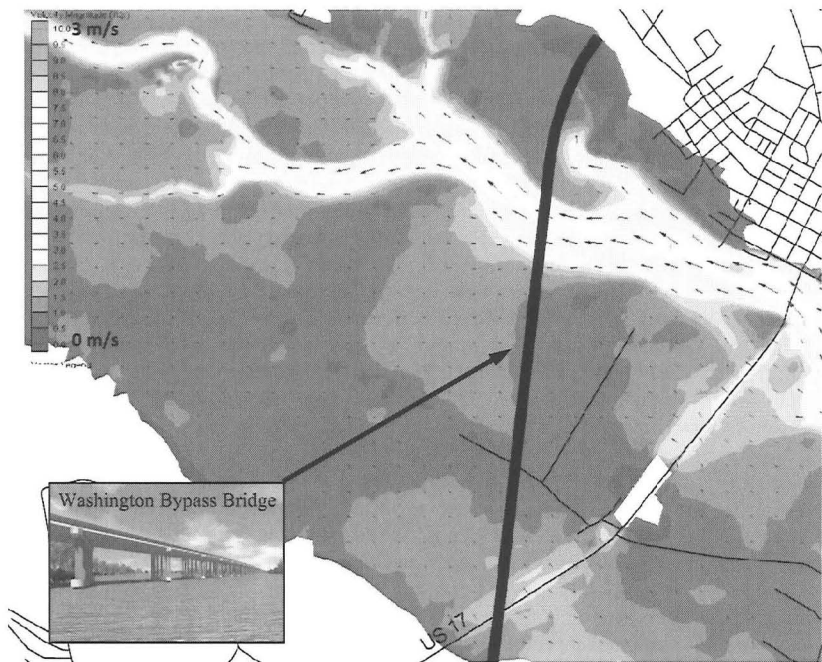


Figure 3. 100-year storm surge depth averaged velocities (red indicates 3 m/s and blue indicates 0 m/s).

Scour Analysis

Scour evaluation and calculations were performed in accordance with the guidelines set forth in the most current editions of the Federal Highway Administration's Hydraulic Engineering Circular (HEC) HEC-20 3rd Edition (Stream Stability at Highway Structures), HEC-18 4th Edition (Evaluating Scour at Bridges),

and HEC-25 1st Edition (Tidal Hydrology, Hydraulics and Scour at Bridges). The hydraulic data required for the scour analysis were extracted from the 2-D model, the soil data were supplied by Mactec Inc., and the preliminary bridge geometry was taken from AECOM's preliminary bridge design plans. All equation constants and coefficients used in the analysis were taken from literature. The following four components of total scour were calculated: aggradation and degradation, general scour, local scour, and lateral stream migration.

Based on the results of the 2D modeling of peak flows caused by rainfall and peak flows due to storm surge hurricane surge conditions (landward flow) produced the worst-case design scour conditions at the proposed bridge location.

Analysis of Long-Term Bed Elevation Change

The analysis consisted of three subtasks. The first subtask involved utilizing historical aerial photographs of the area to digitize the shoreline and observe the evolution of the shoreline changes in time. The second subtask involved obtaining bathymetric surveys conducted at the US 17 Bridge crossing, located about 1.6 km downstream of the Washington Bypass Bridge, and observing the vertical changes on the river bottom. The third subtask was a channel stability assessment performed by riverine geomorphology expert Prof. Stanley Riggs of Eastern Carolina University, who has specific knowledge of the project site.

The historical aerial photograph analysis was performed by digitization of the shoreline in the vicinity of the proposed bridge crossing and then the subsequent observation of the resulting pattern and rate of the channel movement. Analysis showed that no significant changes have occurred over the past 50 years.

The channel stability assessment performed by Prof. Riggs indicated that the Tar River in the vicinity of the Washington Bypass Bridge has been stable vertically (i.e. the channel bed has not experienced significant sediment erosion or accumulation) and laterally (i.e. the channel has not migrated significantly). Considering the current rate of change, significant degradation is not expected.

The conclusion by Prof. Riggs is that the long-term scour component at the site is negligible (i.e. the long-term component of scour is 0 m). However, the analysis indicated that there may be a lateral shift of 0.3 m/year. Therefore, considering the design life of the bridge is 100 years, it was recommended that closest overbank bents to the channel be designed as channel bents.

Scour at Abutments

Per the preliminary bridge design plans, the abutments were determined to be outside of the flood elevation, and were not analyzed further for scour.

Computation of the Magnitude of Local Scour at Piers

Local scour at the proposed Washington Bypass Bridge was computed for hurricane storm surges with recurrence intervals of 100 years and 500 years using the CSU equation as presented in HEC-18. Both simple and complex pier calculations were utilized in calculation of the pier scour as explained below. The hydrodynamic model time step causing the highest scour was used.

During the field inspection, it was determined that the fallen, or eroding, vegetation located at the edge of the channel could potentially become a source of debris that could collect at the channel bents and cause increased scour. However, the established swamp forest in the overbanks acts as a debris deflector for the overbank bents. Debris, therefore, is not expected to be a critical factor for the bents located on the overbanks. The simple pier equation was found to be more suitable for bents in the channel due to its conservative assumption of a solid pier and ability to account for full blockage by debris as described in HEC-18. However, for bents in the overbanks, which have a sufficient forest buffer protecting them from debris, the complex pier equation was found to be more suitable.

A summary of the calculated scour depths is shown in Table 2. For the channel bents, considering that the thalweg in the channel can migrate, the largest scour value (lowest scour-hole bottom elevation) calculated should be used for design of each channel bent. Bents on the overbank which lie outside the potential 30 meters of channel migration should be designed to withstand the smaller calculated scour depths in these areas.

Table 2. Scour Depth Summary Table (m)

	Pile Bent Numbers		
	1 through 81	82 through 99	100 through 127
	Southern Overbank	Channel	Northern Overbank
Storm Event	Avg. (min, max)	Max.	Avg. (min, max)
100-year	3 (1.5, 5.5)	8.2	2.7 (1.5, 4.3)
500-year	4.3 (1.8, 7)	9.1	4 (1.8, 5.5)

CONCLUSION

Adequate data was a key in preparing a comprehensive scour analysis. Obtaining this data involved engaging relevant resources (NCDOT, USGS, Eastern Carolina University, etc.) at the early stages of the project. Especially, the importance of long-term ADCP data and how it can improve the confidence level of sophisticated hydrodynamic model simulations became apparent.

By limiting complex scour equations to simple scour equation, over estimation of scour at the extreme values could be minimized.

A comprehensive long-term aggradation/degradation analysis can indicate maximum expected river bed shift for the design life of the bridge, which minimizes the number of piers to be treated as a channel pier instead of an overbank pier.

Over estimation of scour due to debris accumulation can be minimized by identifying only the piers that are subject to accumulation.

ACKNOWLEDGMENT

The authors would like to acknowledge FLUNJV and NCDOT personnel, Dr. Edward Kent (formerly AECOM), Mr. Ryan Edison, Mr. Wally Jordan, Mr. Tom Shearin (AECOM) and Prof. Stanley Riggs for their contributions to this study.

REFERENCES

- E.V. Richardson and S.R. Davis, 2001, "Evaluating Scour at Bridges," Fourth Edition, FHWA NHI 01-004, Federal Highway Administration, Hydraulic Engineering Circular No. 18, U.S. Department of Transportation, Washington, D.C.
- P.F. Lagasse, J.D. Schall, and E.V. Richardson, 2001, "Stream Stability at Highway Structures," Third Edition, FHWA NHI 01-002, Federal Highway Administration, Hydraulic Engineering Circular No. 20, U.S. Department of Transportation, Washington, D.C.
- P.F. Lagasse, L.W. Zevenbergen, J.D. Schall, and P.E. Clopper, 2001, "Bridge Scour and Stream Instability Countermeasures," Second Edition, FHWA NHI 01-003, Federal Highway Administration, Hydraulic Engineering Circular No. 23, U.S. Department of Transportation, Washington, D.C.
- L.W. Zevenbergen, P.F. Lagasse, and B.L. Edge, December 2004, "Tidal Hydrology, Hydraulics and Scour at Bridges", First Edition, Hydraulic Engineering Circular No. 25, U.S. Department of Transportation, Washington, D.C.
- L.W. Zevenbergen, B.L. Edge, J.H. Hunt, J. Fisher, E.V. Richardson, P.F. Lagasse, March 2002, "Tidal Hydraulic Modeling for Bridges," SCDOT Pooled Fund Study, Ayres Associates, Edge & Associates.
- M.F. Overton, R.R. Grenier, J.S. Fisher, March 1999, "Boundary Conditions For Bridge Scour Analysis", NCDOT, NC State University.
- Federal Emergency Management Agency State of North Carolina, January 2, 2004, Flood Insurance Study, No. 37147CV000A, "A report of Flood Hazards in Pitt County North Carolina and Incorporated Areas"
- J.B. Bradley, D.L. Richards, C.D. Bahner, October 2005, "Debris Control Structures – Evaluation and Countermeasures," Third Edition, Hydraulic Engineering Circular No. 9, U.S. Department of Transportation, Washington, D.C.
- Benedict, S.T., and Caldwell, A.W., "Development and evaluation of clear-water pier and contraction scour envelope curves in the Coastal Plain and Piedmont Provinces of South Carolina", U.S. geological Survey Scientific Investigations Report 2005-5289, 98 p

Re-Classifying Bridges with Unknown Foundations

By Sayed M. Sayed¹, PE, M. ASCE, Hisham Sunna², PE, M. ASCE,
and Pamela R. Moore³, PE

¹ Principal and Director of Engineering, GCI Inc., 2290 North Ronald Reagan Blvd., Suite 100, Longwood, Florida 32750; PH (407) 331-6332; email: smsgci@aol.com

² Vice President, Ayres Associates, 8875 Hidden River Parkway, Suite 200, Tampa, Florida 33637; PH (813) 978-8688, email: sunnah@ayresassociates.com

³ Senior Project Manager, GCI Inc., 1141 Jackson Avenue, Chipley, Florida 32428; PH (850) 638-2288; email: pmoore_gci@bellsouth.net

ABSTRACT

A practical, cost-effective and rational approach to re-classify bridges with unknown foundations is presented in this paper. The method is based on satisfying static equilibrium under appropriate loads for the existing bridge pier/bent conditions using three-dimensional, non-linear finite element analysis. The method is applicable to partially and fully-embedded piled-foundation sub-structures where physical measurements of the super-structure and top of the foundation elements (layout, type, and size) can be made. The computed pile embedment using the proposed method is remarkably in close agreement with the actual embedment for bridges referenced in this paper. The approach presented in this practice-oriented paper can provide confidence in assessing the "unknown foundation" bridges and will expedite the screening of these bridges to protect the public. The methodology can also be used to validate embedment determinations done by Non-Destructive Testing (NDT) methods in previous or current projects and to guide any future NDT.

INTRODUCTION

Since the early 1990's, the Florida Department of Transportation (FDOT) and other transportation agencies in the United States have evaluated the impact of scour on bridges. The efforts of such evaluation focused on assessing the stability of state and locally-owned bridges over tidal and non-tidal waterways with scourable beds and determining the risk of failure due to scour. In general, the bridges fall into three categories; namely, bridges with detailed construction records (Category A); bridges with partial construction records (Category B); and bridges without construction records (Category C). The scour evaluation (Hydraulic Analysis; Soil-Structure Evaluation; and Remedial Measures) of the various categories is basically the same once the sub-structure is defined. Assessment of the stability of Category A (i.e., known foundation) bridges is straightforward and many bridges in various states have been evaluated over the past sixteen years. As a result, hundreds of bridges have undergone monitoring, remedial measures or replacement.

Bridges with unknown foundations (i.e., Category B and C) are much more difficult to evaluate in an efficient manner. With the financial and budgetary constraints currently imposed on transportation agencies throughout the world, there is an urgent need for a practical, cost-effective, and rational approach. For Category B bridges, the inference and/or Back-Calculation (Reverse Engineering) methods initiated by the authors (Sayed 2005) after the FHWA Unknown Foundation Summit (FHWA 2005) are

appropriate and are outlined in a recent paper (Sayed et al. 2009). Category C bridges are the most challenging. The Static/Back-Calculation (S/B-C) method presented herein is suggested as a means of re-classifying unknown foundation bridges to be "known" so that the scour evaluation can be carried out in the conventional way to assess the risk of failure (Stein and Sedmera 2006) due to the design storm events.

PROCEDURE

Background

The approach presented herein to re-classify bridges without construction records from being "unknown" to "known" is applicable to partially and fully-embedded pile groups where physical measurements of the super-structure and top of foundation elements (layout, type, and size) can be made. Table 1 presents the proposed approach of analysis for unknown foundation bridges.

Table 1. Proposed Methodology for Re-Classifying Unknown Foundation Bridges

Bridge Category	Availability of Records	Proposed Approach
B	Bridges with partial construction records	Inference Method and/or Back-Calculation (Reverse Engineering) Method
C	Bridges without construction records	Back-Calculation (Reverse Engineering) Method + Static/Back-Calculation Method

A detailed assessment of available bridge data (bridge inspection reports, site reconnaissance, etc.) is important in this process in order to develop an optimum and cost-effective analysis. A good geotechnical investigation program that incorporates Non-Destructive Testing (NDT), if required by the Owner, and addresses the scheduling of borings and NDT in an optimum manner is a key to minimizing the cost involved.

Static/Back-Calculation (S/B-C) Analysis

The focus of this paper is to address the use of Static Analysis for the existing bridge conditions to back-calculate the embedment of the piled-foundation system supporting the bridge. The question that needs to be asked is as follows: What is a reasonable estimate of minimum pile embedment that satisfies static equilibrium given the design and construction methods used at the time the bridge was built? The answer to this question can be established if one has accurate physical measurements of the components of the super-structure and top of the foundation elements (layout, type,

and size). Such measurements enable the structural engineer via Back-Calculation (Reverse Engineering) to reasonably compute the service loads on the sub-structure. With a reasonable Factor of Safety for traditional Allowable Stress Design (ASD), or appropriate load and resistance factors for Load and Resistance Factor Design (LRFD), the engineer can establish the ultimate load for which the foundation elements were designed. Using this ultimate load and relevant information from the geotechnical investigations, the structure can then be modeled to arrive at a minimum embedment that satisfies static equilibrium for a typical bent or pier as shown in Figure 1.

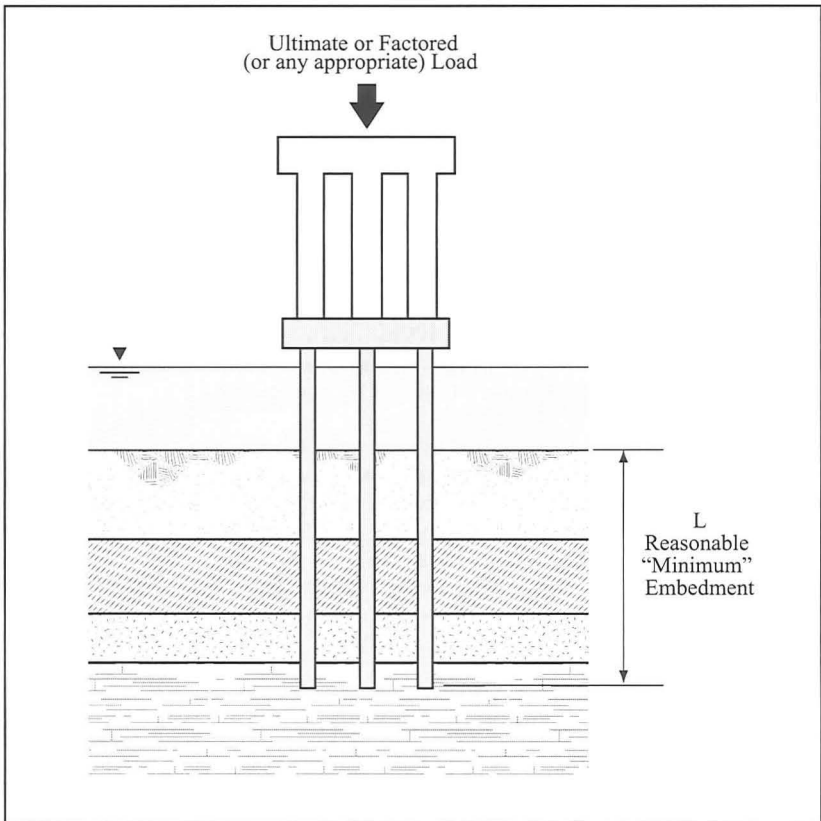


Figure 1. Typical bridge pier/bent over waterway

For older bridges, Allowable Stress Design (ASD) was commonly used. The Static/Back-Calculation Analysis is based on the following relationship:

$$(R)(FS) = \eta_g \Sigma Q_o \quad ; \quad Q_o = Q_o(L) \quad (1)$$

Where

- R = Allowable load per pile bent or pile group;
- FS = Factor of safety;
- η_g = Pile group efficiency; and
- Q_o = Ultimate pile capacity of single pile.
- $Q_o(L)$ = Ultimate pile capacity of single pile expressed as a function of pile embedment (L); and
- L = Reasonable "Minimum" embedment.

It should be noted that the smaller the Factor of Safety (FS), the shorter the embedment. Hence, the proposed method provides a conservative but realistic "current" embedment.

For the most recently designed and constructed bridges, Load and Resistance Factor Design (LRFD) was probably used. The basic equation is, in this case, expressed as:

$$\gamma_d R_{DL} + \gamma_L R_{LL} = \eta_g \Sigma \phi Q_o \quad ; \quad Q_o = Q_o(L) \quad (2)$$

Where

- γ_d and γ_L = Load factors for the dead and live load components;
- R_{DL} and R_{LL} = Dead and live load components of the service load R; and
- ϕ = Resistance (performance) factor.

For locally-owned bridges that are not designed for certain standard loading requirements, an appropriate load per pile would be required to use the S/B-C method as shown in the flowchart in Figure 2. The load posting of these bridges can be used in lieu of the more rigorous Back-Calculation (Reverse Engineering) to arrive at the load per bent/pile needed for using the S/B-C analysis.

The pile group efficiency, η_g , is computed from the following expression (Sayed and Bakeer 1992):

$$\eta_g = 1 - (1 - \eta_s * K) * \rho \quad (3)$$

Where

- η_s = Geometric efficiency;
- K = Group interaction factor; and
- ρ = Friction factor.

The S/B-C computation is carried out by using the three-dimensional, non-linear finite element program FB-MultiPier/FB-PIER (FDOT 2000) iteratively to arrive at the stability/instability embedment. The program considers both axial and lateral pile-soil interaction. Soil is characterized by user-defined parameters. The pile group efficiency and time-dependent soil parameters can be incorporated using the procedure outlined by Sayed and Bakeer (1992). The Static/Back-Calculation process is depicted in Figure 2.

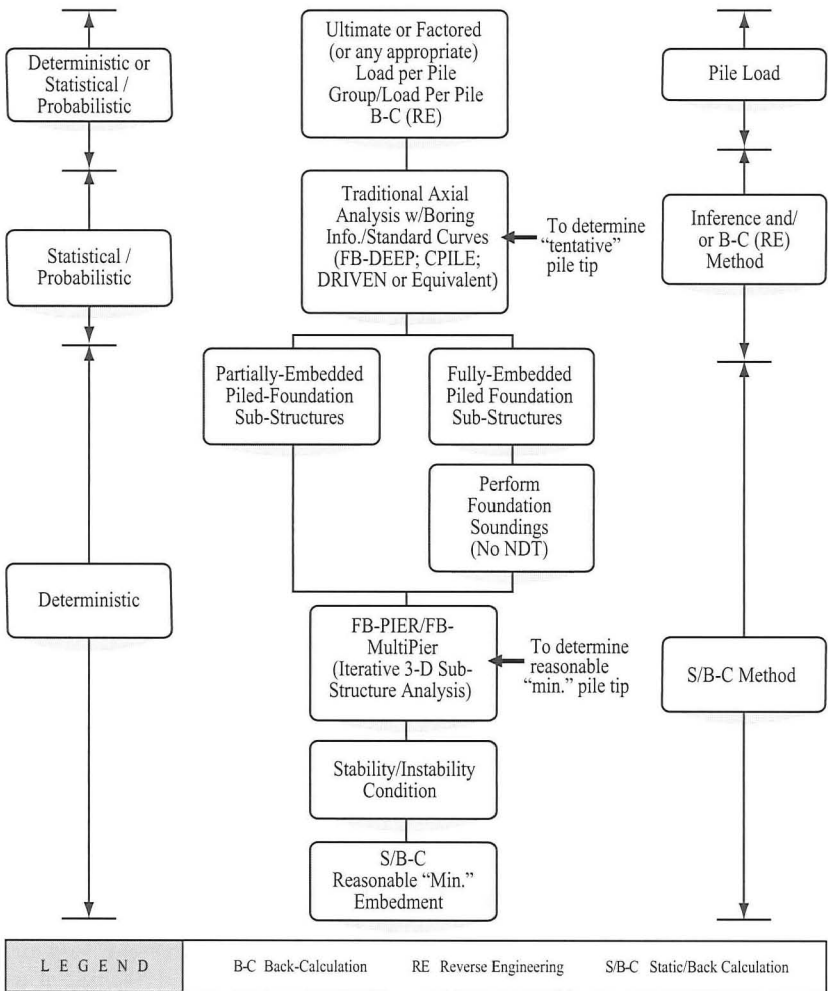


Figure 2. Static/Back-Calculation (S/B-C)

As discussed later in the paper, the proposed method agrees reasonably well with the actual embedment for the "known" foundation bridges used to illustrate the predictive capability of the S/B-C method. Results have shown the actual length is at least equal to the reasonable minimum embedment computed using the Static/Back-Calculation (S/B-C) method added to the known unsupported length. Thus, when implemented with sound engineering judgment, the S/B-C method can be used to analyze bridges with unknown foundations. Subsequent scour evaluations can then

be performed using the S/B-C "reasonable minimum embedment" as the "known" foundation embedment. If a bridge is classified as low-risk based on the scour evaluation using the S/B-C "reasonable minimum embedment", it can be removed from the list of "unknown foundation" bridges. If it is found to be scour critical, further measures can be taken. Thus, the method provides a deterministic, conservative, and practical approach to unknown foundation bridges.

PRACTICAL CONSIDERATIONS

General

Just as the engineer must consider the loading requirements for which a bridge would have been designed, he/she should be aware of the construction methods and specifications typically used at the time of construction. Piles do not always drive as predicted during design or as assumed based on the one or two borings which may be available for the S/B-C analysis. Without driving records, knowledge of construction practices can be critical in correctly using the S/B-C method. Since most of the authors' work has been for structures in Florida, examples of Florida Department of Transportation (FDOT) practices are presented.

FDOT Pre Mid-1990's

Before the mid-1990's, FDOT used a modified Engineering-News Record (ENR) formula to determine the blow count required to achieve design capacity. However, by FDOT Standard Specifications, piles were driven their full length to grade (cut-off elevation) and the driving criteria derived from the ENR formula was used only to assure a minimum capacity was achieved. If a pile was driven its full length without achieving the required blow count, an extension or splice was required. If the blow count was achieved before this, driving continued until the pile reached grade or the "maximum practical resistance" was obtained. Practical refusal was defined as a third of the penetration per blow provided by the required blow count from the bearing formula, maintained over 0.6 m (2 ft). Absolute refusal was defined as a tenth of this same penetration, maintained for 50 blows. Driving was stopped before full penetration only if practical or absolute refusal was achieved. Based on these requirements, it can be concluded that piles driven in accordance with FDOT Standard Specifications on these older bridges were almost always driven at least to the embedments predicted during design. Only in special cases, such as the occurrence of unexpected hard rock or very dense material, might they be shorter. Borings performed as the part of the bridge evaluation can often alleviate concerns that such rock or dense material was encountered.

FDOT Post Mid-1990's

Since the mid-1990's, FDOT has required all structures founded on piles to include dynamic load testing of test piles using Pile Driving Analyzer (PDA) equipment. Based on the results of driving these piles and subsequent CAPWAP analyses, production pile lengths and driving criteria are set. There is confidence that the piles are driven to a required driving resistance which includes a known Factor of Safety (or load and resistance factors), or to a minimum tip elevation, whichever is

deeper. The minimum tip elevation is usually set by the structural engineer to ensure lateral stability, but can also be controlled by potential settlement, punching failure, etc. Scour is accounted for when applicable. Thus, if the structure was designed and constructed in accordance with FDOT procedures, one can be fairly certain that actual embedment is at least as deep as that calculated by the S/B-C method.

General Use of S/B-C Method

With knowledge of the circumstances under which a state or local bridge was constructed, the S/B-C method can be applied to all types of bridge structures founded on piles. As described in this paper, bridges constructed using FDOT Standard Specifications have been analyzed successfully. Non-FDOT bridges, whether in-state or out-of-state, can be analyzed similarly by adapting the methodology to account for the design and construction practices which were in use at the time the bridge was built.

PREDICTIVE CAPABILITY OF S/B-C METHOD

General

The usefulness and predictive capability of the Static/Back-Calculation (S/B-C) analysis presented in this paper are demonstrated by several case studies of bridges with known foundations, one of which is detailed below. In these case studies, the structural loads and geotechnical parameters were considered "known"; the foundation was "unknown". The analysis was carried out using the non-linear, finite element program FB-MultiPier/FB-PIER V4 (FDOT 2000) to determine the pile embedment at which static equilibrium is first encountered. This reasonable minimum embedment was then combined with the known unsupported length and compared to the actual known foundation. In the analysis, piles were modeled assuming no material deficiencies or section property losses and pile creep effects were not considered. The deflected shape (P-delta effects), and possible pile cracked section properties were incorporated and the pile-cap connection was assumed pinned.

Case Study

Bridge Number 030064, US-41 over Outback Canal, Collier County, Florida, is the subject of the case study presented in detail in this section. The bridge was constructed in 1966 and has undergone no repairs or rehabilitation. The bridge structure is approximately 13.6 m (45 ft.) long, consisting of two 6.8 m (22.3 ft.) spans with a superstructure composed of 343 mm (13½ in.) thick simple span cast-in-place slabs. The intermediate pile bent has five 455 mm (18 in.) square prestressed concrete piles with an unsupported length of 1.2 m (3.8 ft.). The soil boring at the bridge bent is shown in Figure 3. Partial geotechnical parameters used in the analysis are provided in Table 2 and more details are given in the report by Ayres and GCI (2007). The total load was computed to be 1775 KN (399 kips) per pile bent or 355 KN (80 kips) per pile. The model geometry was based on the 1965 Bridge Plans. The Static/Back-Calculation (S/B-C) as depicted in Figure 2 and formulated in Equations (1) and (3) was carried-out.

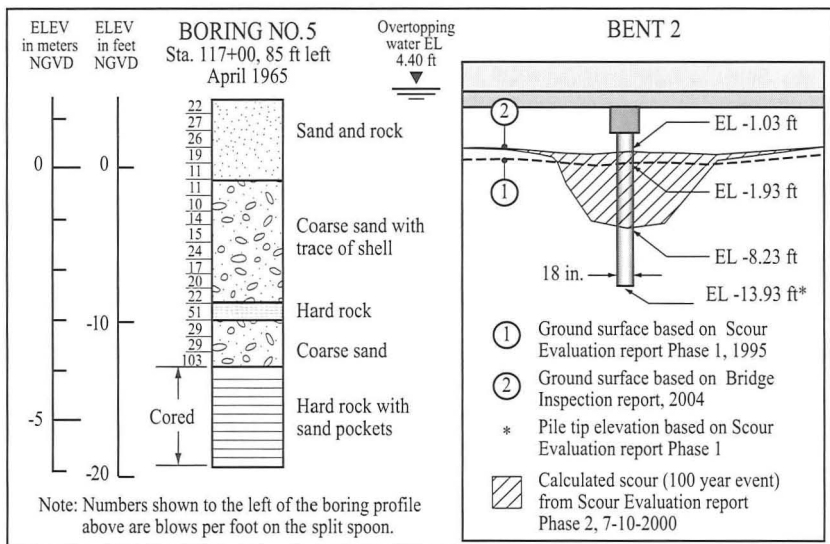


Figure 3. Report of SPT Boring for Bridge 030064

Table 2. Geotechnical Parameters for FB-MultiPier/FB-PIER V4 Model
Bridge No. 030064, US-41 over Outback Canal, Collier County, Florida

SOIL BORING DATA									
Layer No.		1		2		3		4	
Soil Description		Coarse Sand w/trace of Shell		Hard Rock		Coarse Sand		Hard Rock	
Average SPT-N (Blows Per Foot)		17		51		29		100	
Thickness	Feet	6.7		0.9		3.5		6.5	
	Inch	80.0		10.8		42.0		78.0	
Elevation Range (NGVD)	Feet	-1.93 to -8.6		-8.6 to -9.5		-9.5 to -13.0		-13.0 to -19.5	
	Inch	-23.2 to -103.2		-103.2 to -114.0		-114.0 to -156.0		-156.0 to -234.0	
SOIL/ROCK LAYER PROPERTIES									
Geotechnical Parameters		Top	Bottom	Top	Bottom	Top	Bottom	Top	Bottom
Friction Angle (φ) (degrees)		32°	32°	---	---	34°	34°	---	---
Soil Modulus k (kci)		0.06	0.06	0.8	0.8	0.06	0.06	0.8	0.8
Total Unit Weight (γ) (kci) (10 ⁻⁵)		6.7	6.7	6.9	6.9	6.9	6.9	7.0	7.0
Undrained Shear Strength (C _u) (ksi) (10 ⁻³)		---	---	40.0	40.0	---	---	56.0	56.0
Major Principal Strain at 50% (ε ₅₀)		---	---	0.004	0.004	---	---	0.004	0.004
Avg. Undrained Shear Strength (C _{avg}) (ksi) (10 ⁻³)		---	---	40.0	40.0	---	---	56.0	56.0
US-SI CONVERSION FACTORS									
1 in = 25.4 mm				1 kci = 2.71 x 10 ⁻⁴ Kn/mm ³					
1 Kip = 4.45 kN				1 ksi = 6.89 x 10 ⁻³ kN/mm ²					

A Factor of Safety of 2.5 was applied to the axial load for ASD Method. The analysis converged at a pile length of 5.2 m (17 ft.) but failed to converge at a pile length of 4.8 m (16 ft.). Actual average pile length for this bridge bent is 4.9 m (16.1 ft.).

Predicted vs. Actual Length

Results of the various case studies showed a good correlation between predicted pile lengths from the S/B-C analysis and actual average pile lengths. This comparison is graphically summarized in Figure 4.

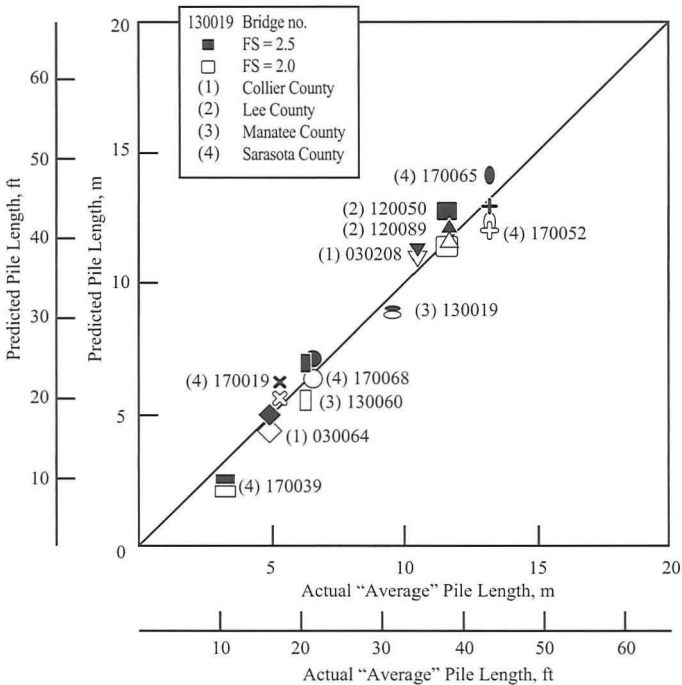


Figure 4. S/B-C Predicted vs. Actual Pile Length

VALIDATION OF NON-DESTRUCTIVE TESTING (NDT)

The S/B-C method can also be used to validate embedment determinations done by NDT methods in previous or current projects. For “high priority” unknown foundation bridges, the S/B-C reasonable minimum embedment can be used along with the embedment required for stability considering the scour to plan and guide any future NDT that may be required by the owner. In general, the S/B-C method can reduce the extent of costly NDT that may be done in the future and presents an alternative to positive discovery of bridge foundations.

SUMMARY AND CONCLUSIONS

Since the mid 1990's, the Static/Back-Calculation (S/B-C) method has been adopted and developed by the authors as a calibration tool for the geotechnical/structural model in the Soil-Structure scour evaluation for several hundred bridges with known foundations in the State of Florida. With the confidence gained from these analyses, the S/B-C method is proposed as a means to re-classify unknown foundation bridges from "unknown" to "known" by determining the reasonable minimum embedment. The method is a practical, cost-effective, and deterministic approach and can reduce or eliminate the use of costly Non-Destructive Testing (NDT). It is based on satisfying static equilibrium under appropriate load for the existing bridge pier/bent conditions using three-dimensional, non-linear finite element analysis. The approach is applicable to partially and fully-embedded (i.e., buried pile cap) sub-structures. Basic geotechnical data, structural loads (ASD, LRFD, or any appropriate load), geometry of the sub-structure (i.e., pile group layout and pile type and size), and knowledge of construction practices and methodologies are all needed to successfully utilize the method. Once the re-classification to "known" from "unknown" is done using the Static/Back-Calculation method, the scour evaluation (Hydraulic Analysis; Soil-Structure Evaluation; and Remedial Measures, if needed) is subsequently done in the conventional manner. The S/B-C method is a powerful tool that removes a major stumbling block in the path of the scour evaluation program for unknown foundation bridges. It alleviates the potential impact of budget cuts experienced by various agencies around the country and accelerates the screening of these bridges in a rational and timely manner to protect the public.

ACKNOWLEDGEMENT

Grateful acknowledgements are due for the support provided by the Florida Department of Transportation (FDOT) District I and VII Maintenance Engineers for allowing the use of some procedures presented in this paper to evaluate FDOT bridges during the course of providing scour evaluation services.

REFERENCES

- American Association of State Highway and Transportation Officials (AASHTO) (2002). *Standard Specifications for Highway Bridges. 17th Edition.*
- Ayres Associates & GCI Inc. (2007). "Phase III Evaluation Report for Bridge No. 030064, Collier County, Florida."
- Federal Highway Administration (FHWA) (2005). *Unknown Foundation Summit.* Lakewood, Colorado.
- Federal Highway Administration (FHWA) (1998). *Driven 1.0: A Microsoft Windows™ Based program for Determining Ultimate Vertical Static Pile Capacity.*
- Federal Highway Administration (FHWA) and Florida Department of Transportation (FDOT) (2009). *"Unknown Foundation Bridges Pilot Study".*
- Florida Department of Transportation (FDOT) (2000). *User's Manual for FB-MultiPier/FB-PIER Program.*
- Florida Department of Transportation (FDOT). (2009). *User's Manual for FB-Deep.*
- Sayed, S. M., and Bakeer, R. M. (1992). "Efficiency formula for pile groups". *J. Geotechnical Engineering Division, ASCE*, 118(2), 278 – 299.

- Sayed, S. M. (2005). Personal Communications, "General approach to unknown foundations." *Scour Technology – FHWA Unknown Foundation Summit*, Lakewood, Colorado.
- Sayed, S. M., Sunna, H., Amaning, K. O., Jetha, N. K., and Garcia, J. (2009). "Stability assessment of bridges impacted by scour." *Proc. 17th Int. Conf. on Soil Mechanics and Geotechnical Engineering (ICSMGE)*, 2, 1333-1336.
- Sayed, S. M., Sunna, H., and Moore, P. R. (2009). "Re-classifying bridges with unknown foundations." Presented at the *41st Southeastern Transportation Geotechnical Engineering Conference (STGEC)*, Wilmington, North Carolina
- Stein, S., and Sedmera, K. (2006). "Risk-based management guidelines for scour at bridges with unknown Foundations." Web-Only Document 107, Project 24-25, *N.C.H.R.P., TRB*, Washington, DC.
- Sunna, H. N., Sayed, S. M., and Jetha, N. K. (2008). "Proposed approach to unknown foundations." presented at the *Geotechnical, Geophysical and Geoenvironmental Engineering Technology Transfer Conference and Exposition (Geo t₃ 2)*, Charlotte, North Carolina.

Guidance on the Design of Berthing Structures Related to the Flow Velocities in Ship Thrusters

Henk Verheij¹, Marc Sas², Marcel Hermans³, and Eckard Schmidt⁴

¹ Delft University of Technology and Deltares, P.O. Box 177, 2600 MH Delft, The Netherlands; email: henk.verheij@deltares.nl

² International Marine and Dredging Consultants, Coveliersstraat 15, B-2600 Antwerp, Belgium

³ Port of Portland, 7200 NE Airport Way, Portland, OR 97218, USA

⁴ Knabe Consulting Engineers GmbH, Gasstrasse 18 Haus 4, 22761 Hamburg, Germany

ABSTRACT

Ships have been getting larger and deeper, and simultaneously the installed power of main propellers and bow thrusters has increased. These changes improve the manoeuvrability, but also result in considerably higher flow velocities in the induced jets. Because the bottom of harbour basins are often not designed for these extreme velocities this can lead to bottom erosion and possibly failure of berthing structures. This paper will discuss the procedure for designing complex new berthing facilities as presented in the new PIANC report on this subject.

Introduction

Marine transport is constantly increasing in scale in order to comply with the ever-changing demands of the international market. Ships are becoming larger and deeper, and to facilitate proper manoeuvring most are equipped with main propellers and bow thrusters. As a result of the increase in size and engine power of the propulsion systems the flow velocities have increased considerably. Because the bottom of harbour basins are often not designed for these extreme velocities this can lead to bottom erosion and possible failure of berthing structures (Figure 1). Because of awareness of damage to existing harbour infrastructure and to provide guidance for properly designing future harbour facilities PIANC (Permanent International Association of Navigation Congresses – www.pianc-aipcn.org) installed a committee to prepare new guidelines for the design of berthing structures related to thrusters. The new guidelines (PIANC, 2010) give an overview of modern berthing structures, thrusters, berthing and departures procedures, the design philosophy, procedures to estimate the flow velocities in the thruster jets, and methods to determine size and extent of bottom protection or to estimate the depth of scour holes. The report replaces an older PIANC report (1997); see also Sas et al (2010). This paper will discuss various aspects related to the design of complex new berthing facilities.

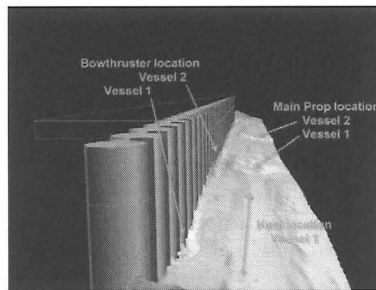


Figure 1. Observed erosion in front of a quay wall

Quay structures

There are many different berth structures in use throughout the world with water depth at the quay up to 20 m. Berth structures can be characterized in two main groups according to their relevance for the impact of thrusters and main propellers as follows (Figure 2):

A) Solid Berth Structures:

- Sheet pile structures, and
- Gravity structures

B) Open Berth Structures

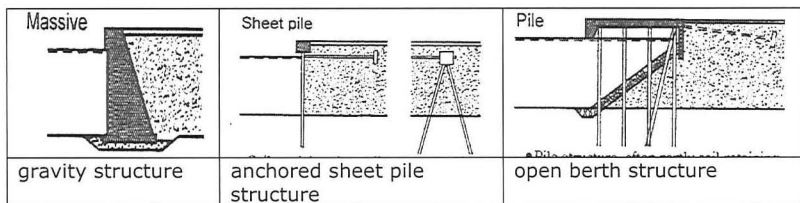


Figure 2. Schematised examples of berthing structures

The scour problem related to Solid Berth Structures is limited to erosion of the bed material in front of the structure, whereas scour related to Open Berth Structures is more complex and can include:

- scour around the piles in particular those near the berthing face, and
- scour of the slope underneath the quay, even up to the top.

Although scour can occur near berth structures due to natural currents as well, berth structures are specifically vulnerable to scour caused by vessel's main propeller action and thrusters. Especially during berthing and unberthing, eroding forces on the seabed in front of the berth or on the slope underneath the berth can be substantial. Resulting current velocities due to the action of the main propellers or thrusters can reach up to 8 m/s near the bed, while for example the tidal current is typically limited to around 1 or 2 m/s.

Propulsion systems

Container vessels, Ro/Ro vessels and ferries are known to be major contributors to erosion near berths. These ship types can be equipped with (Figures 3 and 4):

- Main propellers at the ship’s stern: conventional propellers, azimuthal systems (diameter up to 10 m)
- Thrusters (diameter up to about 3 m)
- Water jets (outflow opening about 1 m)

The advantages of azimuthal systems lie in the capacity for rotating the pods, providing 360° for maneuvering purposes. The total power can reach 25 MW.

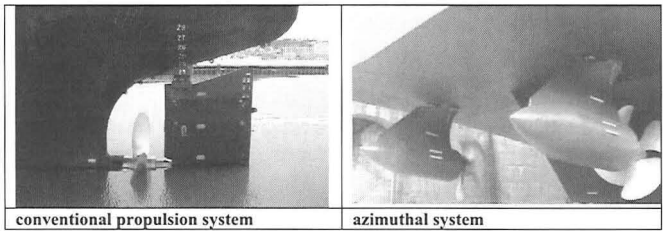


Figure 3. Examples of main propulsion systems

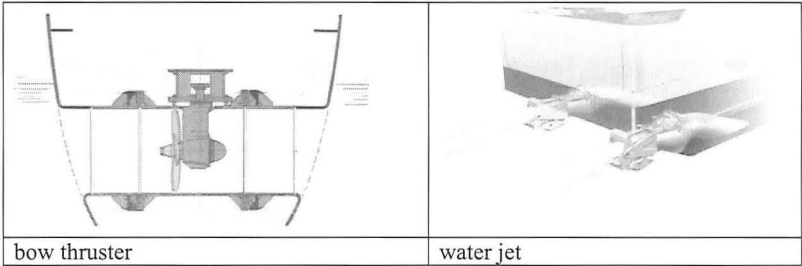


Figure 4. Examples of thrusters and water jets

Thrusters are placed in a smooth tunnel near the bow in single or twin units in different frames, taking in water from one side and expulsing it out the other. They are very useful for turning maneuvers without tug assistance. This subtype is usually called bow thruster when located near the bow, or stern thruster in other positions (aft). Transverse thrusters lose their efficiency at sailing speeds above 2 knots. The power of these systems can reach 4 MW.

Fast ferries are often equipped with water jet systems. Sea water passes through a nozzle where an axial pump is located. A considerable jet of water is impelled backwards through the aft pipe system. These jets are usually installed in pairs. Maneuvering is very easy when one jet is pushing forward and the other pulling backward. The installed power of these systems can reach 26 MW.

Design philosophy

The main distinction in design philosophies is between (Figure 5):

- A. Design to **protect the bottom** in front of the structure in order to **avoid scour**, or
- B. Design to **protect the structure** in order to **avoid negative impacts** to the structure resulting **from scour**

Although in both cases the ultimate goal and result is the protection of the structure, in some cases the designer could decide to accept anticipated scour near the structure but secure the structural integrity in a different way, which in certain cases may be more cost-effective and suitable. It may be more effective and appropriate to design the structure for greater depths taking into account that deep scour holes may develop in front of it, than it would be to put all focus of the design in avoiding any movement or erosion of bed material. Alternatively, a third option of design philosophy could be to focus attention on avoiding scouring forces to happen.

This design philosophy issue is not much different from the usual design question what level of damage to accept in order to optimize a design for long-term functionality and cost-effectiveness over the lifetime of the structure. The answer to that question is highly dependent on the specifics of a situation, and will have to be considered by the designer. Relevant factors that will have to be taken into account are:

- Cost (for both initial construction as well as maintenance)
- Environmental aspects (considerations related to allowing large movements of bed material versus installation of for example a hard bottom protection)
- Options to -and ease of- performing monitoring and any needed maintenance
- Risk to the structure if scour would be more than an acceptable level and/or not detected in time
- Impacts and possibility of performing repair work in case damage to the structure would occur
- Effects on deepening or other berth modifications potentially required in future years
- Any other potential functions of the local bottom (e.g. nearby slopes, buried utilities/outfalls, etc.)

Having made the necessary choices one can start the design. The first step is to compute the outflow velocity taking into account the geometry of the quay structure, berthing procedure, and etcetera.

Berthing and departing procedures

Sailing speed of a vessel during berthing and departure will be relatively low. One consequence of this low speed is that the vessel's manoeuvrability is significantly reduced and that the vessel cannot rely on the rudder to the same level as during regular sailing speeds. For this reason, assistance from tugs and/or bow thrusters is commonly used during berthing and departure. In some cases and to

some degree a bow thruster can substitute the workings and/or need of a tug during berthing or departure.

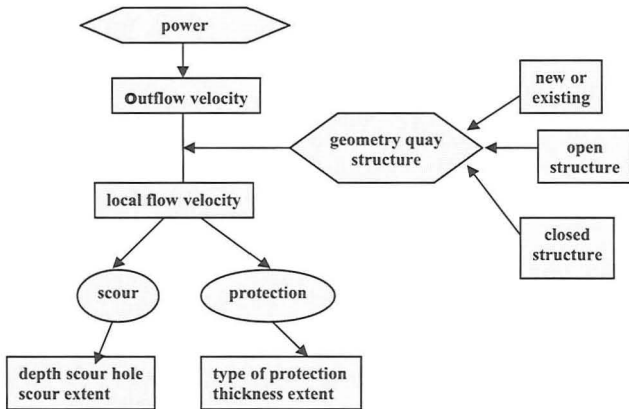


Figure 5. Design process

Main factors in managing a berthing or departure manoeuvre are typically wind and current. Either one can apply great force on a vessel during such manoeuvres and will be a main driver in determining ultimate need for tugs. A certain vessel that may normally depart by use of main propeller and bowthruster may require tug assistance if wind or current are strong. Figure 6 shows berths layouts with unberthing manoeuvres.

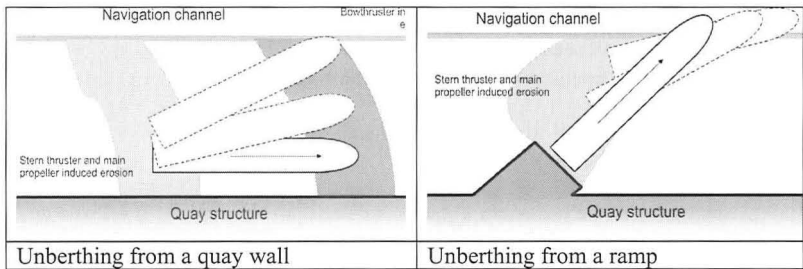


Figure 6. Unberthing manoeuvres

The applied engine power is not constant in time. In the first moments more power will be used. Moreover, the impact of the thrusters depends on the stage of the unberthing manoeuvre. No good data is available on how long captains use their thrusters. Furthermore, it is important to realize that the installed power has increased over time but is not specifically designed for berthing/unberthing but also for carrying out manoeuvres in turning basins in general. In other words: applying

100% of the installed power is a conservative estimate. This is underlined by results of questionnaires of the Harbour Authorities of Antwerp and Rotterdam resulting in the conclusion that use is typically limited to 75% or less of the installed power of the bow thrusters. The same holds true for the main propellers. In general, the applied power is:

- main propellers: $P_{\text{applied}} = (10 - 20\%) \cdot P_{\text{installed}}$ and under strong current and wind conditions the applied power may increase to 40% of the installed power
- thrusters: always 100% of installed power, however for very high powered thrusters this might be a too conservative assumption

This requires information on the installed engine power. The ship owner should be able to provide this information. Sometimes, the ship dimensions can help in selecting a reasonable value, for example for container vessels Roubos (2007) presented relations between the ship width B_s and the installed power P_{thruster} as well as for the propeller diameter of thrusters as function of the ship width:

$$P_{\text{thruster}} = 83B_s - 1400$$

$$D_{\text{thruster}} = 0.05B_s + 0.464$$

Roubos also presented relations for the main propeller system of containers vessels. It should be noted that nowadays the largest container vessels have engines up to 100,000 kW. However, specific equations for all ship types are not available and consequently the designer will have to rely on information from the ship owner.

Flow velocities in thrusters

In general, jets generated by propulsion systems can be distinguished from submerged free jets. A free jet is defined as the water flowing out of an orifice into the surrounding water without any disturbance by lateral boundaries or walls that may hinder the spreading of the jet (Albertson et al, 1950). Main differences are: propeller jets have a rotational flow velocity and swirl at the tip of the propeller blades which results in a higher turbulence level and a shorter length of the flow establishment zone compared to free jets.

Based on the free jet approach formulas have been derived to compute the relevant flow velocities for vertical walls (Schmidt, 1998). The maximum flow velocity at the bed in the corner is (Figure 7):

$$V_{\text{bottom,thruster}} = \alpha_L 1.9 V_{0,\text{thruster}} \left(\frac{x_t}{D_{\text{thruster}}} \right)^{-1.0} \quad \text{with } \alpha_L = 1 \text{ for } h_t/D < 3$$

$$\text{with the outflow velocity } V_{0,\text{thruster}} = 1.15 \left(\frac{P_{\text{thruster}}}{\rho_w D_{\text{thruster}}^2} \right)^{0.33}$$

where x_t is the distance along the jet axis between outflow opening and quay wall.

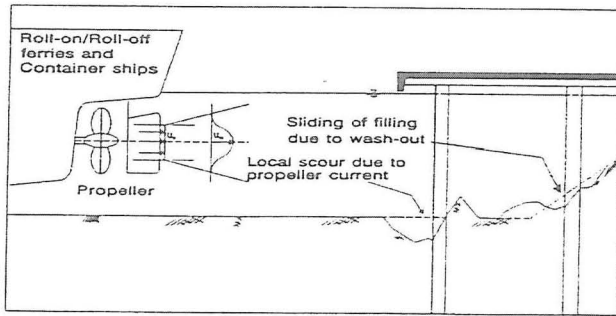


Figure 8. Jet impact on the slope of an open quay structure

The above means that the following situations will have to be considered regarding the flow field and the subsequent scour below the quay deck (see Figure 8):

- Effect of piles
- Effect on the slope
- Effect of oblique jet

The effect of the slope already has been discussed above, while the effect of the oblique jet can be accounted for by a larger distance. Taking into account the effect of the piles on the flow will be more challenging. Considering thrusters, in most situations the flow direction will be perpendicular to the quay structure. In general, the flow velocity directly adjacent to a pile will be about twice the approach flow velocity (Breusers et al, 1977).

Regarding scour, the pile diameter will be much smaller than the water depth allowing the following formula to be used to estimate the final scour depth (Hoffmans & Verheij, 1997):

$$S_e = 2.0b$$

with b = pile diameter.

Mostly, a group of piles supports the superstructure (Figure 9). In those cases, the spacing s between the piles is important as is the flow direction. If the spacing is larger than about $5b$ the scour holes of the individual piles do not impact each other. If the spacing is less than $5b$, particular formulas should be used which take into account the different effects (Richardson & Davis, 2001):

$$S_e = 2.0Kb \text{ with } K = K_{\text{group}} K_{\text{orientation}} K_{\text{shape}}$$

The value of the various K -factors vary between 1.0 and 2.0.

A case study showing how to deal with scour at open quay structures is not available, because to the authors knowledge no particular experiments have been done except by Chin et al (1996). They carried out laboratory tests on scour at quay structures due to propeller jets (Figure 10) and published the results inclusive the following equation for the maximum scour depth S_e :

$$S_e = 0.21 D_0 F_0 \text{ with the densimetric Froude number } F_0 = \frac{V_0}{\sqrt{d_{50} g \Delta}}$$

where D_0 is the outflow diameter, V_0 the outflow velocity, d_{50} the median diameter bed material, g the gravitational constant and Δ the relative density. Note that the equation derived by Chin et al differs considerably with the earlier presented equations for the scour S since it does not contain the pile diameter b . It makes clear that research is required.

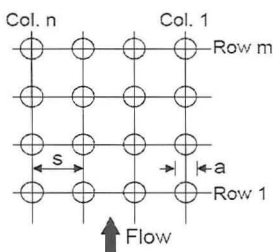


Figure 9. Definition sketch of piles

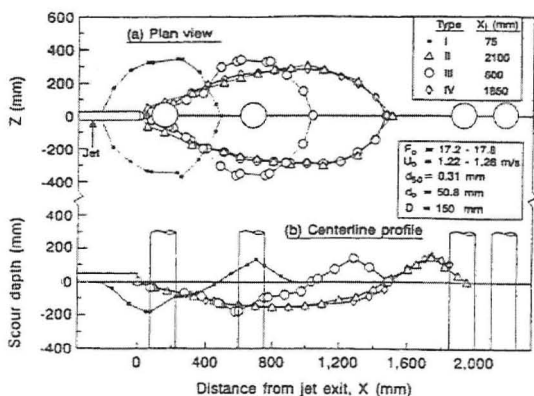


Figure 10. Results of laboratory experiments (Chin et al, 1996)

Conclusions and recommendations

The new PIANC report "Guidelines for berthing structures related to thrusters" presents procedures to design berthing structures taking into account modern thrusters, complex quay walls and berthing and departure procedures. For solid berth structures, such as gravity walls and sheet pile structures, the procedure is straight forward. For open berth structures, such as a superstructure built on piles above a slope, a straight forward procedure is not available. Based on established well-known design rules for pile structures

a procedure is proposed. It is recommended to validate the proposed method by carrying out physical tests. Furthermore, it is recommended to collect data on the use of thrusters, particularly the duration and percentage of use of the installed engine power.

References

- Albertson, M.L. et al (1948). Diffusion of submerged jets. *ASCE, Trans. Paper No. 2409*, pp. 639-664, 1948.
- Breusers, H.N.C., G.Nicolet and H.W.Shen (1977). Local scour around cylindrical piers. *Journ. of Hydraulic Research*, IAHR, 15(3):211-252.
- Chin, C.O., Y.M.Chiew, S.Y.Lim and F.H.Lim (1996). Jet scour around vertical pile. *Journ. of Waterway, Port, Coastal and Ocean Engineering*, Vol.122 No.2, paper No 9787, pg.59-67
- Hoffmans, G.J.C. & Verheij, H.J. (1997). Scour Manual. *Balkema Publishers*, Rotterdam
- Hoffmans, G.J.C.M. and H.J.Verheij (2008). Three dimensional scour. *4rd Intern. Conf. on Scour and Erosion ICSE-4*, paper A-5, pp.128-133, Tokyo, Japan
- PIANC (1997). Guidelines for the design of armoured slopes under open piled quay walls. *PIANC*, report, supplement to Bulletin 22, Brussels.
- PIANC (2010). Guidelines for berthing structures related to thrusters. *PIANC*, Report of working group 48, Brussels, Belgium (in preparation, to be published in 2010).
- Richardson, E.V. and S.R.Davis (2001). Evaluating scour at bridges, *Hydraulic Engineering Circular no 18 (HEC 18, Fourth Edition)*. report FHWA NH1-01-001, *Federal Highway Administration*, Washington DC, USA.
- Römisch, K. (2001). Scouring in front of quay walls caused by bow thrusters and New measures for its reduction. *Vth Intern. Seminar on Renovation and Improvements to existing Quay Structures*, Gdansk, Poland.
- Römisch, K. (2006): Erosion potential of bow thrusters on canal banks (in German). *Binnenschifffahrt – ZfB – Nr.11*.
- Roubos, A.A. (2007). Dealing with uncertainties in the design of bottom protection near quay walls. *MSc thesis*. TU Delft
- Sas, M., H.J.Verheij, M.Hermans, G.Horner, E.Schmidt, C.A.Thoresen, J.van Bogaert and J.L.Zatarain (2010). New PIANC guidelines for berthing structures related to thrusters. *32nd Intern.Congress*, PIANC, Liverpool, UK.
- Schmidt, E. (1998). Diffusion and erosion of a bow thruster jet in front of a quay wall (in German). *MSc thesis*, TU Braunschweig, Mitteilungen des Leichtweiss-Institutes, Heft 143, Braunschweig, Germany.

Georgia DOT's Implementation of BridgeWatch®

Joseph P. Scannell¹, President and Marc K. Baribault², Meteorologist

¹USEngineering Solutions Corporation, 179 Allyn Street, Hartford, CT 06103; PH (860) 524-9110; email: jscannell@usengineeringsolutions.com

²USEngineering Solutions Corporation, 179 Allyn Street, Hartford, CT 06103; PH (860) 524-9110; email: mbaribault@usengineeringsolutions.com

ABSTRACT

Transportation professionals are charged with the formidable task of protecting, maintaining, and replacing bridges in a cost-effective manner to allow safe passage by over 230 million road and rail vehicles daily and commercial vehicles transporting over \$8.4 trillion of cargo annually. A bridge failure is costly in terms of life and property. However, many failures can be prevented, delayed, or mitigated through monitoring, early warning, and well-coordinated emergency response protocols.

During the fall of 2008, the Georgia Department of Transportation ("GDOT") was looking for a way to monitor their scour-critical bridge population and incorporate this effort into the development of plans-of-action ("POA") for seventy-six (76) scour-critical bridges. The monitoring system they chose is a web-based software system known as BridgeWatch®. The system utilizes patented technology that collects and processes real-time data to provide automated early warning to engineers of any potentially-destructive environmental conditions in and around their structures so they can effectively respond to protect life and property.

GDOT engineers were given the ability to populate their BridgeWatch system with inventory data, personnel contact information, and structure specific thresholds, to monitor for environmental conditions such as accumulated precipitation, increased river flows, hurricane induced tidal surge, and seismic events. The system enables owners and operators to make informed decisions about public safety, in real-time, and effectively dispatch emergency personnel, safety inspectors and maintenance workers, prior to flooding or other destructive environmental events which adversely affect bridges.

SYSTEM DESCRIPTION

The GDOT-version of BridgeWatch is a web-based software system designed to access real-time meteorologic, hydrologic, seismologic data sources, analyze site specific data, and evaluate said data against established thresholds pertaining to specific-related structures to determine if, when, and how a user of the system should be alerted. The system enables more effective communication by automatically contacting key personnel and informing them of a potentially destructive event, so they can respond with an appropriate POA protocol. BridgeWatch's capabilities allow for the early detection of potential hazards and allow for the GDOT to initiate their emergency response actions. Through an automated notification process, users receive system-generated watch lists of structures experiencing critical flooding events. A watch list, which can be sorted for specific attributes, establishes a priority list of structures requiring inspections or other emergency actions.

EXTERNAL DATA SOURCES

BridgeWatch accesses several external data sources in real-time, including, but not limited to: data derived by the National Oceanographic Atmospheric Administration ("NOAA"), the United States Geological Survey ("USGS"), and the National Weather Service ("NWS"). The NWS makes available warnings that enable the system to provide early notification for flooding activity. The system gathers and processes relevant river data collected by USGS real-time stream flow stations. NOAA publishes real-time Next Generation Radar ("NEXRAD") rainfall accumulation data sets for processing by the system algorithms. GDOT's version of BridgeWatch has been configured to interact with the above external data sources. The system can be further configured to include other data sources such as, bridge specific monitoring devices, seismic activities, and other related asset location and disposition information.

NWS Data Source

The BridgeWatch system notifies users when the NWS flood and flashflood warnings ("FLW" and "FFW," respectively) are issued and processed. These warnings may or may not require action by the user depending on GDOT's existing protocols. FLW and FFW data are obtained from the Interactive Weather Information Network ("IWIN") web interfaces. The warning data is formatted as Advanced Weather Interactive Processing System ("AWIPS") text data sets as identified in the AWIPS header. Referring to Figure 1, the heading (shaded in yellow), includes an abbreviated World Meteorological Organization ("WMO") code which identify all types of weather data. Imbedded in this weather data are bulletins that represent FLW and FFWs (shaded in red) that are parsed by the system's data handler. Located at the bottom of each warning is a series of four-digit numbers that identify the location of the warning area shaded in green.

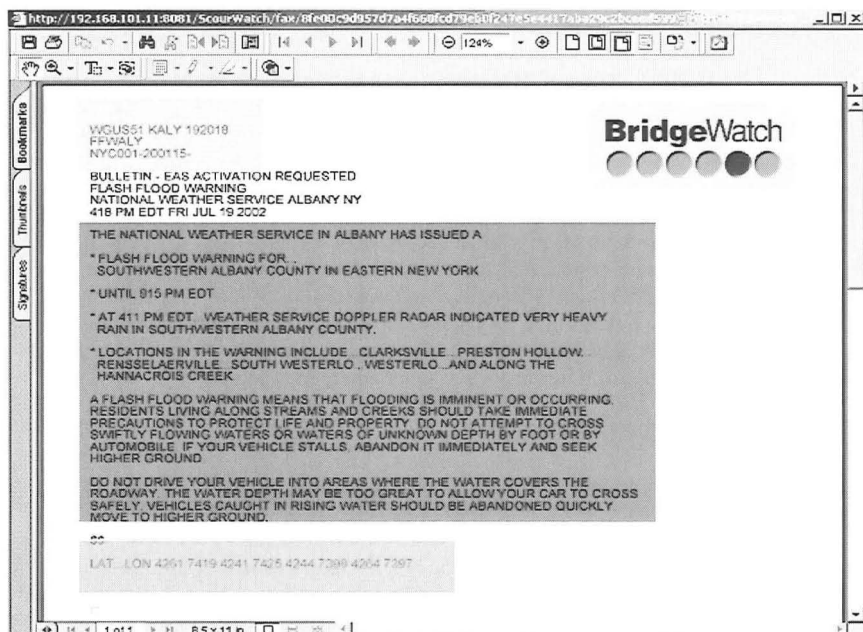


Figure 1. A NWS Flashflood Warning captured and processed by BridgeWatch

USGS Data Source

BridgeWatch accesses USGS' real-time river data from Georgia's gage network at regular intervals. The system gathers and decodes data from real-time stream flow stations for comparison against a static Event Threshold Database ("ETD") as provided by GDOT. The ETD contains thresholds for the 2, 5, 10, 25, 50, 100, 200 and 500-year peak discharge flows for each real-time gage the system interrogates. The system will continually compare data and generate further calculations when one of the thresholds is reached or exceeded. When a threshold is exceeded, the system applies the threshold value to the corresponding bridge associated with that particular gage. GDOT has established the criteria for the bridge associations to a particular gage when the bridge is common to a particular watershed. However, due to the fact that not all watersheds contain gages, not all structures will have associations to gages. The system will generate an event once it has processed the gauged bridge associations and threshold criteria.

NOAA Data Source

The system accesses NEXRAD imagery data sets provided by NOAA in order to perform calculations for threshold comparisons and for direct interface display. GDOT has provided values for these thresholds for each bridge in the system according to six major storm intensities, termed the 2, 5, 10, 25, 50 and 100-year return frequency rainfall intensities. Like the ETD for the stream flows, BridgeWatch will use the rainfall ETD to establish the criteria for creating watch lists. During these rainfall events, NEXRAD binary radar imagery is obtained and decoded by the system data handler. NEXRAD data sets are updated approximately every 5 to 10 minutes, depending on the radar's configuration. However, the most useful data sets are the One-Hour, Three-Hour and Storm Total Precipitation accumulation products. These data sets contain raster imagery identifying accumulated rainfall for the coverage area of each NEXRAD installation. Once a NEXRAD rainfall threshold is exceeded, the system data handler then creates a corresponding watch list of bridges. Threshold exceedance is calculated using the NEXRAD overlay and a bridge's basin of influence.

INTERNAL DATA SOURCES

The system houses several internal data sources as separate databases within the central database: the GDOT BridgeWatch system consists of five primary databases. The first three consist of data provided by the GDOT Bridge Maintenance Unit ("BMU"): profiles, bridges, and threshold databases. The fourth database, gages, consists of a list of real-time gages that are interrogated by the system. The fifth database, tracking hydrologic events, is generated and updated through the use of the application which archives active events.

Profiles and Subscriptions

GDOT user information is maintained in the system's profiles database. Each GDOT has a unique profile containing username, product subscriptions, contact information (cell phone, pager, fax and email) and a geographic area of responsibility. The GDOT BridgeWatch system has over a hundred such profiles, or users, ranging from field staff to GDOT BMU managers. Each profile has a unique set of subscriptions resident the system. The BridgeWatch subscription processor cross-references the profile database to properly disseminate alert notifications as real-time event information is processed and products are generated. User profiles are maintained and updated quarterly by the GDOT BMU.

Bridges and Threshold Databases

The GDOT BridgeWatch database includes seventy-six (76) scour-critical bridges throughout Georgia. This database contains bridge specific information extracted from the reporting items in Georgia's bridge information management system in addition to photos, reports, plans, and digital POAs. Bridge number, carried and crossed features, and item 113 codes are just a few of the many data fields

housed within the system. The system displays bridge data from the bridge database to the user via the web interface.

The thresholds database, generated from data provided by GDOT, contains the exceedance values for rainfall intensity (measured in inches) and stream flow (measured in cubic feet per second) relating to those bridges in the bridge database. The GDOT BridgeWatch data handler is constantly checking thresholds against real-time data sources. Once a threshold exceedance is discovered, the data handler packages the information as a product to be processed by the subscription processor which translates products into alert notifications.

Events and Alert Notifications

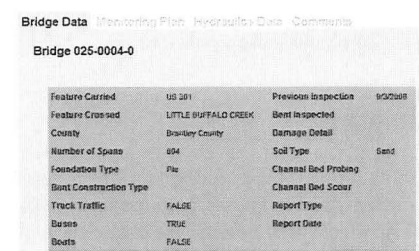
The events database is generated and maintained by the GDOT BridgeWatch system; it records every alert notification generated by the system and maintains an events archive. This archive is useful in reviewing past events and assembling system reports. BridgeWatch displays event data from the events database to the user via the system's administrative panel. Since inception, the GDOT system has identified more than thirty rainfall events and more than a dozen river flow events as associated to Georgia's scour-critical bridge population. Alert bridges will appear on the geospatial environment of the system interface as red icons (Figure 2). Users can click on these icons to learn more about the alert type and review pertinent bridge information. GDOT field engineers can access the system remotely enabling them to publish on-site information in real-time via the system's ticket feature. GDOT staff use tickets to document their response to alert notifications.



Figure 2. Active Alert Bridges displayed as red icons

PLANS OF ACTION

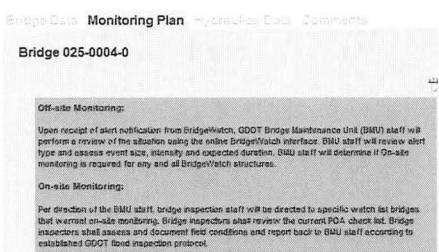
Like all states, Georgia was required to develop POAs in accordance with an FHWA federal mandate related to scour-critical bridges. However, Georgia has uniquely developed, integrated, and maintained POAs for all 76 scour critical bridges using the BridgeWatch system. The GDOT digital POA has four main tabs (Bridge Data, Monitoring Plan, Hydraulics Data, and Comments). The Bridge Data tab can be seen in Figure 3 below.



Bridge Data Monitoring Plan Hydraulics Data Comments			
Bridge 025-0004-0			
Feature Carried	US 501	Previous Inspection	Inspected
Feature Crossed	LITTLE BUFFALO CREEK	Best Inspected	
County	Bartow County	Damage Detail	
Number of Spans	204	Soil Type	Send
Foundation Type	Pile	Channel Bed Probing	
Best Construction Type		Channel Bed Scour	
Track Traffic	FALSE	Report Type	
Beams	TRUE	Report Date	
Boats	FALSE		

Figure 3. Georgia Digital POA's Bridge Data

The Monitoring Plan consists of on and off-site monitoring expectations for each scour-critical bridge. The GDOT system provides the users with the ability to leverage the benefits of off-site monitoring by using the real-time data aggregation capabilities of the system. Many situations can be monitored remotely prior to sending inspection teams to a scour critical bridge site for on-site monitoring. Off-site monitoring is a cost-effective way to only send inspection teams when and where their services are going to be valuable. Figure 4 illustrates Georgia's monitoring plan.



Bridge Data Monitoring Plan Hydraulics Data Comments
Bridge 025-0004-0
Off-site Monitoring: Upon receipt of alert notification from BridgeWatch, GDOT Bridge Maintenance Unit (BMU) staff will perform a review of the situation using the online BridgeWatch interface. BMU staff will review alert type and assess event size, intensity and expected duration. BMU staff will determine if on-site monitoring is required for any and all BridgeWatch structures. On-site Monitoring: Per direction of the BMU staff, bridge inspection staff will be directed to specific watch list bridges that warrant on-site monitoring. Bridge inspection staff review the current POA check list. Bridge inspectors shall assess and document field conditions and report back to BMU staff according to established GDOT flood inspection protocol.

Figure 4. Georgia Digital POA's on and off-site monitoring data

CURRENT UPDATES

Over the past several years, GDOT has become more aware of the capabilities of this population-based approach to monitoring scour-critical bridge populations and have decided to further invest in adding probabilistic storm surge ("P-Surge") data to their monitoring data sources. This will enable GDOT officials to establish thresholds and be alerted when coastline areas are expected to experience coastal inundation from hurricanes making landfall or influencing the eastern coastline of Georgia. GDOT officials will use this data set for the ability to properly allocate assets during and after major hurricanes impact their state. As of the date of this publication, GDOT was still in the implementation phase of this product and therefore no images were available.

CLOSING STATEMENT

The BridgeWatch web-based solution uniquely aggregates public and private data sources that, until now, have been maintained and published independent of one another. The GDOT BridgeWatch system has created a synthesis of these data sources to the extent they are complimentary in providing a comprehensive real-time understanding of the environmental hazards affecting the safe operation of state owned bridges. The GDOT BridgeWatch system has been employed for two years. During this time GDOT bridge maintenance engineers have been notified and responded to more than thirty (30) system-generated alerts which have identified locations where bridges needed to be repaired and even closed due to flood related events.

The employment of new monitoring technology will be the only cost-effective way to increase safety levels and make more timely informed decisions regarding the management of public infrastructure: public safety through real-time structure monitoring.